NUCLEAR ENERGY LEVELS OF ^{37}K

Thesis by
David Reeves Goosman

In Partial Fulfillment of the Requirements

For the Degree of
Doctor of Philosophy

California Institute of Technology
Pasadena, California
1967
(Submitted December 20, 1966)

ACKNOWLEDGMENTS

The author expresses sincere gratitude to all of the Kellogg Radiation Laboratory personnel, and in particular to Dr. R. W. Kavanagh, without whose initiative this project might never have been started. Thanks are due to the Office of Naval Research, which supported the research reported herein, and to the National Science Foundation which kindly granted to me fellowships for four years, and to Dr. J. Bahcall, whose calculations in the mass-37 system have stimulated some of this work.

ABSTRACT

Approximately forty levels in ^{37}K have been established via the reactions $^{40}Ca(p,\alpha)^{37}K$, $^{36}Ar(p,p)^{36}Ar$, $^{36}Ar(p,\gamma)^{37}K$, $^{36}Ar(p,p'\gamma)^{36}Ar$, $^{36}Ar(d,n)^{37}K$ and $^{36}Ar(^{3}He,d)^{37}K$. The analogues in ^{37}K to the first two excited levels in ^{37}Ar were found as a closely spaced doublet at 1368 and 1380 keV excitation energy. The half-life of the latter has been measured electronically to be 9.6 ± 1.4 nanoseconds. Spin and parity assignments have been made to seven of the lowest eight levels in this nucleus and to three higher levels. Approximate values for the elastic and inelastic proton and gamma-ray widths of several levels have been determined. Evidence for the positions and widths of two candidates for the first $T = 3/2$ level is presented. Calibrations of gamma-ray energies with Ge(Li) counters have made possible the determination of level energies with precisions ranging from one to five keV. The mass excess of the ground state is now known to three keV.

TABLE OF CONTENTS

I. INTRODUCTION

One of the most important sources of energy generated in stars like the sun is believed to be the burning of hydrogen in the hot and dense interior of the star. In order to experimentally test this one must be able to observe some kind of radiation emitted from the inside of the sun. The sun is thought to be so dense in its interior that electromagnetic radiation would almost never escape, so that this kind of information is not available for terrestrial observation. To test the theory of energy generation one must observe radiation that has little interaction while escaping the sun.

The conversion of hydrogen to helium in the sun is thought to be initiated by the reaction

$$^{1}H(p, e^{+}\nu)^{2}H(p, \gamma)^{3}He$$

and terminated by the sequences

a. $^{3}He(^{3}He, 2p)^{4}He$

b. $^{3}He(\alpha, \gamma)^{7}Be(e^{-}, \nu)^{7}Li(p, \alpha)^{4}He$

and c. $^{3}He(\alpha, \gamma)^{7}Be(p, \gamma)^{8}B(e^{+}\nu)^{8}Be^{*}(\alpha)^{4}He$.

The rate of the last reaction depends sensitively on the temperature of the solar interior because the thermal energies of the projectiles are small compared to the Coulomb barriers involved. Therefore the

flux of high energy neutrinos (E_{max} = 14 MeV) arising from the decay of ^{8}B is a measure of the temperature of the solar interior.

Although electromagnetic radiation cannot escape the solar interior, the neutrinos from the decay of ^{8}B can escape very easily and thus provide one means of extracting information from the central region of the sun where the nuclear energy is being generated. However, since matter is so transparent to neutrinos their detection is not simple.

Davis (1964) is attempting to measure the solar neutrino flux by measuring the rate of production of ^{37}Ar via the reaction

$$^{37}Cl(\nu_{solar}, e^{-})^{37}Ar \ ,$$

using a detector consisting of 10^5 gallons of C_2Cl_4. The ^{37}Ar atoms are recovered from the liquid by flushing with helium gas and their characteristic radiation is detected in a small proportional counter.

In order to relate the rate of production of ^{37}Ar from the above reaction to the solar neutrino flux one must know the cross section for this reaction. Calculation of this cross section involves knowledge of many excited levels in ^{37}Ar as well as several beta-decay matrix elements within the mass-37 system. It was this need for experimental information that stimulated the research reported in this thesis.

The levels that are most important for the above calculation are the T = 3/2 levels in the T_z = 1/2 nuclei ^{37}Ar and ^{37}K, which are analogues to the ground states of the T_z = 3/2 nuclei ^{37}Cl and

^{37}Ca. Since the same matrix elements for neutrino capture by ^{37}Cl to form ^{37}Ar occur in the beta-decay of ^{37}Ca to ^{37}K, the latter decay has been studied by Poskanzer et al. (1966), Reeder et al. (1964) and Hardy and Verrall (1964). Part of the present work describes a search for the lowest T = 3/2 level in ^{37}K that was carried out simultaneously with the work of Poskanzer et al. (1966), who used the reaction

$$^{36}\mathrm{Ar}(^{3}\mathrm{He}, 2n)^{37}\mathrm{Ca}(\beta^{+})^{37}\mathrm{K}^{*}(p)^{36}\mathrm{Ar}$$

to study the beta decay of ^{37}Ca by observing the energies of the delayed protons to determine which levels in ^{37}K were populated. As is shown in table 3 most of the decay proceeds to the lowest T = 3/2 level in ^{37}K near 5.04 MeV excitation energy. However, since this level is able to emit protons to the first excited level as well as to the ground state of ^{36}Ar, it is important in the analysis of the proton energies to know the ratio of inelastic to elastic proton widths of the T = 3/2 level. It is shown in the present work that this ratio is about 1%.

Experimental information on the levels of ^{37}Ar has been reported by McNally (1964, 1966), Allen (1965), Castro (1964), Hardy and Verrall (1964), Holbrow et al. (1966), Kavanagh and Goosman (1964), Robertson et al. (1960), Rosner and Schneid (1965) and Cerny (1965).

Shell-model calculations of levels in the mass-37 system have been reported by Engelbertink and Brussaard (1966), Glaudemans et al. (1964, 1966), Lande (1965) and Pandya (1958).

It is hoped that future calculations might be more successful in the light of new information on ^{37}K levels presented in this work.

Several investigators have reported experimental results on ^{37}K previous to this work. McNally (1964) saw four levels in ^{37}K via the $^{40}Ca(p, \alpha)^{37}K$ reaction and has measured the ground-state mass excess. Poskanzer et al. (1966) and Cerny (1965) have contributed information on the position of the lowest T = 3/2 level during the course of this work. Kim and Barnard (1961) studied the elastic proton scattering and found only the 3311 keV level, which is shown to have $J^{\pi} = 3/2^-$ in the present work (contradicting the $1/2^-$ assignment of Kim and Barnard). The half-life of the ground state was measured by several investigators and is listed in Endt and Van der Leun (1962) as 1.23 ± .02 sec.; a later measurement by Kavanagh and Goosman (1964) gave 1.25 ± .04 sec. The $^{36}Ar(d, n)^{37}K$ reaction as studied by Yamamoto (1961) revealed the ground state and a possible doublet near 1.46 MeV excitation energy. The $^{36}Ar(p, \gamma)^{37}K$ was investigated by Brostrom et al. (1948) and by Arnell (1964), and the latter found a level at 2.73 ± .02 MeV and put an upper limit of 0.8 keV on the width of the resonance. Val'ter and Kopanets (1964) have studied the inelastic scattering of protons from ^{36}Ar at three resonances and have measured the angular distributions of the de-excitation gamma rays for these resonances. Skeppstedt et al. (1966) have covered the excitation energy region from 5.13 to 6.63 MeV using the reaction $^{36}Ar(p, p'\gamma)^{36}Ar$ with good resolution and have measured the angular distribution of the de-excitation gamma rays. Probable spin assignments were made for four of the twenty-one resonances they found. Definitive work on ^{37}K has been done by Storizhko and Popov

(1964), who studied the elastic scattering of protons on ^{36}Ar for $1.4 < E_p < 3.6$ MeV and found nine resonances. They have made conclusive spin assignments to five of these and have measured the ℓ value of the proton for the other four, and have measured the total width of three of these resonances.

Most of the above work dealt with highly excited levels and a great deal of the present effort was directed toward measuring properties of the low-lying levels, which might be amenable to theoretical interpretation.

II. THE REACTION $^{36}Ar(p, p'\gamma)$ AND THE YIELD OF DELAYED POSITRONS FROM $^{36}Ar(p, \gamma)^{37}K\ (\beta^+)\ ^{37}Ar$

1. Results with coarse resolution

To search for levels in ^{37}K the yield of delayed positrons from the reaction $^{36}Ar(p, \gamma)^{37}K\ (\beta^+)\ ^{37}Ar$ was investigated by bombarding 99% enriched ^{36}Ar gas retained in a small gas cell by a thin foil, as shown in figure 1. The beam entered from the left through two gold collimators and a foil (2.5 μm platinum in this case), through the target of gaseous ^{36}Ar at a pressure of 25 cm of Hg and was finally stopped in a backing of gold or platinum. The entire gas cell was contained in a well-type Pilot-B crystal to detect the positrons from the decay of ^{37}K, which has a half-life of 1.2 seconds. The output of the crystal during the first two seconds after the beam was turned off was routed into one scaler, and the output during the next two seconds into another scaler, after which the beam was turned on and the cycle repeated. The sum and difference of the scaler counts as a function of proton energy are shown in figure 2, which was taken with about 45 keV resolution, due to target thickness and energy straggle. The levels below and including the one at 3.31 MeV were reported previously by Kavanagh and Goosman (1964). The calibration of the excitation energies shown in this figure will be discussed later. Many of these peaks were later found to be doublets.

The prompt 1.97 MeV gamma rays from $^{36}Ar(p, p'\gamma)$ were detected with a 7.6 by 7.6 cm NaI(Tl) crystal as a function of proton energy and the result is shown in figure 3. The excitation energies

shown were derived from later calibrations of the peaks labeled 4.435 and 5.127 MeV.

Figure 4 shows the region from 5.5 to 7.5 MeV excitation taken by detecting prompt 1.97 MeV gamma rays from inelastic scattering and delayed positrons during the same runs. Since the peaks in the 1.97 MeV gamma-ray yield presumably come from compound inelastic scattering, the presence of a peak in both curves of figure 4 for a given proton energy is strong evidence for the existence of a level in ^{37}K. The relative yield of the 1.97 MeV gamma rays is corrected for dead time in figure 3 but not in figure 4.

2. Results with better resolution

Since the lowest T = 3/2 level should appear near 5.1 MeV excitation energy, the region between 4.9 and 5.6 MeV was studied again with better energy resolution than in the previous experiments by replacing the platinum foil with a 0.3 μm gold foil and by reducing the gas pressure to about 5 cm of Hg. The inelastic yield was again taken together with the delayed positron yield and the result is shown in figure 5. The resolution of 15 keV was due mostly to straggle in the foil. The relative heights of the 1.97 MeV gamma-ray yield are greatly distorted by large variations in dead time for the 0^{o} run, and this curve should be taken only as an indication of the resonance energies. The dead time for the gamma-ray yield during the 90^{o} run was always less than 21% because the detector was farther away from the target than during the 0^{o} run.

The peak in figure 2 at 4.42 MeV excitation was also investigated with better resolution by using thin gold entrance foils and is seen in figure 6 to be a doublet separated by 18 keV. The lower member of this doublet is very important to the discussion in part IX in connection with a lifetime measurement.

3. Calibration of the 5048 keV level

The excitation energy of the 5048 keV level was calibrated by using a 10 keV thick gold foil to retain a 7 ± 1.5 keV thick ^{36}Ar gas target in the apparatus shown in figure 1. The yield of delayed positrons as a function of proton energy resulted in the left-hand curve of figure 7. The argon was pumped out of the cell and a natural-silicon target 1 ± 1 keV thick was inserted into the chamber where the "evaporated gold beam catcher" of figure 1 was normally located. Then helium gas of thickness = 0.44 ± 0.2 keV was used in the chamber to cool the thin gold foil (about 0.14 μm thick). The yield of 1.78 MeV gamma rays from the reaction $^{28}Si(p, p'\gamma)$ at the well-known resonance at E_p = 3357 ± 2 keV (total width of 10 keV) (Vorona et al., 1959) was measured as a function of proton energy and the result is shown on the right side of figure 7. The position of the peak is independent of the natural width of the resonance. The observed widths of the peaks in figure 7 are the combined effects of gas pressure, straggle in the entrance foil and the natural widths of the resonances. The thickness of the gold entrance foil almost cancels out in the calibration because both resonances were measured with the beam going through the same foil. There is a 0.3 keV correction due to the change of energy loss in the foil at the two

resonance energies. This procedure established the proton energy of the level as 3280 ± 3 keV. The excitation energy of 5048 ± 3 keV results from the above measurement and the measurement of the ^{36}Ar + proton threshold at 1857.0 ± 1.4 keV (see part X).

4. Calibration of the remaining levels

The energy of the level at 5018 keV in figure 5 was calibrated by measuring the energy difference between it and the 5048 keV level in the reaction ^{36}Ar(p, p) with 2 keV resolution (see part V). The energy calibrations of all the levels shown in figure 5 result from their energy separations from the 5048 keV level. The calibrations of levels between 3311 and 5048 keV shown in figure 2 come from their energy separations in this figure from the 3311 keV level, which was calibrated by its gamma rays in a germanium detector (see part X), by the lower member of the doublet at 4420 keV, which was also calibrated by its gamma rays, and by the doublet at 5.02 and 5.05 MeV.

In later discussions reference will be made to the levels in ^{37}K as found by Storizhko and Popov (1964) in the elastic scattering of protons from ^{36}Ar. Below is a table showing their resonances and the corresponding ones of this work and that of Skeppstedt et al. (1966)

E_p (keV) Storizhko	E_p (keV) This work	E_p (keV) Skeppstedt	Difference (keV) Storizhko - This work
1509 ± 5	1494 ± 4		15 ± 6
2206 ± 5	2184 ± 15		22 ± 16
2727 ± 5	2740 ± 20 ?		-13 ± 21
2800 ± 5	2804 ± 13 ?		- 4 ± 14
3081 ± 5	3059 ± 13		22 ± 14
3269 ± 5	3249 ± 3		20 ± 6
3368 ± 5	not resolved		
3379 ± 5	3359 ± 4	3360 ± 20	20 ± 7
3511 ± 5	3496 ± 5	3490 ± 20	15 ± 7

Question marks indicate uncertain correspondences. The unquestioned correspondences appear to differ by about 18 keV. The correspondence between the 3359 keV resonance of this work and the 3360 keV resonance of Skeppstedt et al. (1966) is certain because of the strength and angular distribution of de-excitation gamma rays following inelastic scattering of protons from ^{36}Ar.

Close examination of figure 5 will reveal that the peaks labeled "5.127" are 5 keV lower in the (p, γ) yield than they are in the (p, p'γ) curve, suggesting that the peak seen in (p, γ) is some average of both the 3368 and 3379 keV resonances of Storizhko and Popov (1964), whereas in (p, p'γ) only their 3379 keV resonance contributes. The latter is confirmed by the results of Skeppstedt

et al. (1966), who had sufficiently good resolution in the (p, p'γ) reaction to resolve the two levels. The correspondence between the resonance of Storizhko and Popov (1964) at 3269 keV and the one of this work at 3249 keV is certain, because their shapes in elastic scattering are very similar. The same argument also definitely confirms the correspondence between their 1509 keV resonance and the one at 1494 keV from this work. The latter was calibrated by means of the Q-value for $^{36}Ar(p, \gamma)^{37}K$ and from a calibration of the excitation energy of this resonance by the gamma rays seen in a Ge(Li) counter (see part X). The 15 keV discrepancy is not understood.

III. GAMMA-RAY ANGULAR DISTRIBUTIONS FROM $^{36}Ar(p, p'\gamma)$

1. Introduction

Figure 5 shows the yield of 1.97 MeV gamma rays following the inelastic scattering of protons by ^{36}Ar over an energy region that will be shown to include the lowest T = 3/2 level. Information on the spins and parities of these levels is contained in the angular distributions of the 1.97 MeV gamma rays. Four resonances are studied in this work.

2. Summary of the theory

The theoretical gamma-ray angular distributions following the inelastic scattering of protons from spin-zero targets are easily calculated from the results derived in appendix A, or by the formulae of Biedenharn (1960). Consider a beam of unpolarized spin one-half particles bombarding a target of spinless nuclei, with the reaction proceeding through a single compound level with sharp spin and parity J^{π}. This compound level can break up into an inelastic particle and an excited state of the target nucleus. The example of $^{36}Ar(p, p'\gamma)$ is illustrated below. The first excited state of ^{36}Ar is at 1.97 MeV ($J^{\pi} = 2^+$, T = 0) (Erne, 1966).

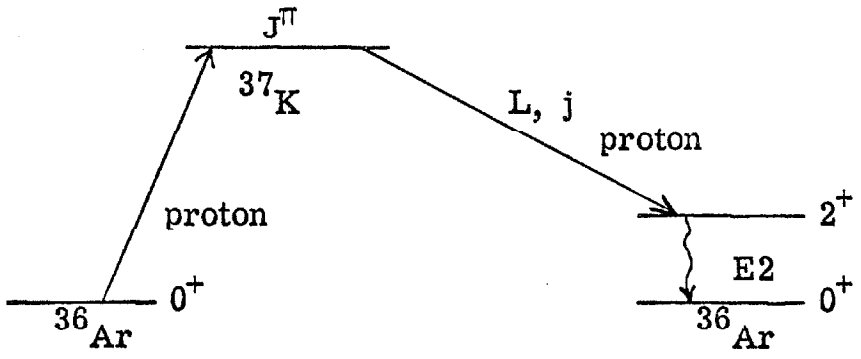

Here L is the orbital angular momentum of the outgoing proton and j is its total angular momentum. For a given J^{π} there are several possible values for j. The value of L is unique once J^{π} and j are specified. When the outgoing proton is not observed it is shown in appendix A that for each possible value of j the gamma-ray angular distribution can be uniquely determined, and that the most general angular distribution is obtained by adding incoherently the angular distributions obtained for each particular value of j. It is also shown in table 1 that the angular distribution depends only upon J and j, and not upon the parity π. Table 1 gives the values for the coefficients A_2 and A_4 which are defined by

$$W(\theta) = 1 + A_2 P_2 (\cos(\theta)) + A_4 P_4 (\cos(\theta))$$

where θ is the angle between the beam and the gamma ray. In fortunate cases where the experimental angular distribution allows only one value for J, one can sometimes also extract the value or values of j which contribute, thus obtaining information on the structure of the compound level relative to that of the 2^+ level of ^{36}Ar. An example of a case where there is a unique value of j determined experimentally is given below.

3. The spin and parity of the 5127 keV level

The gas-cell arrangement shown in figure 1 was used with one 7.6 by 7.6 cm NaI(Tl) crystal placed at 90° to the beam as a monitor and with another similar crystal 14.8 cm from the target free to rotate between zero and 90° to measure the gamma-ray

angular distribution. Pulses from the two crystals were routed into separate halves of a 400-channel pulse-height analyzer so that dead time corrections would be the same for both the monitor and the other crystal. A typical gamma-ray spectrum is shown in figure 8. The corrections to the angular distributions due to the finite size of the gas target (which was 9 mm long) were computed and taken into account, although in no case was the correction larger than 2%.

To avoid any ambiguity in the interpretation of the results to follow, the angular distribution that would result if a detector of negligible solid angle were used is hereafter called the true angular distribution, while that which is observed in a crystal of finite size is defined as the observed angular distribution. Part X discusses in detail the conversion from the observed to the true angular distributions.

The observed angular distribution for the 5127 keV level is shown in figure 9. A background run with helium in the gas cell has been subtracted (a correction of less than 2%). When corrections for the finite size of the detector are taken into account, the true angular distribution becomes

$$W(\theta) = 1 + (0.204 \pm 0.01)\ P_2 + (0.638 \pm 0.01)\ P_4 \ .$$

This angular distribution can be fitted to the theory only if $J = 5/2$ and only then if $j = 3/2$. Since Storizhko and Popov (1964) have shown by elastic scattering that $J^{\pi} = 5/2^-$ or $7/2^-$, the spin and parity is thus $5/2^-$. The unique value of j determined above suggests

that since the yield of inelastic scattering is very strong at this resonance, a large fraction of the 5127 keV level has a nuclear structure similar to a $P_{3/2}$ proton and a core consisting of the first excited state of ^{36}Ar.

4. Results for the 5258 keV level

The same experimental arrangement as that described above (except with the detector 9.0 cm from the target) was used to measure the gamma-ray angular distribution for the 5258 keV level, which is shown in figure 10. This is almost certainly the same resonance seen in elastic scattering by Storizhko and Popov (1964) at 3511 keV bombarding energy, because it has about the same width as they quote (17 keV) and because of the correspondence of levels shown on page 10. These authors have shown conclusively that $J^{\pi} = 3/2^-$ so that no attempt was made to determine the spin from the observed angular distribution. The solid line in figure 10 is the best fit to the data for $J^{\pi} = 3/2^-$ and corresponds to the true angular distribution

$$W(\theta) = 1 + 0.122\ P_2(\cos(\theta))$$

as it would appear with the geometry used for obtaining figure 10.

5. Results for the first two candidates for the lowest T = 3/2 level

As will be discussed in part V, the 5018 and 5048 keV levels are candidates for the lowest T = 3/2 level in ^{37}K, and this is why they have been investigated with several different reactions. Since the spin of the T = 3/2 level, which is the analogue to the ground state of ^{37}Ca, must be $3/2^+$, the author has tried to find some reaction which might show that one of the spins is not $3/2^+$, thus eliminating it as a candidate for the T = 3/2 level.

Figure 11 shows the observed distribution (seen by a 7.6 by 7.6 cm NaI(Tl) crystal 9.0 cm from the target) from the 5018 keV level, which Storizhko and Popov have shown to have $J^\pi = 3/2^+$ or $5/2^+$. (See also part V for a confirming measurement of J^π.) Background runs were taken above and below the resonance energy and the average has been subtracted. The data of figure 11 correspond to a true angular distribution of

$$W(\theta) = 1 + (0.44 \pm 0.03)\, P_2(\cos(\theta)) \ .$$

The solid line in figure 11 is what would result for a spin and parity of $3/2^+$ with a mixture of 88% j = 1/2 and 12% j = 3/2 (see table 1). The dashed line represents what would result for $J^\pi = 5/2^+$ with a mixture of 53% j = 1/2 and 47% j = 3/2. Although the fit for $5/2^+$ is the best fit for this spin and is not as good as that for $3/2^+$, one cannot exclude either spin from these data alone.

Since the yield of the 1.97 MeV gamma rays from the 5048 keV level is so weak (see figure 5), the yield of these gamma rays was measured accurately only at 0° and 90°. A crude measurement

at six angles showed that there was no hope of detecting a P_4 term in the distribution. The anisotropy was measured by using the average of above- and below-resonance background subtractions, and the result was that which would result if the true angular distribution were

$$W(\theta) = 1 + (0.57 \pm 0.15)\ P_2(\cos(\theta)) \quad .$$

It is shown in part V by elastic scattering that this level has $J^{\pi} = 3/2^+$ or $5/2^+$. Unfortunately, as one might expect (Murphy, 1900), the above anisotropy is not sufficient to exclude either of the two possibilities for the spin!

In brief, the inelastic scattering from the two levels which are candidates for the lowest T = 3/2 level has shown that the angular distributions of de-excitation gamma rays from both levels are consistent with $J^{\pi} = 3/2^+$ and $5/2^+$. Part V describes another attempt to distinguish $3/2^+$ from $5/2^+$ for these two levels via the elastic-scattering reaction.

IV. THE EXTRACTION OF $\frac{\omega\Gamma_p\Gamma_{p'}}{\Gamma}$ AND $\frac{\omega\Gamma_p\Gamma_\gamma}{\Gamma}$ FROM THE DATA

1. Theory

The yields of the two reactions shown in figure 5 contain information on the quantities ($\omega = J + 1/2$)

$$\frac{\omega\Gamma_p\Gamma_{p'}}{\Gamma} \qquad \text{and} \qquad \frac{\omega\Gamma_p\Gamma_\gamma}{\Gamma}$$

for each resonance. If a single isolated resonance of spin J is integrated by the target thickness the following relation holds:

$$(J + 1/2)\,\frac{\Gamma_1\Gamma_2}{\Gamma} = \frac{\text{Yield}}{\text{Proton}} \cdot \left(\frac{36}{37}\right)^2 \cdot \frac{\epsilon}{\pi^2\lambda^2}\, m_p\, E_{p_{Lab}}$$

where ϵ is the stopping cross section per atom for the target material. In order to get the correct yield from the observed yield as seen in figure 5, one must correct for the following:

1. the angular distribution of the gamma rays (in the inelastic scattering case)
2. dead time in the pulse-height analyzer ($\leq 21\%$)
3. incomplete integration of the resonance by the beam and target

The angular distribution of 1.97 MeV gamma rays from four of the levels in figure 5 have already been discussed. Angular

distributions for the 5318 and 5468 keV levels have been measured by Skeppstedt et al. (1966). The angular distributions from the levels at 4721 and 4833 keV shown in figure 4 have been measured by Val'ter and Kopanets (1964). In three other cases where there is no information, the angular distribution was assumed to be isotropic and an additional 40% error was included in the result.

The correction factor related to incomplete integration of the resonance is calculated from knowledge of the energy straggle of the beam in the entrance foil, the target thickness, and the natural width of the resonance. The straggle in the foil was measured from the observed width of a resonance known to be narrow (with a known target thickness). The square target thickness was unfolded from the observed width to give the straggle, which was assumed to be a gaussian. Figure 12 facilitates this unfolding process. The straggle for nearby resonance energies was obtained from the calibrated one by employing the formula (Evans, 1955) which shows the slight dependence of the straggle upon the beam energy:

$$\mathrm{FWHM} = 2.35 \sqrt{4\pi z^2 e^4 N Z d \left\{1 + \frac{kI}{m_e V^2} \ln\left(\frac{2m_e V^2}{I}\right)\right\}}$$

where

FWHM	is the full width at half maximum of the beam energy profile
d	is the thickness of the foil
z	is the charge of the projectile

Z	is the charge of the foil atoms
N	is the number of foil atoms per unit volume
I	is the mean ionization potential of the foil atoms
m_e	is the electron mass
V	is the velocity of the projectile
k	is a number which is about unity.

The only energy dependence is in the term in brackets, and for protons of a few MeV energy in gold foils this energy dependence of the straggle is small. It has been found by the author that this formula usually predicts a straggle which is about 25% too large for one- to three-MeV protons on gold, but the energy dependence of the formula is assumed to be sufficiently accurate to allow the calculation of the straggle for all the resonance energies, given its value for one beam energy.

The target thickness was determined from the gas pressure and the stopping power of the gas as determined by the graphs of Whaling (1958).

In many cases the natural width of the resonance was known or was known to be sufficiently narrow (Storizhko and Popov, 1964). In cases where this information was not available, the resonance was assumed to be narrow and the estimated error was increased accordingly.

Having thus determined the straggle, target thickness, and the natural width of the resonance, the observed yield was corrected by dividing it by the fraction of the resonance area that was being

integrated by the beam at the peak of the observed resonance. This fraction was obtained by folding a rectangle of width T into a gaussian of half-width S, and then folding the result into a single-level Breit-Wigner dispersion curve of width Γ, where both the gaussian and dispersion curve have been normalized to unit total area, and then evaluating the resulting curve at its peak. This factor is

$$\frac{1}{\pi^{3/2}} \int_{-\infty}^{\infty} e^{-x^2} \left\{ \tan^{-1}\left[\frac{T + 1.20 \times S}{\Gamma} \right] + \tan^{-1}\left[\frac{T - 1.20 \times S}{\Gamma} \right] \right\} dx .$$

In the special case where the natural width of the resonance is negligible compared with either of the two other widths, one can easily extract the fraction from figure 13.

2. Results

The level at 5127 keV in figure 5 was calibrated by an independent measurement which is described in full detail in appendix B and was found to have $\omega\Gamma_p\Gamma_{p'}/\Gamma = 354 \pm 53$ eV. This same quantity was then extracted for the levels shown in the 90° runs of figure 5 by comparing them with the calibrated 5127 keV level, correcting for angular distributions, dead time, and incomplete integration of the resonance. Figure 3 was then used to extract this quantity for the 4435, 4721 and 4833 keV levels, again normalizing to the 5127 keV level. These results are tabulated in table 2.

Using a procedure very similar to that given in appendix B, a calibration of $\omega\Gamma_p\Gamma_\gamma/\Gamma = 208 \pm 30$ meV was obtained for the 2750 keV level by analyzing the yield of gamma rays from that level. This value was then used to extract approximate numbers for this quantity for the other levels. Since the yield of the (p, γ) reaction was measured by the yield of delayed positrons, there was no correction for the angular distribution because it was isotropic. There was no dead time correction in this case, but the correction for incomplete integration of the resonance was necessary. Values of $\omega\Gamma_p\Gamma_\gamma/\Gamma$ were extracted from figures 2 and 6 for levels below 5.0 MeV and for the 5.21 MeV level, using the result for the 2750 keV level as a calibration. The result obtained for the 5.21 MeV level was then used for the extraction of this quantity for the levels above 5 MeV in figure 5. These results are shown in table 2.

V. THE ELASTIC SCATTERING OF PROTONS FROM ^{36}Ar

1. Introduction

Kim and Barnard (1961) and Storizhko and Popov (1964) have investigated the elastic scattering of protons at the 3311 keV level in ^{37}K and their excitation functions at three angles determined the ℓ value of the proton for this resonance to be unity, so that $J^{\pi} = 1/2^{-}$ or $3/2^{-}$. In order to resolve the remaining ambiguity, one must have a resolution which is known or is known to be negligible compared to the natural width of the resonance. Storizhko and Popov (1964) have investigated the bombarding energy region from 1.3 to 3.6 MeV and by measuring the excitation functions at three angles have determined the proton ℓ values of several resonances. They used targets of 99% enriched ^{36}Ar embedded in carbon foils, and determined uniquely the spin and parity of resonances that were observed to be wider than about 7 keV. They did not attempt to resolve the remaining ambiguity of spin for the narrow levels whose proton ℓ values they had measured.

The purpose for the present investigation of the elastic scattering was to attempt to resolve this ambiguity in a few cases by using thin targets with known resolution to determine the spin from measured magnitudes of scattering anomalies. The author has investigated this reaction at other energies to search for anomalies not previously seen. Of particular interest were the two levels believed to be candidates for the lowest T = 3/2 level.

2. Summary of the theory

The elastic scattering cross section of spin one-half particles upon a spin-zero target in an energy region where there is one isolated resonance of sharp spin and parity is given by Feshbach (1960) and Tombrello and Parker (1963)

$$\frac{d\sigma}{d\Omega}_{cm} = \lambda^2 [\, A + |B + C + D|^2]$$

where

$$A = \left\{ \frac{\Gamma_p}{\Gamma} \right\}^2 \cdot \frac{P_{\ell_o}^{(1)^2}(\cos(\theta))}{4 \left\{ \frac{E - E_r}{\Gamma} \right\}^2 + 1}$$

$$B = \frac{\eta\, e^{-i\eta \ln(\sin^2(\theta/2))}}{2 \sin^2(\theta/2)}$$

$$C = \frac{(J + 1/2)\, e^{2i(\alpha_{\ell_o} + \varphi_{\ell_o})} \left\{ \frac{\Gamma_p}{\Gamma} \right\} P_{\ell_o}(\cos(\theta))}{2 \left\{ \frac{E - E_r}{\Gamma} \right\} + i}$$

$$D = \sum_{\ell=0}^{\infty} (2\ell + 1)\, \sin(\varphi_\ell)\, e^{i(\varphi_\ell + 2\alpha_\ell)}\, P_\ell(\cos(\theta))$$

where

$$\lambda^2 = \left[\frac{M + m}{M} \right]^2 \frac{\hbar^2}{2 m E}$$

$$\alpha_\ell = \sum_{j=1}^{\ell} \tan^{-1}(\eta/j)$$

$$\eta = \frac{z Z e^2}{\hbar V}$$

φ_ℓ are non-resonant non-Rutherford phase shifts

V is the relative velocity

m is the mass of the projectile

M is the mass of the target

J is the spin of the compound level

ℓ_o is the resonant orbital angular momentum of the projectile

P_ℓ is the Legendre polynomial

$P_\ell^{(1)}$ is an associated Legendre polynomial

θ is the center-of-mass angle

z is the charge of the projectile

Z is the charge of the target

E is the lab energy of the projectile

E_r is the lab resonance energy

Γ is the total lab width of the level

Γ_p is the elastic lab width of the level.

The φ_ℓ are assumed to be real and are given approximately in the limit of low energy by their "hard-sphere values"

$$\varphi_\ell \doteq - \tan^{-1}(F_\ell/G_\ell)|_{ka}$$

where F_ℓ and G_ℓ are the regular and irregular Coulomb functions respectively, $k = 1/\lambda$, and a is the value of the nuclear radius, which was taken in this work to be $1.3 \cdot (37)^{1/3}$ fm.

It is noticed that the shape of the anomaly depends upon the ratio Γ_p/Γ because some terms depend linearly upon this ratio while others depend upon its square. When the bombarding energy is high on a light nucleus so that the Rutherford amplitude is small and the non-resonant scattering amplitudes φ_ℓ are not small, then the shape of the anomaly will depend upon the signs and magnitudes of the phase shifts φ_ℓ as well. Unless these are known, the analysis is more difficult. In the present case of a few MeV protons on ^{36}Ar, the Rutherford amplitude is large and the φ_ℓ as estimated by their hard-sphere values are quite small, so that the shape of the various anomalies is not sensitive to the φ_ℓ.

Regardless of the magnitudes of the φ_ℓ, one can make the following remarks about the scattering anomalies. With perfect experimental resolution the cross section at resonance is independent of the total width if $\Gamma = \Gamma_p$. A very useful fact for selecting possible ℓ_o values from observed anomaly shapes at various angles is that if θ is the zero of some Legendre polynomial, then the coefficient C on page 24 is zero and all the resonant interference terms vanish. This means that if the excitation function is taken at the zero of some Legendre polynomial P_ℓ and any part of the observed anomaly dips downward, then that value of ℓ is not the resonant angular momentum ℓ_o.

In the special case where the φ_ℓ can be neglected, the formula on page 24 reduces to

$$\frac{d\sigma}{d\Omega}_{cm} = \frac{\eta^2 \lambda^2}{4 \sin^4(\theta/2)}$$

$$+ \frac{\lambda^2}{4\left\{\frac{E - E_r}{\Gamma}\right\}^2 + 1}\left[\left\{\frac{\Gamma_p}{\Gamma}\right\}^2 \left\{P_\ell^{(1)2}(\cos(\theta)) + (J + 1/2)^2 P_\ell^2(\cos(\theta))\right\}\right.$$

$$\left. + \frac{2J+1}{\sin^2(\theta/2)} \eta \cdot \frac{\Gamma_p}{\Gamma} \cdot P_\ell(\cos(\theta))\left[\left\{\frac{E - E_r}{\Gamma}\right\}\cos(\beta_\ell) + \frac{\sin(\beta_\ell)}{2}\right]\right]$$

where $\beta_\ell = 2\alpha_\ell + \eta \ln(\sin^2(\theta/2))$

and where the resonant value of the orbital angular momentum is now denoted as ℓ.

One notes that as the ratio Γ_p/Γ is decreased from unity the term symmetric in energy about the resonance energy is reduced much more than the other term (which is proportional to P_ℓ), so that the shape of the anomaly will approach that of the last term, provided $P_\ell \neq 0$.

Below 1.9 MeV proton energy the inelastic channel is closed and only the elastic-proton and gamma-ray channels are open. In this case, assuming that $\Gamma_\gamma << \Gamma$, the shape of the anomaly is unique for a given value of E_r, θ, J, and π. When folded into a symmetric energy resolution of unknown width the shape of the observed anomaly is unique for a given value of E_r, θ, and ℓ, but the value of J cannot be extracted. To extract a J value the resolution must either be negligible compared with the natural width of the level, or it must be known within a fractional accuracy that is smaller than

$$\frac{2J_u + 1 - (2J_l + 1)}{2J_u + 1} = \frac{1}{J_u + 1/2}$$

where $J_u = \ell + 1/2$ and $J_l = \ell - 1/2$. For example, to distinguish $J^\pi = 3/2^+$ from $5/2^+$ ($\ell = 2$), the resolution must either be negligible or must be known to a fractional error that is small compared to 33%. When channels other than the elastic channel contribute significantly, the analysis is more difficult. Figures 14-16 show the anomaly shapes for 1.26 MeV protons on ^{36}Ar and illustrate the facts stated above.

3. Method and target preparation

To avoid the loss in resolution due to energy straggling of the proton beam in the entrance foils of a gas target system, "solid targets" of ^{36}Ar were made by bombarding highly polished beryllium disks (4 mm in diameter) with a beam of about 50 microamperes of 5 keV argon ions for 120 seconds. Longer exposure times yielded no more embedded argon than the 120 sec runs, while higher argon energies resulted in broader resolution and only slightly more argon. Bombarding energies of one and two keV were also tried, but very little argon remained in the beryllium. A blank beryllium target was made by bombardment with hydrogen so that corrections could be measured later for contaminants in the beryllium or any that may have been deposited during the production of the targets. For incident protons of 1.25 MeV energy, the best target made had a thickness less than 1.6 keV and a typical target would deteriorate from 2.1 to 2.5 keV resolution after 1500 microcoulombs of beam at a rate of 0.66 microamperes.

The beam was limited to 0.7 microamperes and collimators fixed the size of the beam spot on the target to 1 mm^2. The outgoing protons were analyzed by a 61-cm-radius magnetic spectrometer with a silicon surface-barrier detector at the focal plane. The detector was biased so that it would completely stop the protons, and a 0.5 μm nickel foil placed in front of the counter was used to separate the protons from alpha particles from the reaction $^{9}Be(p, \alpha)^{6}Li$. Deuterons from $^{9}Be(p, d)^{8}Be$ were also present but were well separated from the protons.

In a typical run the width of the outgoing proton group was 2 keV and the energy acceptance of the slit in front of the detector at the focal plane of the magnet was about 14 keV so that the counter detected all the protons in the group even if the field setting on the spectrometer was in error by a few keV. The field setting was checked frequently by taking several runs at a constant bombarding energy with varying magnetic fields in the spectrometer.

4. The spin of the 3311 keV level

Figure 17 shows the 1494 keV resonance which previously had been shown to have $\ell = 1$ by Kim and Barnard (1961) and Storizhko and Popov (1964). The curve on the left of figure 17 shows the spectrum of outgoing protons for a fixed bombarding energy near the resonance energy of the curve on the right. The slit configuration of the spectrometer had a resolution of about 1.86 keV and the observed group had a width of 2.36 keV. Unfolding gives the combined resolution of the beam and target of about 1.5 keV. The background under the left curve in figure 17 is due to a 0.1% iron contaminant in the beryllium. This number was supplied with the impurity analysis of the beryllium (Brush Beryllium Co, 1965) but was checked by calculating it from the observed yield of the background and the two agreed within 20%. This background had to be measured so that it could be subtracted from the observed anomalies. Method one was to use the measured background from the left curve in figure 17. The second method was to re-run the resonance on the beryllium blank which had been bombarded only with hydrogen. The background obtained in this way was very flat in energy and agreed with that

calculated by method one and represented a correction of about 25% to the original data for the 1494 keV resonance. The background for each experimental anomaly presented in this work was measured by both methods, and they yielded essentially the same correction.

Since the ℓ value of this resonance was already known, the anomaly was measured only at 150^{o} in order to try to distinguish between $J^{\pi} = 1/2^{-}$ and $3/2^{-}$. It can be seen from figure 15 that the expected anomaly for $J^{\pi} = 3/2^{-}$ is more pronounced than that for $1/2^{-}$. The data on the right-hand curve of figure 17 are sufficient to determine the spin and width of the level and also the experimental resolution. It is seen that even with perfect resolution, the anomaly could not be as large for a spin of $1/2^{-}$ as that which is observed. Any finite resolution folded into the dashed curve of figure 17 would further reduce the magnitude of the expected anomaly. The inelastic channel is not open and the formula on page 27 with $\Gamma = \Gamma_{p}$ fits the data only for a width of 2.2 ± 0.3 keV, a spin of $3/2^{-}$, and an experimental resolution (target and beam combined) of 1.6 keV. This extracted value of the resolution is close to the measured value of 1.5 keV obtained by unfolding the two curves on the left-hand side of figure 17. The spin assignment is confirmed also by results to be discussed in part X where it is shown that this level emits an anisotropic gamma ray, which eliminates a spin of $1/2^{-}$.

5. Results for the two candidates for the lowest T = 3/2 level

As will be shown on page 35 , the 5018 and 5048 keV levels are candidates for the lowest T = 3/2 level. Figure 18 shows these two resonances in elastic scattering. The 3249 keV resonance has been shown by Storizhko and Popov (1964) to have $J^{\pi} = 3/2^{+}$ or $5/2^{+}$,

while the 3280 keV resonance had not been seen previously. In both cases the inelastic channel is open, so that the theoretical anomalies depend upon the ratio Γ_p/Γ. Information on the inelastic widths of these two levels has been presented in part IV and is in table 2.

Resonance	$\frac{\omega\Gamma_p\Gamma_{p'}}{\Gamma_p+\Gamma_{p'}}$
3249 keV	3.1 ± 0.6 eV
3280 keV	0.84 ± 0.28 eV.

Using the hard-sphere phase shifts and the general formula given on page 24 and using only values of Γ_p and $\Gamma_{p'}$ that are consistent with the above restriction, an acceptable fit for the 3249 keV resonance can be made only for

$J^\pi = 3/2^+$	or	$J^\pi = 5/2^+$
$\Gamma_p = \Gamma = 600 \pm 150$ eV		$\Gamma_p = \Gamma = 400 \pm 100$ eV
Resolution = 2.1 keV		Resolution = 2.3 keV.

The theoretical fit for $J^\pi = 3/2^+$ is shown as the solid line of figure 18. The sensitivity of this fit to the radius used in calculating the hard-sphere phase shifts is not large. The experimental resolution was not known sufficiently accurately to exclude either spin possibility.

Using the same procedure, an acceptable fit to the 3280 keV resonance consistent with the above value of $\omega\Gamma_p\Gamma_{p'}/\Gamma$ can be obtained only for

$$J^{\pi} = 3/2^{+} \qquad \text{or} \qquad J^{\pi} = 5/2^{+}$$

$$\Gamma_p = \Gamma = 40 \pm 20 \text{ eV} \qquad \Gamma_p = \Gamma = 27 \pm 13 \text{ eV}.$$

Here also the resolution was not known sufficiently accurately to exclude either possibility.

Thus once again the author has not been able to distinguish $3/2^{+}$ from $5/2^{+}$; but it has been shown that the elastic width for each case is essentially equal to the total width.

6. Results for the 3083 keV level

A previous publication by Kavanagh and Goosman (1964) has shown evidence for a resonance in ^{37}K near $E_p = 1266$ keV by the yield of delayed positrons following proton bombardment of ^{36}Ar. This level has been seen in the gamma ray work, as will be shown in part X. This resonance was sought by the elastic scattering and the results are shown in figure 19. The resolution before "Run A" started was determined to be 2.1 keV and deteriorated to 2.5 keV after the end of "Run B", as shown in figure 20. The average resolution was taken to be 2.3 keV. By a similar procedure the average resolution for "Run C" and "Run D" was 3.5 keV. Since the previous calibration of the resonance energy shows that the resonance is somewhere in the energy region covered by figure 19, one may put a limit on the width of the resonance from the statistical errors and average fluctuations evident in this figure. The inelastic channel is closed, so that for a given spin and parity, a unique limit on the width may be calculated. It will be shown in part X that there

is evidence that the spin is $5/2^-$, and if one takes 430 counts as the upper limit on the magnitude of any anomaly that may exist in figure 19, then the width of this level is less than 16 eV.

To obtain better resolution a gas target of ^{36}Ar with no entrance foil was used. The beam entered through a stainless-steel tube about 2 cm long and 0.05 cm in diameter, and the gas leaked out of the same hole. A beam catcher of beryllium was placed inside the gas chamber in order to monitor the beam by observing the gamma-ray yield from protons on beryllium. The cell was connected to a small reservoir of ^{36}Ar so that the pressure in the cell decreased slowly during the runs. The resolution of the beam and of the target was checked by investigating the 1.102 MeV resonance in $^{40}Ar(p,\gamma)^{41}K$ and was found to be 650 eV, as shown in figure 21.

Using a silicon surface-barrier detector mounted at 90° to the beam within the gas chamber to detect the protons, the result with ^{36}Ar in the cell is shown in figure 22. Again no anomaly was seen. This curve puts an upper limit on the width of the resonance at 12 eV if $\ell = 2$, but does not reduce the 16 eV limit set by figure 19 for $J^\pi = 5/2^-$.

7. Summary of evidence for the identification of the lowest T = 3/2 level

The position of the first T = 3/2 level in ^{37}K can be calculated to be at about 5.1 MeV excitation energy, and it should have a spin of $3/2^+$. The excitation energy of this level has been shown by the decay of ^{37}Ca (see table 3) to be at 5.021 ± 0.020 MeV (Poskanzer et al., 1966). It is seen in figure 5 that there are two

levels within this energy region at 5018 and 5048 keV, whose energy calibrations have been discussed in part II. It has been shown above that the elastic scattering determines the spin and parity of both these levels to be $3/2^+$ or $5/2^+$. Both the elastic scattering and the angular distribution of gamma rays following inelastic scattering through these levels have failed to distinguish between $J^\pi = 3/2^+$ and $5/2^+$.

Part IV has described the extraction of information on the widths of these levels and the results are summarized in table 2. Since the proton and ^{36}Ar have isospins of 1/2 and zero, respectively, the population of a T = 3/2 level by proton bombardment of ^{36}Ar is isospin forbidden. The breakup of this level into an inelastic proton and the 2^+ level of ^{36}Ar at 1.97 MeV is also isospin forbidden. Therefore, the proton widths of the T = 3/2 level should be very small compared to neighboring levels with T = 1/2. The gamma-ray width of the T = 3/2 level should not be affected by isospin. Thus the T = 3/2 level should not have an abnormally low yield in the (p, γ) reaction whose yield is proportional to

$$\frac{\omega\Gamma_p\Gamma_\gamma}{\Gamma} \doteq \omega\Gamma_\gamma ,$$

but it should have a rather weak yield for the elastic and inelastic scattering reactions.

Examination of figure 5 shows that both the 5018 and 5048 keV levels are moderately strong in (p, γ) relative to their neighbors and quite weak in (p, p'γ). This characteristic is particularly strong for the 5048 keV level. The elastic scattering yield shown in figure 18 reveals that the 5018 keV level has a width of about 600 eV, while

the width of the 5048 keV level is a mere 40 eV or less. For these reasons, the 5048 keV level is favored as the T = 3/2 level, but it is possible that there is some T = 3/2 admixture in eachof the two levels.

VI. THE REACTION $^{40}Ca(p,\alpha)^{37}K$

In order to search for bound as well as unbound levels in ^{37}K, alpha-particles from the reaction $^{40}Ca(p,\alpha)^{37}K$ were analyzed in a magnetic spectrometer with a silicon-surface barrier detector located at the focal plane of the magnet. The counter was biased to just stop alpha particles while not stopping protons of the same energy. Natural calcium (97% ^{40}Ca) was evaporated onto 0.3 μm gold foil backings and transferred under vacuum to the scattering chamber. However, there remained noticeable amounts of ^{16}O and ^{24}Mg on the targets. The yield of alpha-particles at a constant proton bombarding energy at three lab angles is shown in figure 23. The peaks corresponding to levels at 1.368 and 1.380, 2.169 and 2.750 MeV were calibrated by gamma rays as will be discussed in part X. The calibration of the 2.278 MeV level comes from its separation from the 2.169 MeV level. The peak labeled "X" is unknown but is not from a mass-40 target.

Figure 24 shows the separation of the ground-state alpha group and the group at "1.373" MeV excitation energy which is shown in part X to be a doublet at 1368 and 1380 keV. Both the width of this group in figure 24 and its apparent excitation energy suggest that both levels are populated to some extent by this reaction.

Figure 25 shows evidence that the peak at 2.278 MeV is a level in ^{37}K rather than some impurity. The spectrum on the right-hand side of figure 25 shows the separation of the 2.169 and 2.278 MeV levels, which is 109 ± 8 keV in excitation energy. The arrows labeled "41", "40" and "39" indicate where the peak labeled 2.278 on the right-hand side would appear on the left-hand side if the reaction

were originating from a target of mass 41, 40 or 39 respectively. The positions of these arrows of course assume that the 2.169 MeV level is really from ^{37}K, but this will be shown to be true in part VIII, where it has the correct shift at 25 angles as seen in the $^{36}Ar(^{3}He, d)^{37}K$ reaction.

VII. THE REACTION $^{36}Ar(d, n)^{37}K$

1. Introduction

The reaction $^{36}Ar(d, n)^{37}K$ was originally undertaken in order to search for the analogue in ^{37}K to the 1.61 MeV level in the mirror nucleus ^{37}Ar. The $^{40}Ca(p, \alpha)^{37}K$ reaction discussed in part VI revealed a level near 1.37 MeV excitation energy, which was presumed to be the analogue to the 1.41 MeV level in ^{37}Ar. Since the 1.61 MeV level appeared strongly in the stripping reaction $^{36}Ar(d, p)^{37}Ar$ (Rosner, 1965), it was expected to appear strongly in the analogue reaction $^{36}Ar(d, n)^{37}K$.

The gas cell shown in figure 1 was filled with ^{36}Ar gas to a pressure of 43 cm of Hg which was retained by a 2.5 μm platinum foil. The outgoing neutrons were detected in a chilled-silicon surface-barrier detector using a technique recently described by Miller and Kavanagh (1966). The neutrons induce nuclear reactions in the silicon detector and the reaction products produce, for a monoenergetic neutron group, a pulse-height spectrum consisting of many peaks whose positions are a measure of the neutron energy.

2. Analysis of the pulse-height spectra

Figure 26 shows the pulse-height spectrum with ^{36}Ar in the gas cell (after subtraction of a background run with 1 cm of Hg gas pressure of ^{36}Ar) along with the response of the detector to a 8.17 ± 0.03 MeV neutron group from the reaction $^{14}N(d, n_0)^{15}O$. Since there are no excited states below 5 MeV in ^{15}O, this reaction provided a convenient way to measure the response of the detector

to neutrons of variable energies, using the same gas cell as with the ^{36}Ar runs. The peaks in the dashed curve in figure 26 labeled α_m arise from the reaction $^{28}Si(n, \alpha_m)$ and those labeled p_m from $^{28}Si(n, p_m)$. The reactions $^{29}Si(n, \alpha_m)$ with m = 0 and 1 result in peaks whose pulse height is higher than the peak from $^{28}Si(n, \alpha_o)$, so that it is not always a trivial matter to find the $^{28}Si(n, \alpha_o)$ peak to the ground state of the nucleus being studied, unless the Q-value of the reaction is known. In the present experiment the Q-value was known and the identification of the peak labeled "^{37}K Ground State" was straightforward. The higher peak will be explained below. The solid curve in figure 26 represents the response of the counter to all the neutron groups leading to levels in ^{37}K. The dashed curve, which was normalized vertically to fit the corresponding peak in the solid curve, was then subtracted from the latter to remove the effect of the ground-state neutron group. It is important that the neutron energy of the calibration spectrum be within at least 20 keV of the neutron energy leading to the level of ^{37}K in question, because the relative magnitudes of the various peaks due to a monoenergetic neutron group vary rapidly with neutron energy (Miller and Kavanagh, 1966) and (Mainsbridge et al., 1963).

Figure 27 shows the result of the subtraction of the response function due to the ground-state neutrons. The level at 1.37 MeV and one at 2.17 MeV can be unfolded from this curve and their neutron groups each produce peaks which are labeled by single and double primes, respectively. The two large peaks labeled p'_{01} and p''_{01} arise from the neutron groups to the 1.37 and 2.17 MeV levels respectively and the essentially flat region between them shows that there are no

levels between 1.37 and 2.16 MeV excitation that are populated by this reaction. In particular, there is no strong level at 1.6 MeV as there is in the mirror reaction $^{36}Ar(d, p)^{37}Ar$. As will be shown in part X, this is because there are <u>two</u> levels in ^{37}K near 1.37 MeV which are not resolved by the 130 keV resolution of this experiment.

A neutron group of the appropriate energy was used to subtract the effect of the neutrons leading to the 1.37 MeV levels in ^{37}K, and the result of this subtraction is shown in figure 28. The peaks labeled "X" and "Y" are due to improperly subtracted peaks originally present in figure 27. The $^{29}Si(n, \alpha_0'')$ peak in this figure is the one that appears at channel number 148 in figure 26.

This same process was repeated at lab angles of 0° and 30°, but no other levels than those shown above appeared. Angular distributions of these three peaks were not attempted because of the rapidly changing detector efficiency with angle which arises from the rapidly changing efficiency with neutron energy. Stripping patterns to these three levels were more easily measured using the $^{36}Ar(^{3}He, d)^{37}K$ reaction, which is described in part VIII.

VIII. THE REACTION $^{36}Ar(^{3}He, d)^{37}K$

1. Method of taking the deuteron angular distributions

The $^{36}Ar(^{3}He, d)^{37}K$ reaction was undertaken in order to measure the stripping patterns of any groups that might appear to obtain information on the proton ℓ values of levels in ^{37}K. Figure 29 shows the gas cell which was used to contain the ^{36}Ar and the collimator which helped to define the effective target volume. The gas cell contained two entrance foils of 0.5 μm nickel and two exit foils of 1.0 μm nickel. The beam diameter was about 1.1 mm and the outgoing deuterons were required to pass through a series of three rectangular apertures (one of which is not shown in figure 29) before they could enter a magnetic spectrometer and be focused onto an array of 16 silicon surface-barrier detectors at the focal plane of the magnet. By using both of the entrance foils, lab angles from zero to 122° were available for the outgoing deuterons. The three rectangular apertures defined the volume of the target, which changes rapidly with lab angle when the latter is near 0°. The correction for the effective length of the target was computed on an IBM 7094 computer at each of the 25 angles used in the angular distributions. The exit aperture was aligned by measuring the yield of elastically scattered beam as a function of the angular position of the aperture. The cell was fixed rigidly with respect to the target room, but the exit aperture was fixed with respect to the magnet so that it needed to be aligned only once. With a gas pressure of 25 cm of Hg the resolution of this experiment at 40° was about 70 keV and was due mostly to the foils.

There were small amounts of oxygen, nitrogen and carbon in gaseous form in the cell as is evident from a typical profile of the deuterons for a constant bombarding energy, as shown in figure 30. The deuteron groups to the ground state, the 1380 and 2169 keV levels appear strongly, as they do in the $^{36}Ar(d, n)^{37}K$ reaction. The calibration of the energies shown in figure 30 comes from the gamma-ray experiments of part X, where it is shown that there are levels at 1368 and 1380 keV, which are the analogues to the 1st and 2nd excited levels of ^{37}Ar. Rosner and Schneid (1965) have shown that $d\sigma/d\Omega_{max}$ for the $^{36}Ar(d, p)^{37}Ar$ reaction is over eight times as large for the 2nd excited state of ^{37}Ar as it is for the 1st excited state, so that one would expect that the $^{36}Ar(^{3}He, d)^{37}K$ reaction would populate mainly the analogue 1380 keV level in preference to the 1368 keV level in ^{37}K. The energy separation between the ground and "1.38" MeV peaks of figure 30 is 1380 ± 10 keV, and presumably little contribution to this peak comes from the 1368 keV level. A spectrum taken at a higher bombarding energy is shown in figure 31. The impurity peaks due to oxygen were followed at each of the 25 angles so that their effect could be subtracted out for those cases where their energies coincided with those of the levels in ^{37}K.

Because of the possibility of fluctuations in the yield due to non-statistical processes (i.e. the wandering of the centroid of the beam) each of the groups to the ground, 1380 and 2169 keV levels was measured twice at each angle. The average of the two runs was used with an error equal to the difference between the two runs (folded into the statistical counting error). Corrections for the effective lab angle seen by the magnet due to the finite extent of the acceptance slits were

computed with a program written by Moss (1965) but were found to be small.

To measure the relative efficiencies of the 16 solid-state counters at the focal plane of the spectrometer, a 0.4 mm tantalum target was placed into an 8 MeV deuteron beam and the elastically scattered beam at 140^{o} was detected in the 16 counter array. The thick target made a relative flat and smooth spectrum of deuterons which was first scanned with counter 8. Then all 16 counters were connected and the spectrum remeasured at one magnetic field setting. These measurements were made with the same exit collimator and same magnet slit settings as were the angular distributions. The details and results are given in appendix C. The correction factors were measured to about 3% and this error was folded into the other errors in the angular distribution measurements.

2. Results and DWBA analysis for the ground state

Figure 32 shows the experimental angular distribution of the deuteron group leading to the ground state of ^{37}K. The solid line is an optical-model fit with $\ell_p = 2$ to these data using the DWBA computer code of Bassel et al. (1962). The dashed curves represent theoretical curves for the ℓ values one higher and one lower than that for the solid curve. Although the conclusions drawn from the calculations are not sensitive to parameters used in the DWBA theory other than the ℓ value, they are given for completeness. The optical-model potentials used to fit the ground-state pattern were

Entrance channel	Exit channel
V = 76 MeV	V' = 60 MeV
W = 15 MeV	W' = 16 MeV
r_o = 1.3 fermi	r'_o = 1.3 fermi
a = 0.75 fermi	a' = 0.75 fermi

where the symbols are defined by

$$\text{Potential Energy} = \frac{V + iW}{1 + \exp\left[\frac{r - r_o A^{1/3}}{a}\right]}$$

where A in this case was 37. The quantity a is called the diffuseness of the potential. The values above are very close to those given by Hodgson (1963) for these energies and this mass region. It is stressed that the determination of ℓ_p from comparison of theory with the data is quite unique, despite the many parameters in the theory, because of the insensitivity of the position of the first theoretical peak to all the parameters except ℓ. Varying the potentials used by a factor of two only changes the position of the first peak by two or three degrees, while the peak positions for different ℓ values are separated by at least 10 degrees. There is also confirming evidence for the $\ell = 2$ assignment to the ground state given in part X. It is noticed in figure 31 that the experimental position of the secondary hump near 60^o appears there also in the theoretical $\ell = 2$ curve. The spin of the ground state of ^{37}K is thus taken to be $3/2^+$ or $5/2^+$, as the theory used has no J dependence for a given ℓ.

3. Analysis of the 1380 keV level

The experimental stripping pattern to the 1380 keV level is shown in figure 33. In fitting this curve, the entrance-channel parameters were fixed equal to those used in fitting the ground state (because the bombarding energies were the same for the two cases) and the other parameters were varied. However, the position of the first peak was again quite insensitive to the values of the exit-channel parameters used, which were

Exit channel

$V' = 60$ MeV

$W' = 16$ MeV

$r'_o = 1.3$ fermi

$a' = 0.5$ fermi .

The only difference between these parameters and those on page 45 is the change in a'. The 1380 keV level is fitted only for $\ell = 3$, which means that $J^{\pi} = 5/2^-$ or $7/2^-$.

4. Results for the 2169 keV level

Figure 34 shows the angular distribution of deuterons leading to the 2169 keV level. Fitting this curve involves an extrapolation in the binding energy of the level, because the computer code does not accept unbound levels, and the 2169 keV level is unbound by 312 keV. The level is "almost" bound, however, because if it is $\ell = 1$, the

Wigner limit on its width is about 1 eV. Fortunately the theoretical results are not sensitive to the binding energy of the level, as shown in figure 34. The parameters used in this fit were the same as those for the ground and 1380 keV levels except that a' was equal to 0.6 fermi. Since the three curves of figure 34 are very similar and since the level must be very narrow, it is hoped that the theory is sufficiently valid to determine the correct ℓ value. Figure 35 shows fits for three ℓ values, showing that only the fit for $\ell = 1$ is acceptable, so that $J^{\pi} = 1/2^{-}$ or $3/2^{-}$ if the theory is valid.

The effect of changing a' from 0.6 to 0.5 fermi may be seen by comparing figures 35 and 36: the height of the secondary hump is sensitive to a', but the determination of the ℓ value is not changed.

IX. THE LIFETIME AND SPIN OF THE 1380 keV LEVEL VIA THE $^{36}Ar(p, \gamma\gamma)^{37}K$ REACTION

1. Introduction

Of all the reactions discussed so far, none has provided as much information as the reaction $^{36}Ar(p, \gamma)^{37}K$. This is because of the known behavior of gamma radiation and the favorable Q-value for the reaction of 1857.0 ± 1.4 keV (see part X for this result).

Because of the large cross section for the reaction $^{19}F(p, \alpha\gamma)^{16}O$, it was necessary to use very clean entrance foils and beam catchers in the gamma-ray work. For a proton bombarding energy of 2.6 MeV, an impurity content of 0.1 parts per million by weight of ^{19}F in the gold beam stopper would produce as many gamma rays as does the strongest known (p, γ) resonance in ^{37}K. The most satisfactory entrance foils to the gas cell shown in figure 1 were made by evaporation of a layer of BaI_2 about 2 micrograms/cm^2 onto a glass micro-slide followed by a layer of gold evaporated upon the BaI_2 film to the desired thickness. The gold was then floated off the glass in distilled water, and the foils epoxied onto the stainless steel holder shown in figure 1. See appendix D for full details. Unfortunately, almost all of the foils revealed small pinholes, and in experiments where accurate charge integration was needed (as in the angular distribution measurements), only the hole-free foils could be used.

The most satisfactory beam catcher for the gas cell was made by cleaning a disk of commercial gold sheet about 0.1 mm thick and evaporating a layer of gold of equal thickness upon it so that the beam stopped in the evaporated layer. As shown in figure 1, gold

collimators were employed and tantalum liners caught most of the scattered beam.

Heavy lead shields about 10 cm thick were used to shield the NaI(Tl) crystals from the gamma radiation due to ^{40}K and radio-thorium in the concrete walls of the target room, which would produce in an unshielded crystal one hundred times more gamma-ray counts than some of the gamma-ray resonances in ^{37}K that are reported in part X, using beam currents of about one microampere. In the control room of the tandem facility an unshielded 7.6 by 7.6 cm NaI(Tl) crystal has a counting rate from the 1.46 MeV gamma ray from ^{40}K of about 600 photopeak counts per minute.

2. Gamma-ray decay of the 4417 keV level

Figure 37 shows the gamma-ray decay of the 4417 keV level, which is the lower member of the doublet shown in figure 6. The 1976 keV gamma ray comes from the inelastic scattering of protons from the ^{36}Ar target. The yield of this gamma ray is so strong for higher resonances (figure 4) that the 4417 keV level is the highest one for which investigation of the gamma rays from the $^{36}Ar(p,\gamma)^{37}K$ reaction was feasible. Figure 38 shows the gamma-ray spectrum from the same level as seen by a Ge(Li) counter. The 1380 keV gamma ray was calibrated four times by comparison with the 1368.5 keV gamma ray (Ewan and Tavendale, 1964) from the decay of ^{24}Na, and the mean of the measurements gives 1380 ± 2 keV. Calibration of the other gamma rays in this figure was accomplished by using various other well-known gamma-ray energies (Ewan and Tavendale, 1964) as shown in figure 39. The excitation energy of this level in ^{37}K was

determined as 4417 ± 5 keV, and the energy of the first excited level of ^{36}Ar is 1976 ± 4 keV.

3. The lifetime of the 1380 keV level

a. Significance of the lifetime

The 4417 keV level is of particular interest because it is the strongest way to selectively populate the 1380 keV level, which has been shown in part VIII to have $J^{\pi} = 5/2^-$ or $7/2^-$. The latter is seen from figure 37 to decay directly to the ground state, which has been shown in part VIII to have $J^{\pi} = 3/2^+$ or $5/2^+$. This leaves four possibilities for the spins of both the 1380 keV level and the ground state. Only one of these, namely $7/2^-$ to $3/2^+$ cannot proceed by an E1 transition, but must result from an M2-E3 transition. The Weisskopf estimate (Wilkinson, 1960) for the lifetime of an E1 transition of this energy is about $3 \cdot 10^{-16}$ seconds, while that for an M2 transition is about one nanosecond. If the measured lifetime were greater than a few nanoseconds, this would determine the spin of the 1380 keV level as $7/2^-$ and that of the ground state as $3/2^+$.

b. Electronic apparatus

Figure 40 shows the block diagram for the electronics designed to measure the half-life of the 1380 keV level. Two 5.04 by 5.04 cm NaI(Tl) crystals situated at 90° to the beam and 180° apart detect the two gamma rays from the cascade from the 4417 keV level. The discriminator on the start side passes a timing pulse to the time-to-pulse-height converter only if the energy loss of the gamma ray in

the start crystal is greater than 1.5 MeV. Thus the start side cannot trigger on the second gamma ray of the cascade. The crystal on the stop side passes a stop pulse to the converter if the energy loss in this crystal is greater than 0.7 MeV. The output of the converter feeds the vertical input of a two-dimensional analyzer, and a linear pulse-height spectrum from the start crystal provides the horizontal input to the analyzer. The analyzer stores a count in a channel whose vertical coordinate is proportional to the time delay between the start and stop pulses, and whose horizontal coordinate is proportional to the pulse height from the start crystal. A pulse in the stop crystal corresponding to the photopeak of a 1380 keV gamma ray provides a coincidence input to the analyzer. The analyzer does not store a count in any channel unless all three of its inputs occur within two microseconds.

This configuration eliminates the effect of resolution broadening due to the fast amplifier on the start side producing a trigger pulse whose timing depends upon the input pulse height (time slewing), because counts corresponding to different start input pulse heights are stored in different horizontal channels. If the 1380 keV level has a measurable half-life, there should be tails in the vertical (time) direction as long as the horizontal channel number corresponds to a start energy of less than 3.04 MeV, but there should be no tails for horizontal channel numbers larger than this.

c. Results and analysis

Figure 41 shows part of the analyzer output with ^{36}Ar in the cell. As explained in the caption, there are long time tails as long as the energy of the gamma ray detected in the start side is less

than the 3.04 MeV gamma ray which initiates the cascade, but no tails above this. This is confirmatory evidence that the tails are due to ^{37}K and not some impurity.

However, since there is a fair amount of prompt coincidences due to impurities in the gold and the gas, a background run with identical electronics and beam was taken with the ^{36}Ar replaced by helium. This is shown in figure 42. This run must be multiplied by 1.7 before comparison with figure 41. It is seen that there is a large amount of prompt-coincidence background, but no tails in the time direction other than that due to the resolution.

The resolution of the electronics was checked by using a source of ^{24}Na, which produces 2754 and 1368.5 keV gamma rays in coincidence. The result is shown in figure 43, indicating a resolution with a FWHM of 3.2 nanoseconds. This source also provided the gain calibration for the horizontal (energy) scale of the analyzer and a check on the proper setting of the 1.38 MeV coincidence window in figure 40.

The result with ^{36}Ar in the chamber, when summed for start pulse heights between 2.1 and 3.0 MeV and corrected for the background run taken at the original beam energy, is shown in figure 44. The tails in the time direction occurred only when the pulse height in the start side was less than 3.1 MeV; no tails occurred when the coincidence window was moved from 1.38 to 1.7 MeV, and there were no tails when the ^{36}Ar was replaced by helium. Because the beam energy hitting the beam stopper was slightly higher when helium was used in the cell than when ^{36}Ar was used, a background run was also taken with the beam energy raised 12 keV, and no tails occurred. These three background checks make it extremely improbable that the

time tails are due to an impurity. There is a 10% uncertainty in the horizontal scale of figure 44, which when folded into the statistical uncertainty in the half-life, results in 9.6 ± 1.4 nanoseconds for the half-life of the 1380 keV level. This value is close to the 1.29 MeV $7/2^-$ to $3/2^+$ transition in ^{41}K which has a half-life of 6.7 nanoseconds (Elliot, 1952). Assuming that the decay of the 1380 keV level is not due to an E1 transition which is weaker than its Weisskopf estimate by a factor of $0.5 \cdot 10^{-8}$, the arguments given above thus show that the spin of this level is $7/2^-$ and that of the ground state is $3/2^+$. Perdrisat (1966) has summarized hindrances for E1 transitions and for this mass region they are such that

$$\frac{\Gamma_{E1}}{\Gamma_{Weisskopf}} \geq 2 \cdot 10^{-5} .$$

X. GAMMA-RAY ANGULAR DISTRIBUTIONS AND ANISOTROPIES FROM THE REACTION $^{36}Ar(p,\gamma)^{37}K$

1. Introduction

In the measurement of anisotropies or angular distributions of the gamma rays produced by the reaction $^{36}Ar(p,\gamma)^{37}K$, hole-free gold entrance foils were used in the gas-cell arrangement in figure 1. This is because a gas leak in the region of the foil where the beam was entering could cause the charge integration to be in error. Commercial foils of nickel and platinum are obtainable hole-free, but were unsuitable because of the background gamma-ray counts they produce under proton bombardment.

There are sharp resonances in many impurity reactions such as $^{19}F(p,\alpha\gamma)^{16}O$ which can confuse the results because the beam energy impinging upon the beam catcher is in the order of 10-20 keV higher during the helium background runs than during the runs with ^{36}Ar in the cell. Since it was not possible to increase the helium pressure so that its energy loss equaled that of the ^{36}Ar, two background runs with helium were taken at all the resonances reported below. One was taken at the original energy and the other with the beam energy raised by the difference between the energy losses in the ^{36}Ar and the helium. The results were similar. In all the gamma-ray spectra in NaI(Tl) crystals reported below the helium background at the original beam energy has been subtracted.

2. Geometrical considerations

The center of the target chamber was aligned over the center of the steel gamma-ray table in the tandem target room to within 1/2 mm, and with the geometries and gamma-ray energies used in the work reported below, this could cause no error larger than 2% in the measured anisotropies.

The length of the target chamber was 9 mm and its effect on the observed anisotropies was calculated by computing with an IBM 7094 computer the efficiency change of the crystals when the source is placed off axis by 4.5 mm, as the extreme ends of the target are when the crystal is at 90^{o}. Then the difference between the efficiency for a point source and that for two point sources on axis separated by 9 mm at the same average distance from the crystal was also calculated. In the geometries used the net effect on the anisotropy was a correction of about 2% or less.

The thin-walled aluminum chamber (0.4 mm thick) caused an attenuation of about 1% and its effect on the angular distributions was negligible.

Since the spectra obtained usually contained several gamma rays, the angular distributions or anisotropies were measured by taking the number of counts in the photopeak at each angle. The effect of the solid angle of the detector was calculated by the method of Rose (1953) who gives formulae for the angular attenuation coefficients Q_L which are defined as follows. If the truc angular distribution of a gamma ray is

$$1 + \sum_{L=1} A_L P_L (\cos(\theta))$$

then the observed angular distribution will be (for cylindrical symmetry)

$$1 + \sum_{L=1} Q_L A_L P_L(\cos(\theta)) \ .$$

For perfect angular resolution, the Q_L equal unity, but for the experiments reported below, Q_2 ranged from 0.62 to 0.85, as calculated by a Kellogg subroutine BAZKJL.

The method of calculation of the Q_L assumed that the photofraction is independent of the angle that the gamma rays enter the crystal (with respect to the crystal axis). This is not valid near the corners of the crystal, but it is here that the total efficiency is low, so that this part of the crystal does not have much weight in the calculation of the Q_L. As discussed in more detail in the thesis of Pearson (1963), the photofraction decreases with increasing theta, and the true Q_L are slightly closer to unity than the numbers which are calculated by assuming that the photofraction is constant. The error for Q_2 for 4 MeV gamma rays as seen by a 12.7 by 10.2 cm NaI(Tl) crystal located 8 cm from the target is about 5% (Pearson, 1963). This means that the effective solid angle of the crystal is smaller. In comparing the observed photopeak anisotropies with calculations for various spin and parity assumptions, one must keep in mind that the real anisotropies might not have been washed out as much as the calculations by the code BAZKJL would predict. See the analysis of the 3083 keV level below for further discussion and illustration.

3. Gamma-ray decay of the 3311 keV level

a. Results

The 3311 keV level has been shown to have $J^{\pi} = 3/2^-$ so that none of its cascade gamma rays can have P_4 terms in their angular distributions, and therefore the yield was measured only at 0^o and 90^o. The experimental setup is shown in figure 45. The lead collimator used for this resonance was not used in any of the other resonances. The angular attenuation factors were calculated by the code BAZKJL with a cutoff at 30^o and the result for Q_2 was 0.82. The gamma-ray decay scheme of the 3311 keV level is shown in figure 46. This level cascades through a level at 1368 ± 3 keV the energy of which was measured with a 4 cm^3 Ge(Li) crystal placed at 90^o to the beam to avoid doppler shifts (figure 47). The well-known 1368.5 keV gamma ray from the decay of ^{24}Na (Ewan and Tavendale, 1964) provided a convenient calibration. A calibration of the 1943 keV gamma ray gives the excitation energy of the upper level as 3311 ± 5 keV. When combined with the result of Kavanagh and Goosman (1964), the final result is 3311 ± 4 keV.

It is thus seen that there are levels at 1368 ± 3 keV and 1380 ± 2 keV in ^{37}K, the latter of which was shown to have $\ell_p = 3$ in part VIII and is presumably the analogue to the $\ell_n = 3$ level at 1.611 MeV in the mirror nucleus ^{37}Ar (Rosner and Schneid, 1965). The lower member of this doublet in ^{37}K is presumably the analogue to the $1/2^+$ level at 1.41 MeV in ^{37}Ar (Rosner and Schneid, 1965).

After correcting for summing in the crystal, the peak in figure 46 at 3.3 MeV indicates a ground-state branch of $5 \pm 2\%$. Although the spin of the ground state was established as $3/2^+$ in

part IX, there is further evidence from figure 46 that it is not $5/2^+$. Assuming that a $3/2^-$ to $3/2^+$ or $5/2^+$ transition would be pure E1, the expected anisotropies for this geometry would be 1.60 and 0.78, respectively. The observed anisotropy $W(0^o)/W(90^o)$ corrected for summing is 1.8 ± 0.6, thus discriminating against the assignment of a spin of $5/2^+$ to the ground state.

b. Determination of the spin of the 1368 keV level

What information on the spin of the 1368 keV level can be obtained from figure 46? The calculated anisotropy of the 1943 keV gamma ray populating it from the $3/2^-$ level depends upon the spin assumed for the terminal level. The analysis is somewhat simplified if one makes the assumption that a magnetic L + 1 - pole cannot compete with an electric L-pole transition. The following table summarizes the possibilities for the expected anisotropies with this geometry, which were calculated from the general formulae given by Poletti and Warburton (1965) used in the Kellogg subroutine DRGGAD.

Assumed Transition	Assumed Multipolarity	Expected Anisotropy	Observed Anisotropy
$3/2^- - 1/2^+$	E1	0.492	0.49 ± 0.03
$3/2^- - 1/2^-$	M1	0.492	"
$3/2^- - 3/2^-$	44% or 84% E2	0.492	"
$3/2^- - 3/2^+$	E1	1.585	"
$3/2^- - 5/2^+$	E1	0.882	"
$3/2^- - 5/2^-$	12% or 99% E2	0.492	"
$3/2^- - 7/2^-$	E2	1.185	"

In the cases of M1-E2 mixtures, the amounts of E2 used were chosen so that they fit the observed anisotropy. Spins of $7/2^+$ or higher are extremely improbable because decays from a $3/2^-$ level to a $7/2^+$ level should not compete with the ground-state transition which can proceed by E1. From the above table it is seen that if one assumes that a magnetic L+1-pole cannot compete with an electric L-pole transition, then the spin of the 1368 keV level is not $3/2^+$, $5/2^+$ or $7/2^-$. Exclusion of some of the remaining possibilities ($1/2$, $3/2^-$ and $5/2^-$) has been attempted using the fact that the 1368 keV gamma ray in figure 46 is isotropic, but the data are insufficient for this purpose. On the assumption that this level is the analogue to the 1.41 MeV $J^\pi = 1/2^+$ level in ^{37}Ar, a tentative assignment of $(1/2^+)$ is made for this level.

4. Gamma-ray decay of the 2750 keV level

The gamma-ray spectrum from the decay of the 2750 keV level is shown in figure 48. The excitation energy of this level was calibrated by comparison with the 2753.9 keV gamma ray (Ewan and Tavendale, 1964) from the decay of ^{24}Na. A line source of ^{24}Na was placed in a target chamber very similar to the one used in obtaining the spectrum of figure 48 and similarly placed relative to the 4 cm^3 Ge(Li) counter. The source strength of the ^{24}Na was adjusted to be close to that from ^{37}K, and several measurements yielded the excitation energy as 2750 ± 1 keV. The proton energy of this resonance as seen by ^{36}Ar(p, γ)^{37}K was measured as 918 ± 4 keV by Kavanagh and Goosman (1964) and as 918 ± 1 keV by Arnell (1964). This provides the mass excess of ^{37}K on the ^{12}C = 0 scale as

$$(M - A)_{^{37}K} = -24799.6 \pm 2.7 \text{ keV},$$

using the mass excess for ^{36}Ar as given by Mattauch (1965).

There is a weak branch of about 1.4% from the 2750 keV level to the doublet near 1.38 MeV as seen in figure 48. It is essentially impossible to tell by energy measurements alone which of the two members of the doublet is being populated because one would see the same two gamma-ray energies to within one keV for either cascade.

The angular distribution of the 2750 keV gamma ray was taken and the runs were normalized to the yield of positrons from the decay of ^{37}K as seen by a 3.7 by 1.3 cm anthracene crystal placed vertically over the target so that the positrons scattered into the vertical monitor would be independent of the position of the NaI(Tl) crystal which moved in a horizontal plane to measure the distribution. Corrections for the finite length of the chamber and attenuation through the walls of the chamber were made. The entire angular distribution was remeasured on the tandem-accelerator gamma-ray table using the yield of gamma rays at 90^{o} as seen by a 7.6 by 7.6 cm NaI(Tl) crystal as a monitor. The results were the same within statistics as that of the previous measurement and the result is shown in figure 49.

This angular distribution definitely excludes spins of 1/2, 7/2 and 9/2 for any mixing of the lowest two allowed multipolarities. Spins higher than or equal to 11/2 are extremely unlikely because the ground-state transition to a $3/2^{+}$ level (98%) would then have to proceed by E4 or M4, even though a $7/2^{-}$ level at 1380 keV is

available. Thus the spin is determined to be 3/2 or 5/2. Negative parity is also very unlikely because $3/2^-$ or $5/2^-$ to $3/2^+$ requires at least 62% M2 mixed with 38% E1 to fit the angular distribution. The distinction between the two remaining possibilities, $3/2^+$ and $5/2^+$, is difficult. Figure 49 shows that $5/2^+$ to $3/2^+$ by 1.5% E2 fits the data quite well, but also that $3/2^+$ to $3/2^+$ by 62% E2 fits the data almost as well. It is noted that the anisotropy $W(0^o)/W(90^o)$ tends toward unity if the M1-E2 mixture for the $3/2^+$ to $3/2^+$ transition is changed in either direction. A least-squares analysis of the data yields the true angular distribution corrected for geometry,

$$W(\theta) = 1.000 \pm 0.009 - (0.620 \pm 0.021)\ P_2 + (0.003 \pm 0.032)\ P_4 \ .$$

The establishment of a non-zero P_4 term would definitely exclude $J^\pi = 3/2^+$, but the above angular distribution shows no evidence for this. This result is in contradiction to the result quoted for this transition by Arnell (1964),

$$W(\theta)_{\text{Arnell}} = 1 - (0.74 \pm 0.04)\ P_2 + (0.05 \pm 0.02)\ P_4 \ .$$

The value of the observed anisotropy given in figure 49 is slightly lower than that allowed by a $3/2^+$ to $3/2^+$ transition for any mixing of M1 and E2, and the best fit for $3/2^+$ to $3/2^+$ requires 62.5% E2, which is 68 ± 10 times the Weisskopf estimate for an E2 width (Wilkinson, 1960). One cannot definitely exclude a spin of $3/2^+$ for this level, however, and it is assigned as $(5/2)^+$ in table 2.

5. Gamma-ray decay of the 3083 keV level

a. Calibration of gamma-ray energies

This level is the weakest of the gamma-ray resonances in ^{37}K reported in this work. The level was populated by the reaction $^{36}Ar(p,\gamma)^{37}K$ and background runs were taken with helium in the gas cell. Because of the low counting rate the spectra were taken only at 0^{o} and 90^{o}. Figure 50 shows the gamma-ray spectra taken with a 12.7 by 10.2 cm NaI(Tl) crystal at a distance of one cm from the target. This geometry severely washes out information on the angular distributions of the gamma rays, but is quite sensitive for determining what gamma rays exist. Figure 50 shows that the 3083 keV level decays mainly to the 1380 keV level; the remainder decays to the 2169 keV level and to the ground state. The summing of the various cascade gamma rays has been taken into account in determining the true number of ground-state gamma rays in the peak at 3.083 MeV in figure 50.

Figure 51 shows the gamma rays from this level as seen by a 20 cm^3 Ge(Li) counter placed at 90^{o} to the beam. The 1380 ± 2 keV gamma ray energy was measured by comparison with the 1368.5 keV gamma ray from the decay of ^{24}Na (Ewan and Tavendale, 1964) and the result is the average of several runs. The other gamma ray of the dominant cascade mode at 1703 ± 3 keV was measured by comparison with the 1731.9 keV pair peak to the 2753.9 keV gamma ray from ^{24}Na (Ewan and Tavendale, 1964). These two results provide the excitation energy of this level as 3083 ± 4 keV. This last result and a calibration of the 914 keV gamma ray in the

spectrum of figure 51 provide the excitation energy of the other level populated by this decay as 2169 ± 5 keV.

b. The anisotropies and spin assignments for the 3083 and 2169 keV levels

Since the spectra of figure 50 were taken with close geometry and hence contained little angular information, another set of runs was taken at this resonance as seen by a 7.6 by 7.6 cm NaI(Tl) crystal placed 2.8 cm from the center of the target. In this geometry the angular attenuation factors as calculated by the code BAZKJL were $Q_2 = 0.64$ and $Q_4 = 0.17$ for the 1.7 MeV gamma ray. Figure 52 shows the spectra. Since the spin of the 1380 keV level is known and the spin of the 2169 keV level is $1/2^-$ or $3/2^-$ (part VIII), the observed anisotropies of the 1703 and 914 keV gamma rays provide information on the possible spins of the 3083 keV level. The runs of figure 52 were taken with a hole-free gold foil to assure that gas leakage near the beam entrance region did not affect the charge integration. Corrections for the finite length of the target and attenuation through the target chamber were in the order of two percent. The observed anisotropies for this geometry were

Gamma-ray energy	$W(0^o)/W(90^o)$
1703 keV	0.60 ± 0.04
914 keV	0.41 ± 0.16 .

Despite this apparent paucity of information, tentative spin assignments for both the 3083 and 2169 keV levels may be

inferred from these data. Considering first only the anisotropy of the 1703 keV gamma ray which terminates on the $7/2^-$ level, and assuming that magnetic L+1-pole transitions do not compete with electric L-pole transitions, what spins for the 3083 keV level can be eliminated?

Assumed 1.7 MeV Transition	Assumed Multipolarity	Expected Anisotropy	Observed Anisotropy
$1/2^- - 7/2^-$	any	1.00	0.60 ± 0.04
$3/2^- - 7/2^-$	E2	1.16	"
$3/2^+ - 7/2^-$	35% or 99% E3	0.60	"
$5/2^+ - 7/2^-$	E1	0.87	"
$5/2^- - 7/2^-$	5% or 99% E2	0.60	"
$7/2^- - 7/2^-$	76% or 97% E2	0.60	"
$7/2^+ - 7/2^-$	E1	1.54	"

In cases where M1-E2 or M2-E3 mixtures are possible, the mixtures used in each case were chosen to fit the observed anisotropy.

It will be recalled that in calculating the Q_L the assumption was used that the photofraction was independent of the angle between the axis of the NaI(Tl) crystal and the gamma ray. Page 56 showed that the experimental angular resolution might be slightly better than the calculated values of Q_L would predict. It is seen in the table above that the spin assignment of $5/2^+$ is rejected because it predicts an anisotropy of 0.87 while the observed is 0.60 ± 0.04. But if the real angular resolution is better than that calculated, the expected anisotropy for $5/2^+$ would be lower than 0.87

(i. e., more anisotropic). Fortunately, for perfect resolution with $Q_L = 1$ the expected anisotropy for $5/2^+$ is 0.80, so the rejection of $5/2^+$ persists.

It is thus seen that under the assumptions stated above, spins of 1/2, $3/2^-$, $5/2^+$ and $7/2^+$ are excluded. A spin of $3/2^+$ is extremely unlikely because the transition $3/2^+$ to $7/2^-$ should not compete with transitions to other states that could proceed by multipolarities lower than M2 or E3. Since 79% of this decay width is through the $7/2^-$ level, $3/2^+$ is excluded. Spins higher than $7/2^+$ are quite unlikely because 11% of the decay width is through a level believed to be $1/2^-$ or $3/2^-$.

Consider the anisotropy of the 914 keV gamma ray which originates from the 3083 keV level and terminates on the 2169 keV level ($J^\pi = 1/2^-$ or $3/2^-$). Can either of the two spin possibilities not eliminated by the previous argument, namely $5/2^-$ and $7/2^-$, be eliminated by the observed anisotropy of the 914 keV gamma ray? The following table illustrates the possibilities.

Assumed 914 keV Transition	Assumed Multipolarity	Expected Anisotropy	Observed Anisotropy
$5/2^- - 1/2^-$	E2-M3	≥ 1.21	0.41 ± 0.16
$5/2^- - 3/2^-$	5% or 73% E2	0.41	"
$7/2^- - 1/2^-$	M3-E4	≥ 1.88	"
$7/2^- - 3/2^-$	E2-M3	≥ 0.88	"

In all cases above except the second one, the expected anisotropy is the minimum possible for any mixing of the assumed multipolarities. Thus it is seen that even allowing magnetic L+1-pole transitions to

compete with those of electric L-poles, a spin of $7/2^-$ for the 3083 keV level is excluded, and thus

$$J^\pi_{3083\ \mathrm{keV}} = (5/2^-)$$

$$J^\pi_{2169\ \mathrm{keV}} = (3/2^-) \ .$$

Since it was assumed that an M2 could not compete with an E1 transition in the first argument, and because the $\ell_p = 1$ assignment to the 2169 keV level arose from extrapolation of the DWBA theory to unbound levels, parentheses are included around the spin assignments for these two levels.

But what becomes of this analysis if the 1380 keV level is in fact $5/2^-$ instead of the assigned value of $7/2^-$ and decays by an E1 transition with a strength $0.5 \cdot 10^{-8}$ times its Weisskopf estimate? In the remote chance that this may be the case, the analysis of the gamma decay of the 3083 keV level has been carried out on the assumption that the 1380 keV level has a spin of $5/2^-$. Using the same assumptions as before, the anisotropy of the two decay gamma rays is consistent only with the following spin assignments:

Possible spin assignments if $J^\pi_{1380\ \mathrm{keV}} = 5/2^-$

3083 keV level		2169 keV level
$5/2^-$	and	$3/2^-$
$3/2^-$	and	either $3/2^-$ or $1/2^-$.

It is seen that the assignments given on page 66 of $(5/2^-)$ and $(3/2^-)$ are possible even if the spin of the 1380 keV level is $5/2^-$.

6. Gamma-ray decay of the 3962 and 3982 keV levels

The yield of the reaction $^{36}Ar(p,\gamma)^{37}K$ was investigated near 3.97 MeV excitation in ^{37}K and the peak in figure 2 at this energy was found to be a doublet. The lower member at 3962 keV is less than 10 keV wide and appears to decay to the ground state and through the doublet near 1.37 MeV excitation; the upper member at 3982 keV is about forty keV wide and appears to decay through the 2169 keV level. This broad level at 3982 keV is presumably the $1/2^-$ level seen in elastic scattering by Storizhko and Popov (1964).

XI. SUMMARY OF THE EXPERIMENTAL RESULTS

Figure 53 shows the energy levels of the mirror nuclei ^{37}Ar and ^{37}K below 4 MeV, and the dashed lines relate levels believed to be analogues. The spin assignments for ^{37}Ar are due to Rosner and Schneid (1964) except for that of the 2.797 MeV level. The $1/2^-$ assignment to the 3.982 MeV level in ^{37}K is due to Storizhko and Popov (1964). Only the principal modes of gamma-ray decay are shown for ^{37}K and those in ^{37}Ar are due to Allen (1966).

It is believed that the 2.498 MeV level in ^{37}Ar and the 2.169 MeV level in ^{37}K are analogues because both have large yields in the stripping reactions, as compared to the 2.217 MeV level in ^{37}Ar and the 2.278 MeV level in ^{37}K, which are about 100 times weaker.

Kavanagh and Goosman (1964) have shown that the 2.797 MeV level in ^{37}Ar has $J^\pi = 1/2^+$, $3/2^+$ or $5/2^+$ and Rosner and Schneid (1965) have shown that $\ell_n = 1$ or 2, so that $J^\pi = 3/2^+$ or $5/2^+$. This level is believed to be the analogue to the 2.750 MeV level in ^{37}K because both appear in the stripping reactions and have similar gamma-ray decay modes. The $(5/2)^+$ assignment in ^{37}Ar is based upon the assumption that the 2.797 MeV level is the analogue to the 2.750 MeV level in ^{37}K.

The 3.525 MeV level in ^{37}Ar and the 3.311 MeV level in ^{37}K are presumed to be analogues because they have the same spin and parity and both appear moderately strong (see the caption to figure 30) in the stripping reactions. This correspondence should not be considered definite.

It would appear that there is one level missing in ^{37}K between the 2.750 and 3.311 MeV levels, but re-investigation of this region with the $^{36}Ar(^{3}He, d)^{37}K$ reaction has revealed no evidence for more levels than those shown in figure 53.

A brief summary of evidence for the spins and parities of levels in ^{37}K is given below (see also figure 54):

Ground state - from the $\ell_p = 2$ stripping pattern and the half-life of the 1380 keV level; confirmed by the anisotropy of the ground-state gamma ray from the 3311 keV level; or from the superallowed beta decay to the $3/2^+$ ground state of ^{37}Ar which is its analogue.

1368 keV level - from the anisotropy of the gamma ray populating it from the 3311 keV level, which requires $J^\pi = 1/2,\ 3/2^-$ or $5/2^-$, and the assumption that it is the analogue to the $1/2^+$, 1408 keV level in ^{37}Ar.

1380 keV level - from the $\ell_p = 3$ stripping pattern and its 9.6 nanosecond half-life; or from the assumption that it is the analogue to the $7/2^-$, 1611 keV level in ^{37}Ar.

2169 keV level - from the anisotropy of the gamma ray populating it from the 3083 keV level and the $\ell_p = 1$ stripping pattern; or from the assumption that it is the analogue to the $3/2^-$, 2498 keV level in ^{37}Ar.

2750 keV level - from the angular distribution of the ground-state gamma ray which requires $J^\pi = 3/2^+$ or $5/2^+$, the former spin being less probable because of the large E2

strength required to fit the angular distribution and the actual value of the observed anisotropy.

3083 keV level - from the anisotropies of the gamma rays from it which populate the $7/2^-$ level and the $\ell_p = 1$ level at 2169 keV.

3311 keV level - from the elastic scattering of protons.

5018 keV level - from the elastic and inelastic scattering of protons.

5048 keV level - from the elastic scattering of protons, and confirmed by the inelastic scattering of protons.

The spin and parity assignments made to other levels are given in table 2 with a list of references.

The excitation energies of all levels below 3.4 MeV in table 2 were measured from their gamma rays as seen with a Ge(Li) detector with the exception of the 2278 keV level, which was measured from its proximity to the 2169 keV level in the $^{40}Ca(p, \alpha)^{37}K$ reaction. The calibration of the other excitation energies for levels below 5.6 MeV is described in detail in part II. The proton energies of some of the levels as determined by Storizhko and Popov (1964) which differ significantly from some of the author's excitation energies given in table 2 are tabulated in part II. The region between 5.6 and 6.65 MeV excitation energy was covered with excellent resolution by Skeppstedt et al. (1966) and their proton resonance energies supercede several of those inferred from figure 4. The proton resonance energies observed by Skeppstedt et al. (1966) for

levels below 5.6 MeV agree very well and are in one-to-one correspondence with the resonance energies determined by the present work. Where a number not due to the present work is quoted in table 2 a reference is supplied.

Table 3 gives the levels in ^{37}K that are populated by the beta decay of ^{37}Ca, as determined by Poskanzer et al. (1966). Figure 55 shows the gamma-ray branching ratios for levels in ^{37}K as determined by the present work.

Using the 1964 mass tables of Mattauch et al. (1965) and the ^{37}K mass excess reported in part X, one arrives at the following Q-values in the $^{12}C = 0$ scale:

Reaction	Q-value (keV)
$^{33}Cl(\alpha,\gamma)^{37}K$	6211 ± 12
$^{35}Cl(^{3}He,n)^{37}K$	2645.0 ± 3.0
$^{36}Ar(p,\gamma)^{37}K$	1857.0 ± 1.4
$^{36}Ar(d,n)^{37}K$	-367.5 ± 1.4
$^{36}Ar(^{3}He,d)^{37}K$	-3636.6 ± 1.4
$^{40}Ca(p,\alpha)^{37}K$	-5183.7 ± 4.2
$(M - A)_{^{37}K}$	-24799.6 ± 2.7

APPENDIX A GAMMA-RAY ANGULAR DISTRIBUTIONS FROM $^{36}Ar(p, p'\gamma)$ WHEN THE PROTON IS NOT OBSERVED

In this appendix the following notation is used:

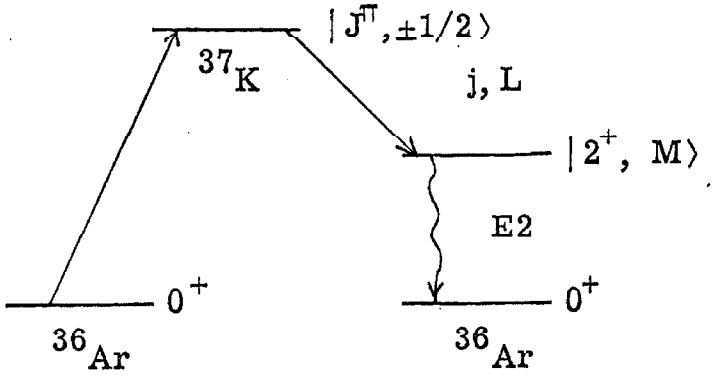

J is the spin of the compound level

L is the orbital angular momentum of the inelastic proton

j is the total angular momentum of the inelastic proton

M is the z-component of the angular momentum of the excited ^{36}Ar nucleus. The beam is in the z-direction.

Since the bombarding proton has $L_z = 0$, only the $\pm 1/2$ magnetic substates of the compound level in ^{37}K are populated. They are populated equally by the unpolarized beam, and the amplitudes for each substate do not have a definite phase relationship. For this reason the contributions to the correlations due to the +1/2 and -1/2 magnetic substates are treated incoherently. The calculation will be done only for the +1/2 magnetic substate because the result is identical for the -1/2 substate.

When the compound level decays into a proton and the excited 2^+ level of the target, it may in general leave the ^{36}Ar nucleus in any of its five possible projections. The population of these substates determines uniquely the angular distribution of the gamma rays to the 0^+ ground state, because the transition proceeds by pure electric quadrupole radiation. Since the ground state has only one substate, the gamma-ray decay of each substate of the 2^+ level proceeds by an E2 photon of definite and unique J_z. This means that for each value of M there is a unique angular distribution of the photon given by the absolute square of the M^{th} standard component of the vector spherical harmonic of degree two. The amplitudes for photon emission from the various projections of the 2^+ level add incoherently because the photon from each magnetic substate has a unique value of J_z which could have been measured as part of the experiment.

The compound level in ^{37}K decays to the 2^+ level of ^{36}Ar by the emission of a proton which may have any of several values of its total angular momentum j. The purpose of this appendix is to demonstrate that the amplitudes for proton emission with definite values of j can be treated incoherently for purposes of computing the angular distribution of the de-excitation gamma rays when the proton is not observed. For this purpose it is sufficient to demonstrate that the interference terms due to different values of j vanish upon integration over all possible directions of the proton. In what follows all magnetic projections and wave functions will be written in a coordinate system which has the beam direction as its z axis, except for the initial description of the inelastic-proton wave function.

The transition probability for the +1/2 substate of ^{37}K breaking up into a proton in any direction and leaving the excited ^{36}Ar in a substate with projection M upon the z axis is proportional to

$$P_M = \int d\Omega \sum_{m'} |(2\ M\ e^{ikz'}\ m'|\ H|\ J\ 1/2)|^2$$

where the z' axis points in a direction Ω in the original coordinate system and $m' = \pm 1/2$ is the helicity of the proton. Expanding the proton wave function into eigenstates of the operators J^2 and J_z gives

$$e^{ikz'}\,|\,m'\rangle = \sum_L A_L\, Y_L^0(\Omega')\,|\,m'\rangle$$

$$= \sum_L A_L \sum_j (j\ m'|\ L\ 0\ 1/2\ m')|\ j\ m'\rangle$$

$$= \sum_L A_L \sum_j (j\ m'|\ L\ 0\ 1/2\ m') \sum_m D^j_{m',m}(\Omega)\,|\,j\ m\rangle$$

where the states $|\,j\ m\rangle$ for the inelastic proton are expressed in the z' coordinate system. $D^j_{m',m}(\Omega) = D^j_{m',m}(\varphi, \theta, 0)$ where the first two Euler angles are the usual spherical angles and the third angle represents rotations of the coordinate system about the z' axis and may be set equal to zero because the description of the inelastic proton emerging in the z' direction with helicity m' is invariant under rotations about the z' axis. Thus one can write

$$P_M = \int d\Omega \sum_{m'} \Big| \sum_{L} \sum_{m,j} A_L (jm'|\ L0\ \ 1/2\ m')\ D^j_{m',m}(\Omega)\ (2M\ jm|\ H|\ J\ 1/2)\Big|^2.$$

Since the Hamiltonian is assumed to commute with $\hat{J}_z$, $M + m = 1/2$ and the sum over m is omitted below. The entire dependence upon Ω is contained in the D function so that all the interference terms due to the various values of j of the proton are proportional to (Preston, 1962)

$$\int D^{j}_{m',m}(\Omega)\, D^{*j'}_{m',m}(\Omega)\, d\Omega = f(j)\delta_{j,j'}$$

where $f(j)$ is a function only of j and the integral is over the first two Euler angles φ and θ, and the third angle in the argument of the D functions is arbitrary. Thus the contributions due to different values of j add incoherently when the proton is not observed.

To compute the angular distribution of the gamma rays for a definite value of j of the proton and J of the compound level, one notes that the integral of the square of the two D functions is independent of M. The entire M-dependence is contained in the matrix element of the Hamiltonian. Thus

$$P_M = \text{constant} \cdot |(2\ M\ j\ m|H|\ J\ 1/2)|^2$$

where the constant is independent of M. The matrix element is decomposed into a reduced matrix element and a Clebsch-Gordan coefficient: (Biedenharn, 1953)

$$P_M = \text{constant} \cdot \text{RME} \cdot (2\ M\ j\ m|J\ 1/2)^2$$

where RME is also independent of M. Since one needs only the relative population of the various M substates, it is sufficient to write

$$P_M = (2\ M\ j\ m|J\ 1/2)^2 .$$

The angular distribution of gamma rays with respect to the beam direction is given for definite values of J and j by

$$W_J^j(\theta) = \sum_M (2\ M\ j\ m\ |\ J\ 1/2)^2\ |\ X_2^M\ |^2$$

where the last symbol is the M^{th} component of the vector spherical harmonic of degree two (Jackson, 1962). Table 1 shows the coefficients A_2 and A_4 for these angular distributions when written as

$$W_J^j(\theta) = 1 + A_2\ P_2(\cos(\theta)) + A_4\ P_4(\cos(\theta)).$$

These coefficients may also be deduced from a table of unnormalized coefficients given by Sheldon and Van Patter (1966).

The general gamma-ray angular distribution for a given J of the compound level is an incoherent sum of the contributions from different values of j:

$$W_J(\theta) = \sum_j a_j\ W_J^j(\theta)$$

where the a_j are arbitrary coefficients.

APPENDIX B MEASUREMENT OF $\frac{\omega\Gamma_p\Gamma_{p'}}{\Gamma}$ FOR THE 5127 keV LEVEL

As shown on page 18, when a beam of protons undergoes a nuclear reaction with a spinless target which proceeds through a resonant compound state of spin $J = \omega - 1/2$, then the widths of the compound level for the entrance and exit channels, Γ_p and $\Gamma_{p'}$, are related to the yield of the reaction by the formula:

$$\frac{\omega\Gamma_p\Gamma_{p'}}{\Gamma} = \frac{(\text{yield per proton}) \cdot \varepsilon \cdot m \cdot E}{\pi^2\hbar^2} \left(\frac{M}{m+M}\right)^2$$

where m is the proton mass, M is the target mass, E is the proton lab energy and ε is the atomic stopping cross section. This expression assumes that the resonance is completely integrated by the beam. This means that every proton has, at some time during its passage through the target, the correct energy for this resonant reaction. In most cases this is not true, because the beam-energy profile is broadened by straggle in the entrance foil and the gas-target thickness (pressure) cannot be made large enough without rupturing the foil. On page 21 the general formula was given for the fraction of the incident beam that was available for the reaction. Since the natural width of the 5127 keV level is 0.5 keV and is negligible compared to the target thickness or straggle in the foil, a simple method using figures 12 and 13 is used to extract this fraction, which is called the resolution factor.

In the special case of protons on ^{36}Ar, the formula on page 77 becomes

$$\frac{\omega\Gamma_p\Gamma_{p'}}{\Gamma} = \frac{3.71 \cdot 10^{-4}(\text{yield per microcoulomb}) \cdot \varepsilon \cdot E}{\text{Resolution factor}} \text{ eV}$$

where εE is in units of 10^{-14} eV MeV cm^2/atom.

The 5127 keV level was calibrated by measuring the yield of 1.97 MeV gamma rays following inelastic scattering of protons from a ^{36}Ar target, as shown in figure 8. The target was contained in a stainless-steel target chamber 0.5 mm thick and 0.87 cm deep by a gold foil about 0.8 mg/cm^2 thick. A 7.6 by 7.6 cm NaI(Tl) crystal was placed 14.8 cm from the center of the gas target. A flat sheet of lead 1.75 mm thick was placed in front of the detector to reduce the number of x-rays entering the crystal. The following factors enter into the calculation:

Target pressure was 4.14 cm of Hg ± 3% as read by a mercury manometer.

Temperature of the gas was estimated as 35 ± 15°C. The chamber was air-cooled and the power dissipation was 0.6 watts.

Target thickness in 0.87 cm of target chamber plus an estimated 0.07 cm for the bulge in the entrance foil was 5.78 keV ± 12%, where the error on the number of targets per unit area was 6% and the error on the atomic stopping cross section was taken as 10%. As will be explained, this

error on the stopping cross section essentially cancels out and is therefore not important.

Resolution was 13 ± 1 keV FWHM as measured by running the resonance yield as a function of bombarding energy.

Straggle of the beam upon leaving the entrance foil was therefore 12.4 ± 1 keV, because figure 12 shows that a straggle of 12.4 keV folded into a target thickness of 5.8 keV results in a yield with a FWHM of 13 keV.

Resolution factor was then taken from figure 12. The ratio of target thickness to straggle was 0.468 ± 14% and from the graph one obtains the resolution factor as 0.42 ± 0.05.

Photofraction or the fraction of events in the detector that result in the loss of all the energy of the gamma ray within the crystal was taken from graphs of Heath (1957) as 0.265 ± 10%. This value is consistent with the actual gamma-ray spectrum used in this calculation which is shown in figure 8.

Attenuation of the gamma rays due to the 1.75 mm of Pb and 0.5 mm of stainless steel was obtained from tables given by Grodstein (1957) and was 11% for gamma rays incident perpendicular to the face of the lead.

Total efficiency including solid angle for this geometry and including the attenuation of the lead was calculated by a Kellogg computer code BAZKJL and was 0.00707 ± 7% for an isotropic source. This number is the fraction of the number of gamma rays emitted by the source at any angle

which lose some energy in the crystal.

Observed angular distribution for this geometry is plotted in figure 9 and is given by

$$W(\theta) = 1 + (0.197 \pm 0.01)\, P_2 + (0.564 \pm 0.01)\, P_4 .$$

The actual number of gamma rays emitted by the source is given by

$$\frac{\text{Observed yield at any angle } \theta}{\text{Total efficiency} \cdot \text{Photofraction} \cdot W(\theta)} .$$

Charge was read off the tandem current integrator as 22.5 microcoulombs.

Yield at 20° was taken from figure 8 for this charge and was $15390 \pm 3\%$ counts in the photopeak. This was corrected for the background with helium in the gas cell, which was 350 counts on resonance and 330 counts above resonance. The net yield was $15050 \pm 3\%$ counts.

Proton energy in the lab was 3359 ± 4 keV.

Dead time correction was computed as the ratio of clock to live time and was 1.036.

Stopping cross section as given by Whaling (1958) was $0.46 \cdot 10^{-14}$ eV cm^2/atom $\pm$ 10%.

The desired formula in terms of these quantities is

$$\frac{\omega\Gamma_p\Gamma_{p'}}{\Gamma} = \frac{3.71 \cdot 10^{-4} \cdot Y \cdot \epsilon \cdot E \cdot \text{Dead time correction}}{Q \cdot PF \cdot EFF \cdot W(20^{\circ}) \cdot \text{Resolution factor}} \text{ eV}$$

where Y is the corrected yield at 20°, ϵ is the stopping cross section, E is the lab proton energy, Q is the charge, PF is the photofraction, and EFF is the total efficiency.

One notices in examining figure 13 that when the resolution factor is about 0.42 or lower, the resolution factor becomes proportional to the target thickness, and hence is proportional to the stopping cross section. The error on the stopping cross section in the numerator of the equation above cancels the error in the resolution factor that is due to the stopping cross section. For this reason the error on the resolution factor is taken as 6% and the error on the ϵ in the numerator above is taken as zero. Thus

$$\frac{\omega\Gamma_p\Gamma_{p'}}{\Gamma} = \frac{3.71 \cdot 10^{-4}(15050 \pm 3\%)(0.46)(3.359 \pm 0.1\%)(1.036 \pm 1\%)}{(22.5 \pm 5\%)(0.265 \pm 10\%)(0.00707 \pm 7\%)(1.43 \pm 2\%)(0.42 \pm 6\%)}$$

$$= 354 \pm 53 \text{ eV for the 5127 keV level.}$$

This result was used to normalize the value of this quantity obtained for the other levels which are tabulated in table 2.

The 5127 keV level is different from most of the levels in ^{37}K below 6 MeV in that the inelastic width is not negligible compared to the elastic proton width. Thus its elastic-scattering-anomaly shape

will be affected, and the analysis of the widths is more complicated than when the elastic width is essentially the total width. The values in table 2 for the various widths of this level were calculated in the following manner.

If one assumes that the gamma-ray width is negligible, then the only open channels for the 5127 keV level are the elastic and inelastic widths (to the 1.97 MeV level of ^{36}Ar). As seen in figure 5 the inelastic yield is very strong. The spin is $5/2^-$ so that $\omega = 3$ and thus

$$\frac{\Gamma_p \Gamma_{p'}}{\Gamma_p + \Gamma_{p'}} = 0.118 \pm 0.018 \text{ keV}.$$

Thus

$$\Gamma_p = \Gamma \left[\frac{1 \pm (1 - 0.472/\Gamma)^{1/2}}{2} \right]$$

and

$$\Gamma = \frac{\Gamma_p^{\,2}}{\Gamma_p - 0.018} .$$

This means that $\Gamma \geq 0.472 \pm 0.07$ keV and that $\Gamma_p \geq 0.118 \pm 0.018$ keV. The following table lists possible solutions to these equations

Γ_p (keV)	Γ
0.160	0.610
0.200	0.488
0.230	0.473
0.250	0.474
0.300	0.495
0.400	0.568
0.500	0.655 .

Storizhko and Popov (1964) have investigated the elastic scattering of protons from this level at 141° with an experimental resolution of 2.5 keV. The error on their resolution as estimated by the author of the present work is about 35%. Since the magnitude of the elastic scattering anomaly depends on the ratio of Γ_p/Γ and on the resolution, it was possible to get a rough measure of both Γ_p and Γ. The background phase shifts were taken to be the hard-sphere values ($|\varphi_\ell| < 5^\circ$). Of all the solutions consistent with the above restrictions only the solution for

$$\Gamma_p = 0.30 \text{ keV} \quad \text{and} \quad \Gamma = 0.50 \text{ keV}$$

fits the magnitude of the observed anomaly of Storizhko and Popov (1964). Because of the uncertainty in their experimental resolution, an error of 35% was included in the results shown in table 2. The inelastic width of this level was then calculated from these results and the value of $\omega\Gamma_p\Gamma_{p'}/\Gamma$ quoted in table 2.

Very rough measures of the proton widths for the 4523, 4833 and 5116 keV levels were estimated in the same way from the data of Storizhko and Popov (1964) and are shown in table 2.

APPENDIX C. CORRECTION FACTORS FOR THE 16-COUNTER ARRAY

In the analysis of the $^{36}Ar(^{3}He, d)^{37}K$ reaction the deuterons were detected by an array of 16 surface-barrier counters placed at the focal plane of a magnetic spectrometer. In order to analyze the angular distributions, it was necessary to measure the correction or efficiency factors for this array. The slit width in front of each counter was 0.125 inches and the counters were about 0.25 inches apart, so that roughly half of the deuterons proceeding through the magnetic spectrometer were never detected, and this correction is important in absolute cross-section measurements. However, even in relative measurements like angular distributions, the various efficiencies of the counters must be measured because the particle group may not always be in the same group of counters throughout the angular distribution measurements. As in the $(^{3}He, d)$ work the entrance slits on the magnet were 8^{o} and 3^{o} total separation in the φ and θ directions, respectively. 8 MeV deuterons were scattered off a thick tantalum target and viewed at 140^{o} through the same exit collimator as that used in the $(^{3}He, d)$ work (see figure 29).

All counters except counter 8 were disconnected and the spectrum of deuterons was scanned with counter 8 by varying the field of the magnet. This yield as a function of the frequency of counter 8 is defined as $N_8(f)$. Then the same spectrum was measured with all counters connected. This yield defines 16 numbers which are called $N(f_j)$ where f_j is the frequency corresponding to the j^{th} counter for that magnetic field. Then 16 new numbers are defined by

$$P_j = \frac{N_8(f_j)}{N(f_j)} \quad .$$

The number of deuterons per unit frequency interval in the spectrometer is simply

$$N_f = \frac{N_8(f)}{FA_8(f)}$$

where $FA_8(f)$ is the frequency acceptance of counter 8 at a frequency f. The total number of deuterons in the entire group within the spectrometer in the frequency range of the 16 counters is

$$\int_{f_1}^{f_{16}} N_f \, df \doteq \sum_{i=1}^{16} \frac{P_i \cdot N_{obs}(i) \cdot (f_{i+1} - f_i)}{FA_8(f_i)}$$

where $N_{obs}(i)$ is the observed number of counts in counter i. The number $FA_8(f)$ is proportional to f, and for 0.125" slits,

$$FA_8(f) = \frac{f_8}{720} \quad .$$

The factor 1/720 is the frequency resolution with 0.125" slits. Because of this proportionality a simplification can be introduced by defining a set of 16 numbers

$$D_i = \frac{f_{i+1} - f_i}{FA_8(f_i)} \cdot$$

The D_i are independent of the magnetic field of the spectrometer. One can make these numbers independent of the slit size by normalizing them to unity for counter 8, so one defines

$$C_i = \frac{D_i}{D_8} \cdot$$

For 0.125" slits the numerical value of D_8 is 1.85. The number of deuterons in a certain group within the magnetic spectrometer can then be written as

$$D_8 \sum_{i=1}^{16} N_{obs}(i) \cdot P_i \cdot C_i \cdot$$

The numbers C_i are calculated from the frequency-factors book for the spectrometer and are independent of slit size and magnetic field. The numbers P_i are the measured numbers defined on page 86, and D_8 depends only upon the slit size as long as the dispersion of the magnet is independent of frequency.

Once the numbers P_i are measured, they can be combined with the calculated numbers C_i to form a set CF_i which is unity for counter 8 and which are multiplied by the observed number of counts in each counter to yield the actual number of deuterons in the group:

$$\text{True yield} = 1.85 \sum_{i=1}^{16} CF_i \cdot N_{obs}(i) \quad \text{where } CF_i = C_i P_i \, .$$

The numbers CF_i are called the "correction factors" for the 16 counter array. The following table lists the calculated numbers C_i, the measured numbers P_i and the correction factors CF_i used in this work:

Counter	C_i	P_i	$CF_i \pm 3\%$
1	1.06	0.87	0.923
2	1.08	1.121	1.21
3	1.08	0.995	1.07
4	1.06	0.948	1.00
5	1.03	0.951	0.98
6	1.00	1.011	1.01
7	0.983	0.978	0.96
8	1.00	1.00	1.00
9	0.95	1.022	0.97
10	0.96	1.063	1.02
11	0.91	1.11	1.01
12	0.88	1.12	0.99
13	0.89	1.105	0.98
14	0.92	1.13	1.04
15	0.84	1.21	1.02
16	0.84	1.18	0.99

These correction factors CF_i were measured for 3^o and 8^o slit openings in the θ and φ directions, respectively, with 0.125" counter slits for 6.3 MeV deuterons on 11/12/65, and since counters have been replaced since then, the numbers P_i and CF_i may no longer be valid.

APPENDIX D THE PRODUCTION OF HOLE-FREE GOLD FOILS FOR GAS CELLS

This appendix treats in detail the procedure used to make the hole-free gold entrance foils used in this work. The author does not have a recipe which is guaranteed to work; rather the fraction of foils that are good is very low (around one percent).

The basic problems are the cleaning of the substrate and the removal of all dust particles before evaporation, and the evaporation of the gold without allowing micro-globules of gold to be emitted from the boat toward the substrate.

Glass microslides 1" by 3" were chosen as the substrate because of their availability, low cost, and transparency. The latter factor allows one to view the hot boat through the film of gold that is being deposited, and to gauge the thickness of the film. A commercial thickness monitor was used to measure the film thickness at one position in the bell jar, but the transparent microslides allowed the visual measurement of film thickness for five or six slides. A good rough rule is that when a boat that is hot enough to evaporate gold becomes invisible through a thin gold film, that film is greater than about 0.3 μm thick. Most of the films used in this work were in the 0.1 to 0.3 μm range in experiments where good resolution was necessary.

To start the procedure, six microslides were selected for their freedom from pit marks, scratches and dirt. Although most containers of microslides state that their slides are "pre-cleaned" etc., examination of them usually reveals that they are anything but

clean. They invariably have dust and dirt on them, and the following cleaning procedure was used.

The microslides are first rinsed with tap water to remove the dust: wiping them directly as they come from the box may scratch them. Then they are immersed in a warm solution of sodium dichromate and sulphuric acid, which is sometimes called "cleaning solution". A warm solution may be most easily obtained by diluting one unit of the concentrated solution with one unit of cold water (carefully!). Cleansers such as "Lava" soap or "Alcinox" are not recommended, because they are very hard to dissolve completely in water, and the author has made gold foils using Alcinox which later under proton bombardment revealed intolerable amounts of aluminum on them. After being immersed in the cleaning solution for a few minutes, the microslides are rinsed for about two minutes with cold tap water and then rinsed immediately with distilled water for about 30 seconds. They are then quickly transferred to a clean bench which flows filtered air over them to evaporate the water remaining on the microslides. They are placed nearly vertical on a dry paper towel to help drain away the water. After drying they are inspected in the clean bench for dust, and if satisfactory are placed in a covered plastic box to keep out dust until they are to be used.

A small tantalum boat containing BaI_2 (the release agent) is placed adjacent to a covered tungsten boat for the gold evaporation. Tantalum boats cannot be used for gold, because molten gold alloys with the tantalum and destroys the boat. A covered boat is used so that the surface of molten gold is not exposed directly to the substrate. The gold is required to evaporate within the boat and

bounce around a few times before streaming out a small hole at the end of the boat. This is done in an effort to reduce the number of micro-globules of gold which are deposited on the gold film.

Both boats are previously outgassed at white heat in vacuum while they are empty. Commercial gold (99.9%) 35 mils thick is cut into small pieces and cleaned with cleaning solution in the same manner as the microslides. The tungsten boat is then filled with some gold and the tantalum boat with BaI_2. The microslides are placed about five inches away from the boats.

The release agent chosen was BaI_2 rather than the usual $BaCl_2$ because the former has a lower melting point, is five times as soluble in water, and has a minimum Z of 53 as opposed to 17. Should any of the release agent remain on the foil, the high Coulomb barrier for iodine would reduce the extent of nuclear reactions due to the release agent.

During the evacuation of the bell jar, the microslides are subject to a glow discharge for about three minutes in an effort to unseat dust particles still remaining on the microslides. Unfortunately the slides are not electrical conductors and the process is therefore not very effective. Metal substrates would be more effective. With a shield covering the microslides and in a vacuum of about 10^{-7} mm Hg, the BaI_2 is slowly heated until it fuses. Rapid heating will cause it to jump out of the boat. When the BaI_2 is in liquid form, the microslide shield is removed and a layer of BaI_2 about 2 micrograms/cm^2 (as measured by the thickness monitor) is deposited on the glass surface. The gold is then heated with the shield again covering the slides, and when gold is seen to be evaporating from the boat, the shield is removed and a gold film of the desired

thickness is deposited. A device to heat the slides during the evaporation process was tried, but no improvement in the quality of the films was noticed.

After the slides are removed from the bell jar, they are inspected in a dark room with a bright penlight for pinholes. A small "O-ring" glued to the penlight helps to reduce the amount of scattered light. It takes about 15 minutes of dark adaptation before some of the holes become visible. A good microslide will have less than about 200 pinholes in it. Areas which appear to be large enough for a foil with no visible holes are then marked by cutting the foil with a knife while it is still on the glass slide. Unless a procedure which makes much better films is discovered, simply cutting the foil into eight or six equally spaced areas will have little chance of producing a hole-free foil. In a good batch of six microslides, usually about one region large enough for a foil 0.30" in diameter that appeared hole-free was found. Of these that were floated off with distilled water, most of them revealed pinholes unseen in the first examination. The author made about ten hole-free gold foils (as determined by a helium mass-spectrometer leak detector) during the course of this project. Some of the early foils were contaminated with NaCl, and for this reason it is recommended that for gamma-ray work the experimenter wear surgical gloves and mask while inspecting the microslides for pinholes.

It is suggested that the process of sputtering be investigated for the production of these foils, as the process itself helps to clean dust from the substrate before the gold is deposited.

Gold foils will take three microamps of 1 MeV protons without rupturing, but they almost never take more than 24 hours of bom-

bardment with about one microampere of protons before they develop very small leaks. The author suggests that this is possibly due to gold atoms being kicked about or completely out of the foil due to the proton bombardment. The Coulomb cross section for 1 MeV protons on gold is high enough so that if one integrates it from 5^{o} to 180^{o}, corresponding to gold recoils of at least 40 eV energy, a calculation shows that in a day's bombardment at one microampere about one-fifth of the gold atoms in the region of the foil through which the beam passes have at some time at least 40 eV of energy.

The author's experience has shown that it is not advisable to store gold foils for long periods of time in vacuum systems which have mercury manometers, as the vapor pressure of Hg is 10^{-3} mm of Hg at room temperature and the vapor will eventually destroy the gold foil!

REFERENCES

Allen, J., 1966, private communication.

Arnell, S. E., 1964, Ark. för Fys. 26, 153.

Bahcall, J. N., 1964, Phys. Rev. 135, B137.
1966, Phys. Rev. Letters 17, 398.

Bassel, R. H., Drisko, R. M. and Satchler, G. R., 1962, O. R. N. L. 3240.

Biedenharn, L. C., 1960, in "Nuclear Spectroscopy Part B", Ajzenberg-Selove, F., Academic Press, New York, 777.

Biedenharn, L. C, and Rose, M. E., 1953, Rev. Mod. Phys. 25, 733.

Brostrom, K. J., Huus, R. and Koch, J., 1948, Nature 162, 695.

Brush Beryllium Co., 17876 St. Clair Ave., Cleveland, Ohio, 44110, private communication.

Castro, M. B., 1964, M. A. Thesis, Massachusetts Institute of Technology.

Cerny, J., 1965, private communication.

Davis, R., 1964, Phys. Rev. Letters 12, 302.

Elliot, L. G., 1952, Phys. Rev. 85, 942.

Endt, P. M. and Van der Leun, C., 1962, Nucl. Phys. 34, 1.

Engelbertink, G. A. P. and Brussaard, P. J., 1966, Nucl. Phys. 76, 442.

Erné, F. C., 1966, Nucl. Phys. 84, 241.

Evans, R.D., 1955, "The Atomic Nucleus", McGraw-Hill, New York, 661-2.

Ewan, G.T. and Tavendale, A.J., 1964, Can. J. of Phys. 42, 2286.

Feshbach, H., 1960, in "Nuclear Spectroscopy Part B", Ajzenberg-Selove, F., Academic Press, New York, 651.

Glaudemans, P.W.M., Wiechers, G. and Brussaard, P.J., 1964, Nucl. Phys. 56, 529.

Glaudemans, P.W.M., Wildenthal, B.H. and McGrory, J.B., 1966, Physics Letters 21, 427.

Grodstein, G.W., 1957, N.B.S. Circular 583.

Hardy, J.C. and Verrall, R.J., 1964, Phys. Rev. Letters 13, 764.
1965, Can. J. Phys. 43, 418.

Heath, R.L., 1957, "Scintillation Spectrometry - Gamma Ray Catalogue", Phillips Petroleum Co., Atomic Energy Division.

Hensley, D.C., 1966, private communication.

Hodgson, P.E., 1963, "The Optical Model of Elastic Scattering", Oxford, London, 119 and 127.

Holbrow, C.H., Hewka, P.V., Wiza, J. and Middleton, R., 1966, Nucl. Phys. 79, 505.

Jackson, J.D., 1962, "Classical Electrodynamics", Wiley & Sons, New York, 551.

Kavanagh, R.W. and Goosman, D.R., 1964, Physics Letters 12, 229.

Kim, C.C. and Barnard, A.C.L., 1961, Nucl. Phys. 28, 438.

Lande, A., 1965, U.C.R.L. report 16304.

Mainsbridge, F., Bonner, R.W. and Robson, T.A., 1963, Nucl. Phys. 48, 83.

Mattauch, J.H.E., Thiele, W. and Wapstra, A.H., 1965, Nucl. Phys. 67, 1.

Miller, R. and Kavanagh, R.W., 1966, to be published in Nucl. Inst. and Methods.

McNally, J.H., 1964, private communication
1966, Nucl. Phys. 88, 257.

Moss, C.E., 1965, private communication.

Pandya, S.P., 1958, Progress in Theoretical Physics 19, 404.

Pearson, J.D., 1963, Ph.D. Thesis, California Institute of Technology, 92.

Perdrisat, C.F., 1966, Rev. Mod. Phys. 38, 63.

Poletti, A.R. and Warburton, E., 1965, Phys. Rev. 137, 595.

Poskanzer, A.M., McPherson, R., Esterlund, R. A. and Reeder, P.L., 1966, Phys. Rev. 152, 995.

Preston, M.A., 1962, "Physics of the Nucleus", Addison-Wesley, Reading, Mass., 613.

Reeder, P.L., Poskanzer, A.M. and Esterlund, R.A., 1964, Phys. Rev. Letters 13, 767.

Robertson, M.M., Mack, J.E., Cohen, V.W. and Davis, R., 1960, Bull. Amer. Phys. Soc. 5, 441.

Rose, M.E., 1953, Phys. Rev. 91, 610.

Rosner, B. and Schneid, E. J., 1965, Phys. Rev. 139, B66.

Schweizer, F., 1958, Phys. Rev. 110, 1414.

Sheldon, E. and Van Patter, D., 1966, Rev. Mod. Phys. 38, 176.

Skeppstedt, L., Jonsson, A., Hasselgren, A. and Arnell, S. E., 1966, Ark. för Fys. 31, 83.

Storizhko, V. E. and Popov, A. I., 1964, Bull. of the Acad. of Sciences of the USSR, Vol 28, No. 7, 1048.

Tombrello, T. A. and Parker, P. D., 1963, Phys. Rev. 130, 1112.

Val'ter, A. K., Kopanets, E. G., L'vov, A. N. and Tsytko, S. P., 1964, Bull. of the Acad. of Sciences of the USSR, Vol 28, No. 7, 1040.

Vorona, J., Olness, J. W., Haeberli, W. and Lewis, H. W., 1959, Phys. Rev. 116, 1563.

Whaling, W., 1958, Handbuch der Physik 34, 193.

Wilkinson, D. H., 1960, in "Nuclear Spectroscopy Part B", Ajzenberg-Selove, F., Academic Press, New York, 859.

Yamamoto, S. S. and Steigert, F. E., 1961, Phys. Rev. 121, 600.

Table 1.

Coefficients for the angular distribution of gamma rays from the decay of a 2^+ level to a 0^+ level initiated by the compound resonant inelastic scattering of spin one-half particles upon spinless targets. The example $^{36}Ar(p, p'\gamma)^{36}Ar$ is illustrated. J^π is the spin and parity of the compound level, L_p is the resonant orbital angular momentum of the projectile, L is the outgoing orbital angular momentum of the proton and j is its total angular momentum. As shown in appendix A, when the outgoing proton is not observed the angular distribution of the gamma rays is an incoherent mixture of those tabulated for a unique value of j. Coefficients for only the lowest two allowed values of L are tabulated. For example the angular distribution with respect to the beam direction for $J^\pi = 5/2^-$ with $j = 3/2$ is

$$W(\theta) = 1 + 0.2041\ P_2(\cos(\theta)) + 0.6530\ P_4(\cos(\theta)) \quad .$$

This particular case is the actual angular distribution of gamma rays for the 5127 keV level (see figure 9).

Table 1

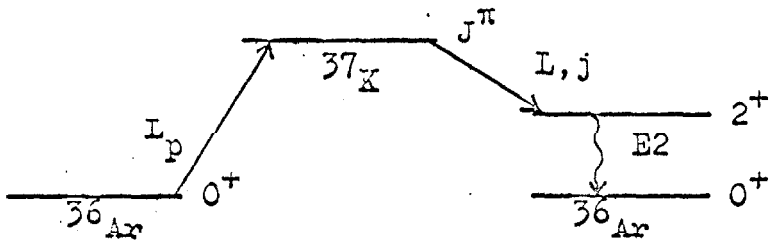

J^π	L_p	L	j	A_2	A_4
$3/2^-$	1	1	1/2	0.5000	0.
			3/2	0.	0.
		3	5/2	-0.3571	0.
			7/2	.1429	0.
$3/2^+$	2	0	1/2	0.5000	0.
		2	3/2	0.	0.
			5/2	-0.3571	0.
$5/2^+$	2	0	1/2	0.5714	-0.5714
		2	3/2	0.2041	0.6530
			5/2	-0.2041	-0.3673
$5/2^-$	3	1	1/2	0.5714	-0.5714
			3/2	0.2041	0.6530
		3	5/2	-0.2041	-0.3673
			7/2	-0.3469	0.1088
$7/2^-$	3	1	3/2	0.5102	-0.3673
		3	5/2	0.0850	0.6530
			7/2	-0.2721	-0.4898
$7/2^+$	4	2	3/2	0.5102	-0.3673
			5/2	0.0850	0.6530
		4	7/2	-0.2721	-0.4898
			9/2	-0.3231	0.1781
$9/2^+$	4	2	5/2	0.4762	-0.2857
		4	7/2	0.0216	0.6233
			9/2	-0.3030	-0.5454

Table 2.

The present information on ^{37}K. Information that is not due to the present work is labeled with letters:

a - Storizhko and Popov (1964).
b - The author's analysis of the data of ref. a. See appendix B for an example.
c - Val'ter and Kopanets (1964).
d - Arnell (1964).
e - This level was found by Storizhko and Popov (1964) but the energy quoted was determined by the author from its proximity to the 5127 keV level.
f - Schweizer (1958).
g - This spin results from this report or that of ref. c, in conjunction with that of ref. a.
h - Assumes J = 3/2. Multiply by 2/3 for J = 5/2.
i - This is the unresolved sum for the 3962 and 3982 keV levels.
j - This follows from the allowed beta decay of ^{37}Ca (Poskanzer et al., 1966).
k - This level is not definitely established by figure 2 alone, but it also appears in the beta decay of ^{37}Ca (Poskanzer et al., 1966).
m - This letter denotes a pair of close levels at least one of which is seen by reaction H and has $J^{\pi} = 1/2^+$, $3/2^+$ or $5/2^+$ (Poskanzer et al., 1966).
n - Skeppstedt et al. (1966).

The symbol ω is an abbreviation for J + 1/2. The code for the reactions is:

A - $^{36}Ar(p,\gamma)^{37}K$
B - $^{36}Ar(p,\gamma\gamma)^{37}K$
C - $^{36}Ar(p,p'\gamma)^{36}Ar$
D - $^{36}Ar(p,p)^{36}Ar$
E - $^{36}Ar(d,n)^{37}K$
F - $^{36}Ar(^{3}He,d)^{37}K$
G - $^{40}Ca(p,\alpha)^{37}K$
H - $^{37}Ca(\beta^+)^{37}K^*$
I - Either or both of reactions E and G.

Numbers in parentheses are not certain.

Excitation Energy (keV)	Proton Energy (keV)	J^π; T	Γ (keV) or $\tau_{\frac{1}{2}}$	θ^2 (r=4.3 fm)	$\omega\Gamma_p\Gamma_\gamma/\Gamma$ (meV)	$\omega\Gamma_p\Gamma_{p'}/\Gamma$ (eV)	Γ_p (keV)	$\Gamma_{p'}$ (eV)	Γ_γ (meV)	Reactions
0	-	$3/2^+$	1.23±0.02 s [f]	-	-	-	-	-	-	B,E,F,G
1368 ± 3	-	$(1/2^+)$	-	-	-	-	-	-	-	B,I
1380 ± 2	-	$7/2^-$	9.6±1.4 ns	-	-	-	-	-	-	B,I,F
2169 ± 5	321 ± 5	$(3/2^-)$	-	-	-	-	-	-	-	B,E,F,G
2278 ± 9	433 ± 9	-	-	-	-	-	-	-	-	G
2750 ± 1	918 ± 1[d]	$(5/2)^+$	≤0.8[d]	≤57	208±30	-	≤0.8[d]	-	(69±10)	A,F,G
3083 ± 4	1260 ± 4	$(5/2^-)$	(≤0.016±0.003)	(≤1.5)	13±2	-	(≤0.016±0.003)	-	(4.3±0.7)	A
3311 ± 4	1494 ± 4	$3/2^-$	2.2±0.3	0.22	31±4	-	2.2±0.3	-	15±2	A,D,F
(3498 ± 20)	(1686 ± 20)	-	-	-	8±3	-	-	-	-	A
3623 ± 15	1815 ± 15	$1/2^+,3/2^+,5/2^+$ [j]	-	-	14±3	-	-	-	-	A,H
3844 ± 10	2042 ± 10	$1/2^+,3/2^+,5/2^+$ [j]	-	-	21±6	-	-	-	-	A,H
3962 ± 15	2163 ± 15	-	≤10±4	-	70±21[i]	-	≤10±4	-	-	A
3982 ± 15	2184 ± 15	$1/2^-$ [a]	35[a]	0.34		-	35[a]	-	-	A,D
4127 ± 15[k]	2333 ± 15[k]	$1/2^+,3/2^+,5/2^+$ [j]	-	-	-	-	-	-	-	A,H
4281 ± 20	2491 ± 20	-	-	-	23±12	-	-	-	-	A
4417 ± 5	2631 ± 5	m	-	-	170±50	-	-	-	-	A,(H)[m]
4435 ± 5	2649 ± 5	m	-	-	113±34	0.75±0.27	-	-	-	A,C,(H)[m]
4523 ± 20	2740 ± 20	$1/2^+$ [a]	0.5±0.3[b]	0.0005	29±23	-	0.5±0.3[b]	-	29±23	A,D
4585 ± 13	2804 ± 13	$1/2^-$ [a]	90[a]	0.24	700±210	-	90[a]	-	700±210	A,D
4659 ± 10	2880 ± 10	$1/2^+,3/2^+,5/2^+$ [j]	-	-	53±20	-	-	-	-	A,H
4721 ± 10	2944 ± 10	≥5/2[c]	-	-	98±42	18±5	-	-	-	A,C,D
4833 ± 13	3059 ± 13	$3/2^+,5/2^+$ [a]	0.20±0.08[b,h]	0.002	52±21	32±10	0.20±0.08[b,h]	16±5[h]	26±11[h]	A,C,D
5018 ± 3	3249 ± 3	$3/2^+,5/2^+$; (3/2)	0.60±0.15[h]	0.004	33±17	3.1±0.6	0.60±0.15[h]	1.6±0.3[h]	17±9[h]	A,C,D,(H)[m]
5048 ± 3	3280 ± 3	$3/2^+,5/2^+$; (3/2)	0.04±0.02[h]	0.0003	110±50	0.84±0.28	0.04±0.02[h]	0.42±0.14[h]	55±25[h]	A,C,D,(H)[m]
5116 ± 5[e]	3348 ± 5[e]	$1/2^+$ [a]	0.2±0.1[b]	0.0001	50±30	-	0.2±0.1[b]	-	50±30	A,D
5127 ± 4	3359 ± 4	$5/2^-$ [g]	0.5±0.2[b]	0.036	50±30	354±53	0.3±0.1[b]	200±110	17±10	A,C,D
5207 ± 8	3444 ± 8	-	-	-	180±80	3±2	-	-	-	A,C
5258 ± 5	3496 ± 5	$3/2^-$ [a]	17[a]	0.018	139±60	316±50	17[a]	158±25	70±30	A,C,D
5318 ± 6	3558 ± 6	3/2 [n]	-	-	48±24	200±60	-	-	-	A,C
5339 ± 9	3580 ± 9	-	-	-	-	-	-	-	-	C
5415 ± 6	3658 ± 6	-	-	-	-	-	-	-	-	A,C
5449 ± 6	3693 ± 6	-	-	-	-	-	-	-	-	A,C
5468 ± 6	3713 ± 6	3/2 [n]	-	-	-	-	-	-	-	A,C

Table 2

Table 2 continued.

Levels of ^{37}K above 5.56 MeV. See page 101 for the meaning of the superscripts with the addition that the superscript p denotes excitation energies that were derived from the proton resonance energies of reference n (page 101) and the 1857 keV Q-value for $^{36}Ar(p,\gamma)^{37}K$.

Table 2 continued.

Excitation Energy (keV)	Proton Energy (keV)	J^{π}	Reactions
5571 ± 15	3816 ± 15	$(5/2^-)^n$	A, C
5711 ± 20[p]	3960 ± 20[n]		C
5730 ± 20[p]	3980 ± 20[n]		A, C
5778 ± 20[p]	4030 ± 20[n]		A, C
5928 ± 20	4184 ± 20	m	A, C, (H)[m]
6012 ± 20[p]	4270 ± 20[n]	m	C, (H)[m]
6041 ± 20[p]	4300 ± 20[n]		A, C
6109 ± 20[p]	4370 ± 20[n]		C
6128 ± 20[p]	4390 ± 20[n]		A, C
6217 ± 20[p]	4480 ± 20[n]		A, C
6276 ± 20[p]	4540 ± 20[n]		C
6344 ± 20[p]	4610 ± 20[n]	m	A, C, (H)[m]
6375 ± 20[p]	4640 ± 20[n]	m	C, (H)[m]
6450 ± 20[p]	4720 ± 20[n]		A, C
6527 ± 20[p]	4800 ± 20[n]	m	A, C, (H)[m]
6625 ± 20[p]	4900 ± 20[n]	m	A, C, (H)[m]
6688 ± 15	4965 ± 15		A, C
(6865 ± 15)	(5147 ± 15)		C
6974 ± 20	5259 ± 20	$1/2^+, 3/2^+, 5/2^+$ [j]	A, C, H
7093 ± 15	5382 ± 15		A, C
(7518 ± 20)	(5818 ± 20)		A

Table 3.

The decay of ^{37}Ca to various levels in ^{37}K as reported by Poskanzer et al. (1966). The first column represents the delayed proton energy following the decay of ^{37}Ca plus 1857 keV, which represents the excitation energy in ^{37}K. The second column represents the level or levels taken from table 2 which corresponds to the number in the first column. The third column is the percentage of all decays proceeding to a given level and column four is the log ft value for that level. About 16% of the decay is presumed to populate the ground state of ^{37}K, and the rest is not yet accounted for but may involve transitions to bound levels in ^{37}K (Poskanzer et al., 1966). Each of the levels populated by the allowed decays should have a spin of $1/2^+$, $3/2^+$, or $5/2^+$, as is indicated in table 2 and figure 54. Most of the decay is to the T = 3/2 level or levels near 5.04 MeV excitation energy. (page 71)

Table 3

E_{cm} + 1857 (keV)	^{37}K level (keV)	%	log ft
	Ground State	(16)	(5.06)
3597 ± 30	3623 ± 15	4.0	4.8
3827 ± 40	3844 ± 10	3.0	4.8
4097 ± 60	4127 ± 15	1.5	5.0
4397 ± 60	4417 ± 5 4435 ± 5	3.0	4.7
4627 ± 60	4659 ± 10	3.5	4.5
5021 ± 20	5018 ± 3 5048 ± 3	50.0	3.2
5977 ± 30	5928 ± 20 6012 ± 20	1.0	4.5
6347 ± 60	6344 ± 20 6375 ± 20	0.5	4.7
6557 ± 60	6527 ± 20 6625 ± 20	0.5	4.6
6987 ± 30	6974 ± 20	0.4	4.5

Figure 1.

The gas cell used for most of the gamma-ray work. The entrance foil was epoxied in place and the beam catcher was made of platinum or rolled gold for the early experiments and was changed to evaporated gold for the later experiments. The suppressor ring was found to be unnecessary and was later removed. The thin-walled chamber presents very little attenuation to positrons and gamma rays with energies above 1 MeV. (page 6)

Figure 1

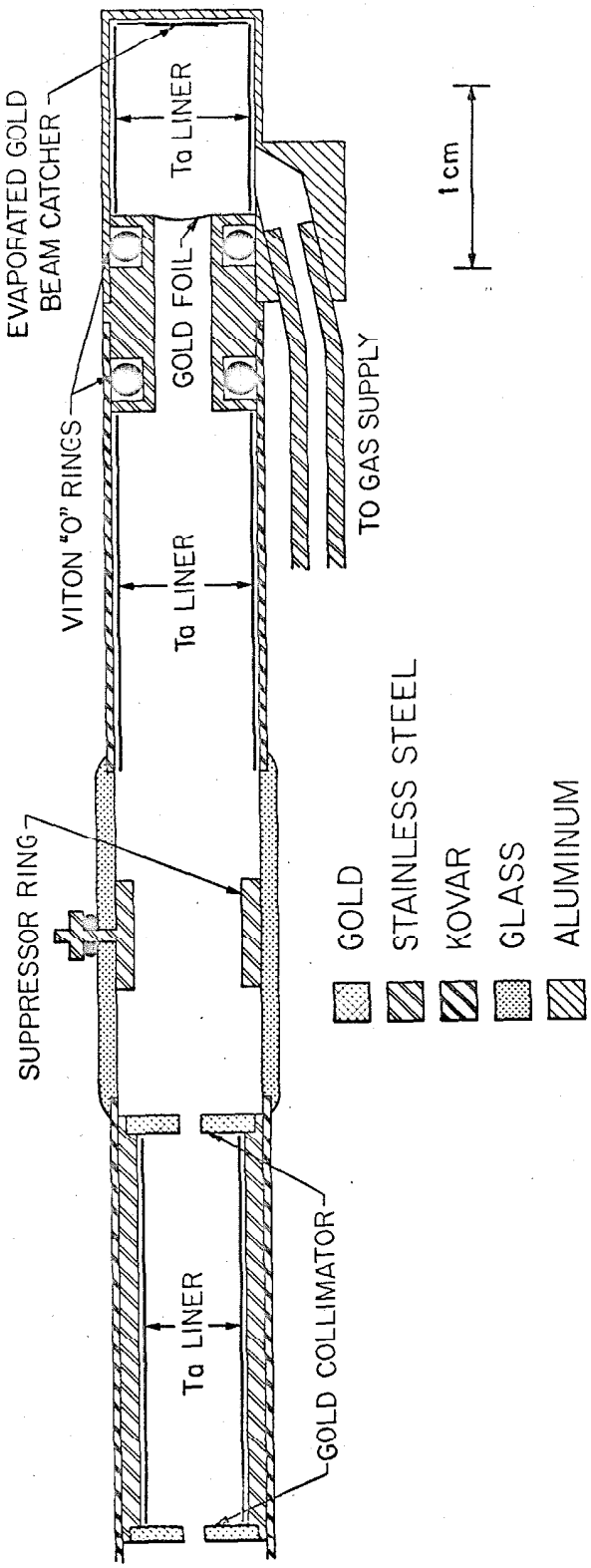
EVAPORATED GOLD BEAM CATCHER
Ta LINER
GOLD FOIL
VITON "O" RINGS
TO GAS SUPPLY
Ta LINER
SUPPRESSOR RING
Ta LINER
GOLD COLLIMATOR
1 cm
GOLD
STAINLESS STEEL
KOVAR
GLASS
ALUMINUM

Figure 2.

The yield of delayed positrons vs. bombarding energy from the reaction $^{36}Ar(p,\gamma)^{37}K(\beta^{+})^{37}Ar$ seen with 45 keV resolution. The abscissa includes energy loss in the entrance foil. The upper curve is the number of counts (above about 1 MeV positron energy) occurring within four seconds after chopping the beam and the lower curve is the difference between those occurring in successive two-second intervals. The lower curve discriminates against long-lived activity. The peak labeled 3.50 MeV is uncertain. (page 6)

Figure 2

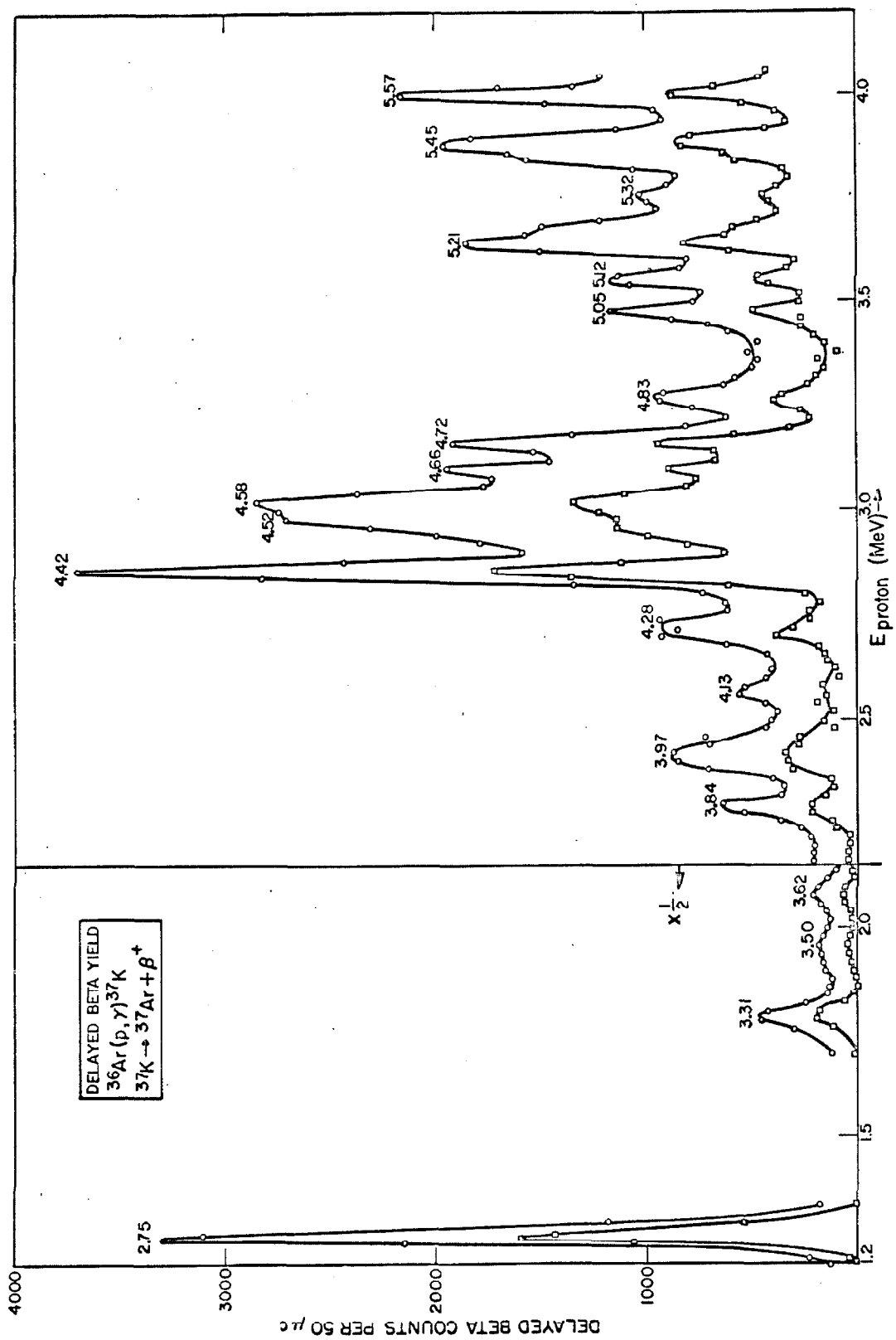
DELAYED BETA YIELD
$^{36}Ar(p,\gamma)^{37}K$
$^{37}K \rightarrow {}^{37}Ar + \beta^+$
DELAYED BETA COUNTS PER 50 μc
4000
3000
2000
1000
$\times\frac{1}{2}$
2.75
3.31
3.50
3.62
3.84
3.97
4.13
4.28
4.42
4.52
4.58
4.66
4.72
4.83
5.05
5.12
5.21
5.32
5.45
5.57
1.2
1.5
2.0
2.5
3.0
3.5
4.0
E_{proton} (MeV)

Figure 3.

The yield of 1.97 MeV gamma rays from inelastic scattering as seen by a 7.6 by 7.6 cm NaI(Tl) crystal with about 35 keV resolution. The abscissa includes energy loss in the entrance foil. Below 2.8 MeV the yield is very weak, but above this energy its strength made the investigation of gamma rays from $^{36}Ar(p,\gamma)^{37}K$ not feasible. (page 6)

Figure 3

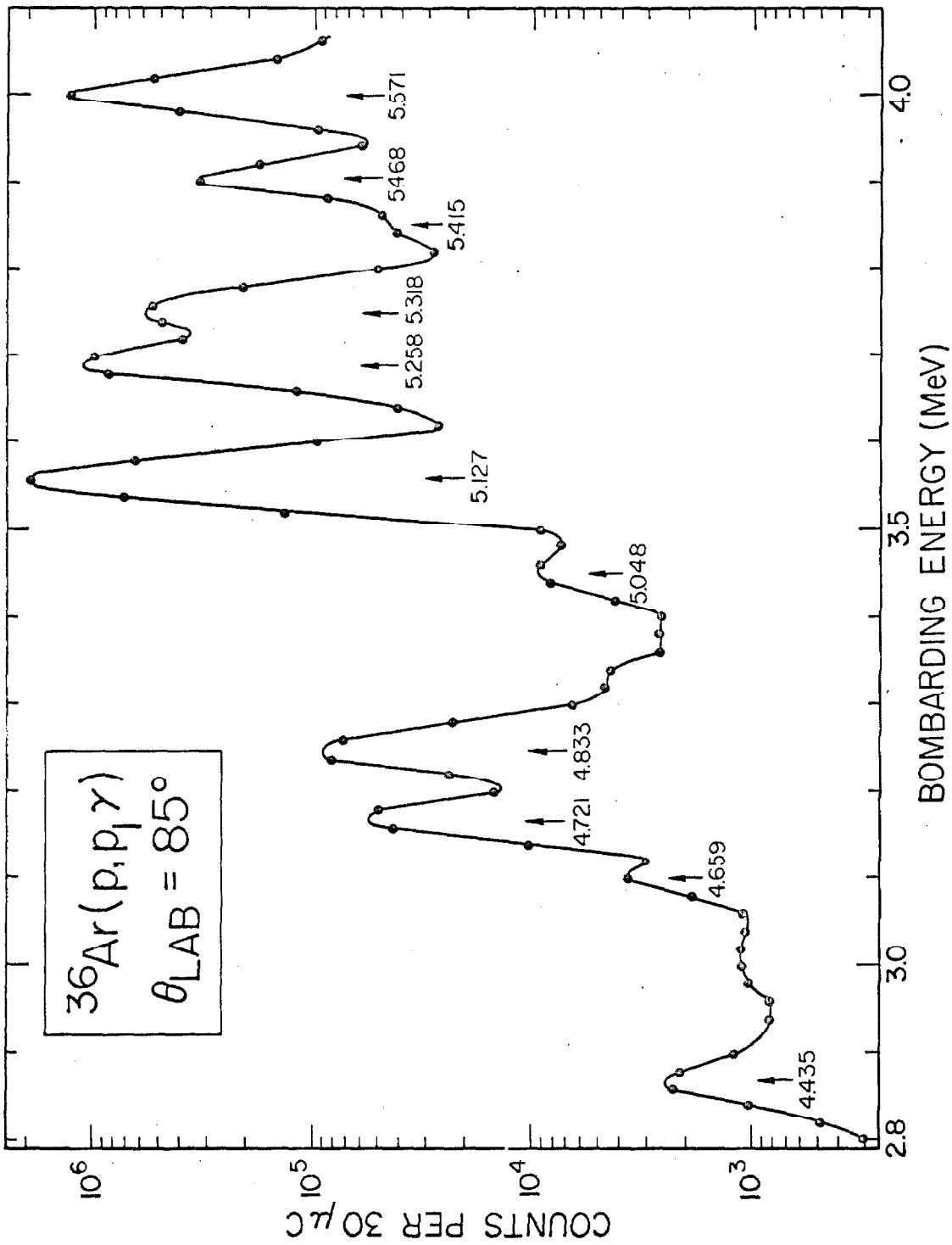
$^{36}Ar(p,p_1\gamma)$
$\theta_{LAB} = 85°$
4.435
4.659
4.721
4.833
5.048
5.127
5.258
5.318
5.415
5.468
5.571
COUNTS PER 30 μC
BOMBARDING ENERGY (MeV)
2.8
3.0
3.5
4.0

Figure 4.

The yield of delayed positrons and 1.97 MeV gamma rays from the proton bombardment of ^{36}Ar vs. proton energy seen with about 40 keV resolution. The lower curve represents delayed positrons as counted by the difference scaler (see page 6), and the upper curve is the yield of 1.97 MeV gamma rays seen by a 7.6 by 7.6 cm NaI(Tl) crystal placed at 90^{o} to the beam and outside of the positron counter. The upper curve is distorted vertically because of dead time, which was about 55% for the peak labeled 6.14 MeV. The numbers by each peak represent excitation energies in MeV. The abscissa includes energy loss in the foil. The region of excitation energy between 5.6 and 6.68 MeV has been covered in the inelastic scattering reaction with better resolution by Skeppstedt et al. (1966) who finds that several of these bumps are at least double. (page 7)

Figure 4

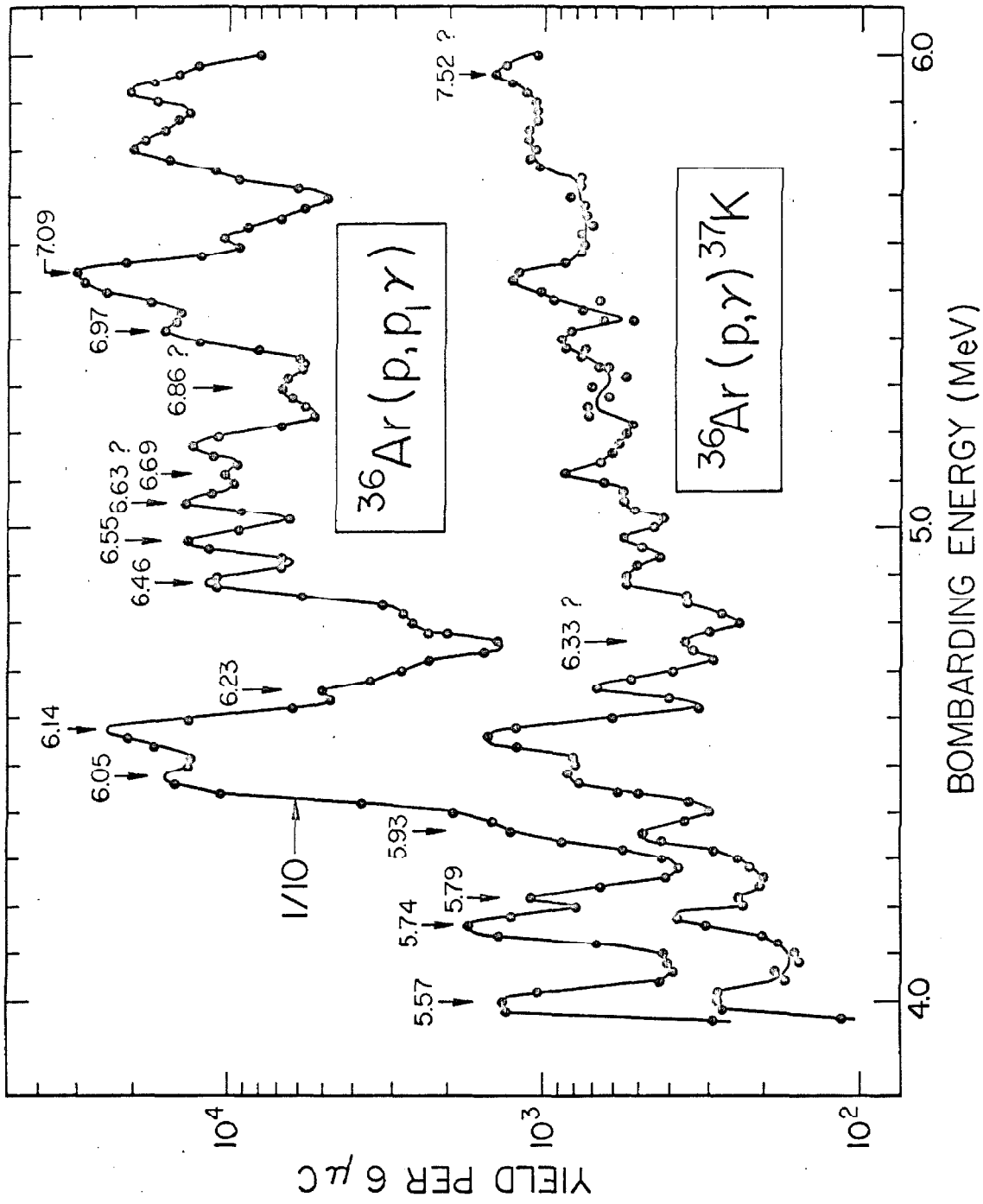
YIELD PER 6 μC
BOMBARDING ENERGY (MeV)
$^{36}Ar(p,p_1\gamma)$
$^{36}Ar(p,\gamma)^{37}K$
1/10
6.14
6.05
6.23
6.46
6.55
6.63 ?
6.69
6.86 ?
6.97
7.09
5.57
5.74
5.79
5.93
6.33 ?
7.52 ?

Figure 5.

The region of excitation energy between 4.9 and 5.5 MeV as seen by simultaneous runs measuring the yield of delayed positrons and gamma rays from inelastic scattering with about 15 keV resolution. The abscissa includes energy loss in the entrance foil. The middle curve represents counts in the sum scaler and the lower curve those in the difference scaler (see page 6). The two vertical lines denote the addition of target gas to compensate for leaks in the thin gold entrance foil. The curve on the right was taken with the positron counter removed, and is distorted vertically in a smooth way due to dead-time variations. The existence of the bump labeled 5.339 on the right-hand curve is confirmed by the results of Skeppstedt et al. (1966). (page 7)

Figure 5

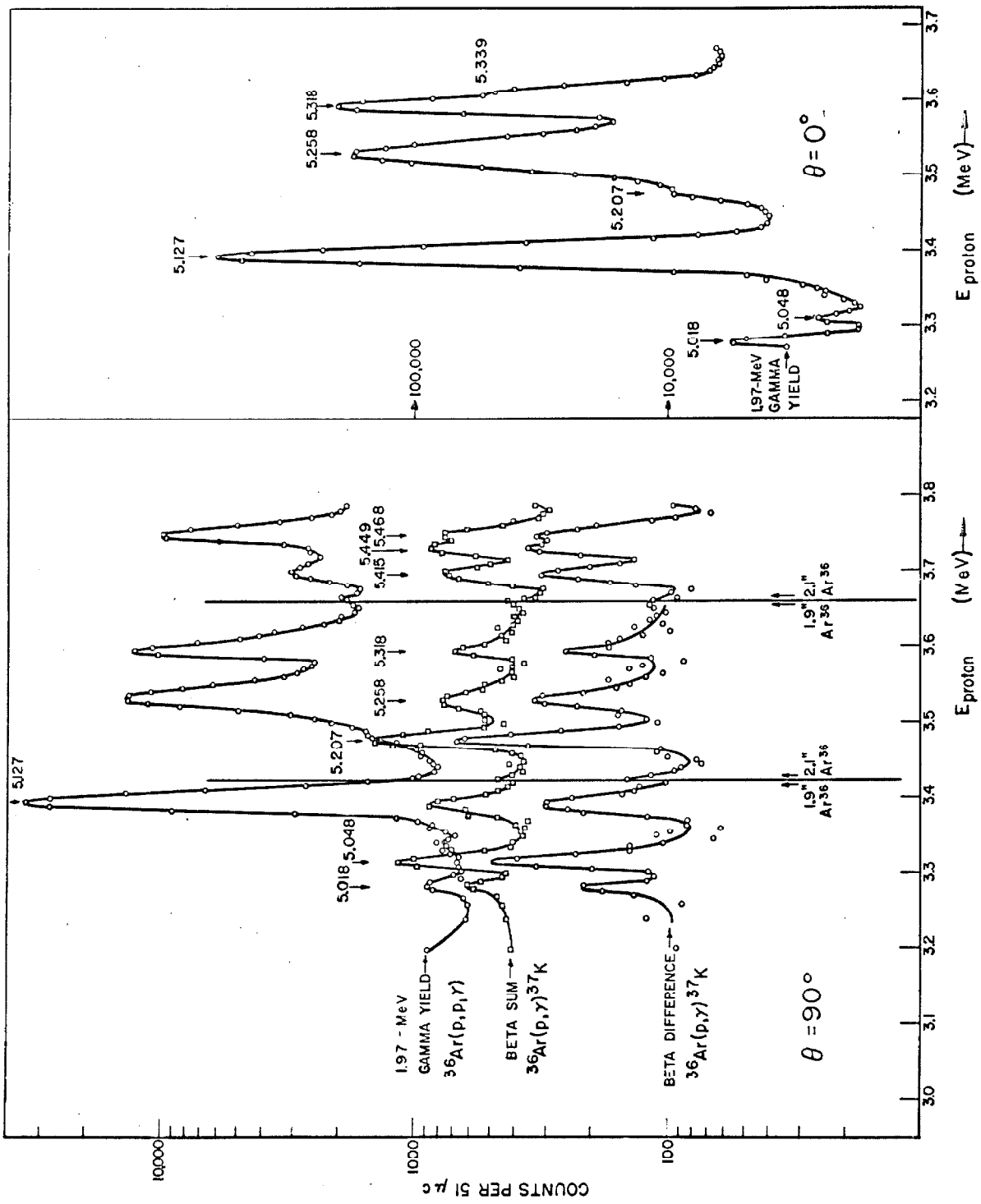
θ = 0°
θ = 90°
5.127
5.339
5.316
5.258
5.207
5.048
5.018
1.97-MeV GAMMA YIELD
100,000
10,000
5.449
5.415
5.468
1.9" Ar36
2.1" Ar36
1.97 - MeV GAMMA YIELD
36Ar(p,p,γ)
BETA SUM
36Ar(p,γ)37K
BETA DIFFERENCE
36Ar(p,γ)37K
COUNTS PER 51 μc
E proton (MeV)

Figure 6.

The peak labeled 4.42 MeV excitation energy in figure 2 as seen with about 16 keV resolution. The bottom curve shows that inelastic scattering is relatively weak for the lower member of the doublet. (page 8)

Figure 6

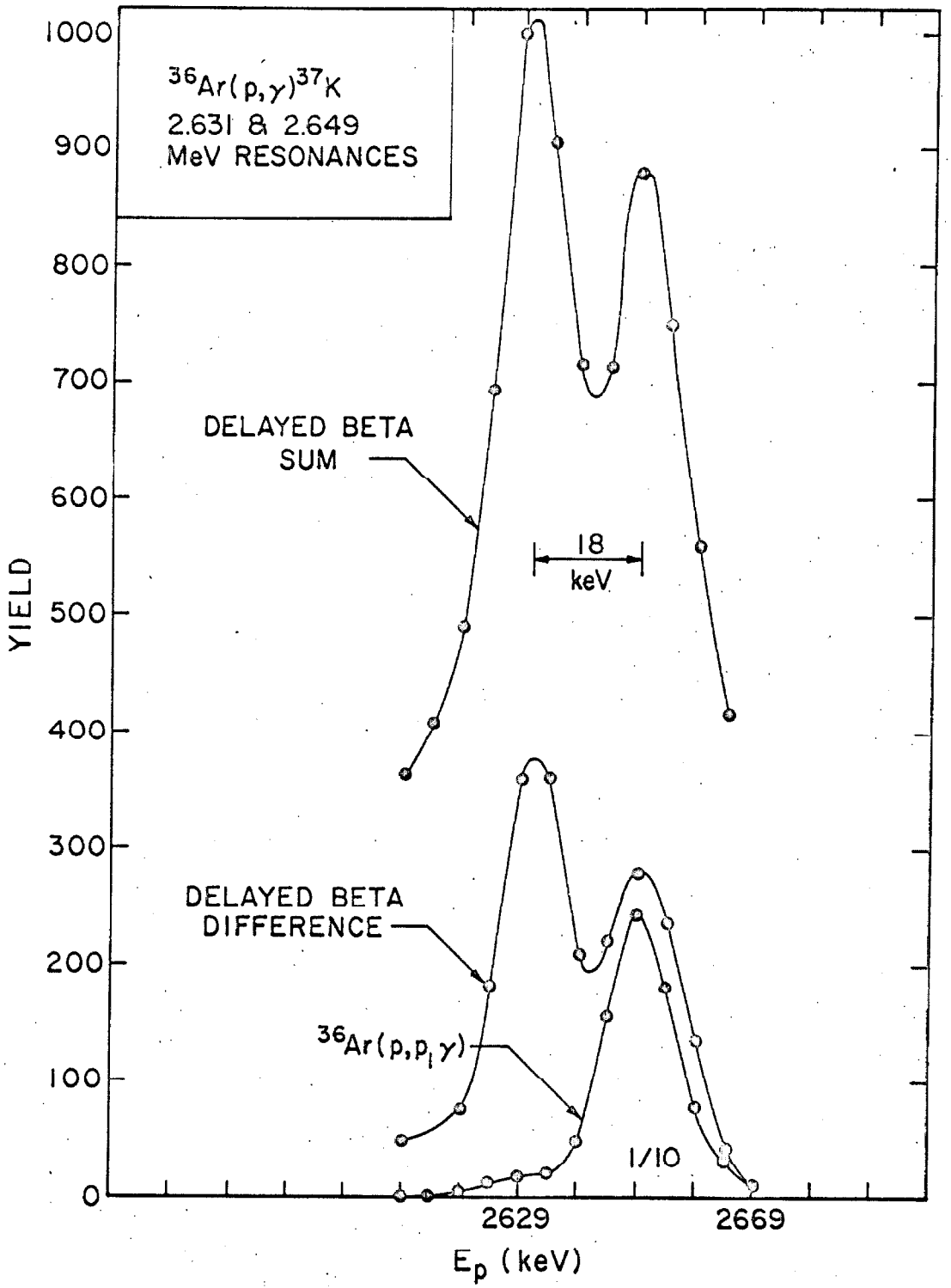
$^{36}Ar(p,\gamma)^{37}K$
2.631 & 2.649
MeV RESONANCES
DELAYED BETA
SUM
18
keV
DELAYED BETA
DIFFERENCE
$^{36}Ar(p,p_1\gamma)$
1/10
YIELD
1000
900
800
700
600
500
400
300
200
100
0
2629
2669
E_p (keV)

Figure 7.

The calibration of the proton bombarding energy of the 5.048 MeV level by comparison with a $^{28}Si(p, p'\gamma)$ resonance nearby. The natural width of the silicon resonance is 10 keV, and the resolution is 8.5 keV. The proton momentum is in frequency units of the NMR device used to determine the field in the analyzing magnet. (page 8)

Figure 7

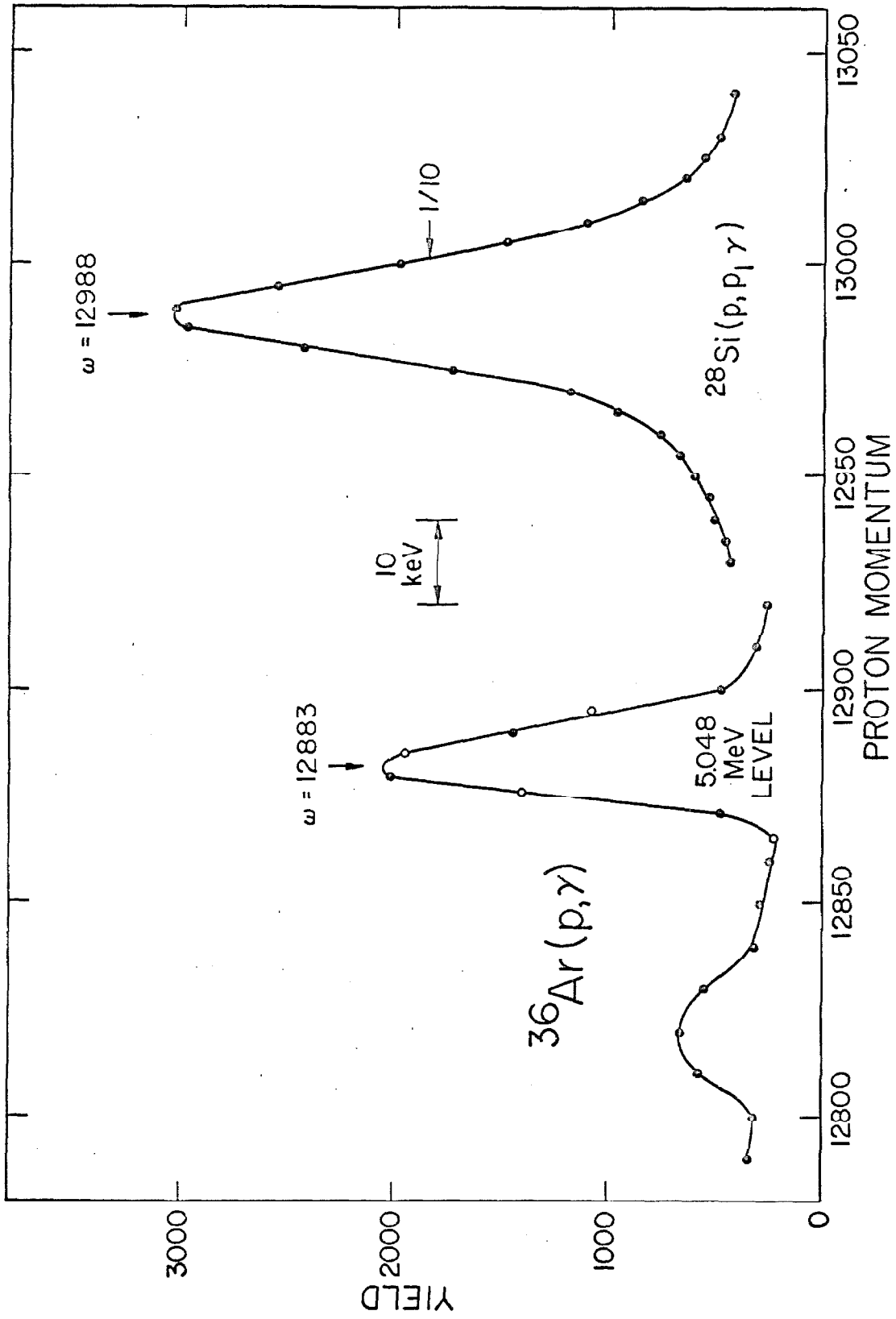
YIELD
3000
2000
1000
0
12800
12850
12900
12950
13000
13050
PROTON MOMENTUM
$^{36}Ar(p,\gamma)$
$^{28}Si(p,p_1\gamma)$
ω = 12883
ω = 12988
5048 MeV LEVEL
10 keV
1/10

Figure 8.

The 1.97 MeV gamma-ray spectrum from inelastic scattering seen in a 7.6 by 7.6 cm NaI(Tl) crystal. This spectrum was used in calibrating the widths of the 5127 keV level. See appendix B for details. (page 14)

Figure 8

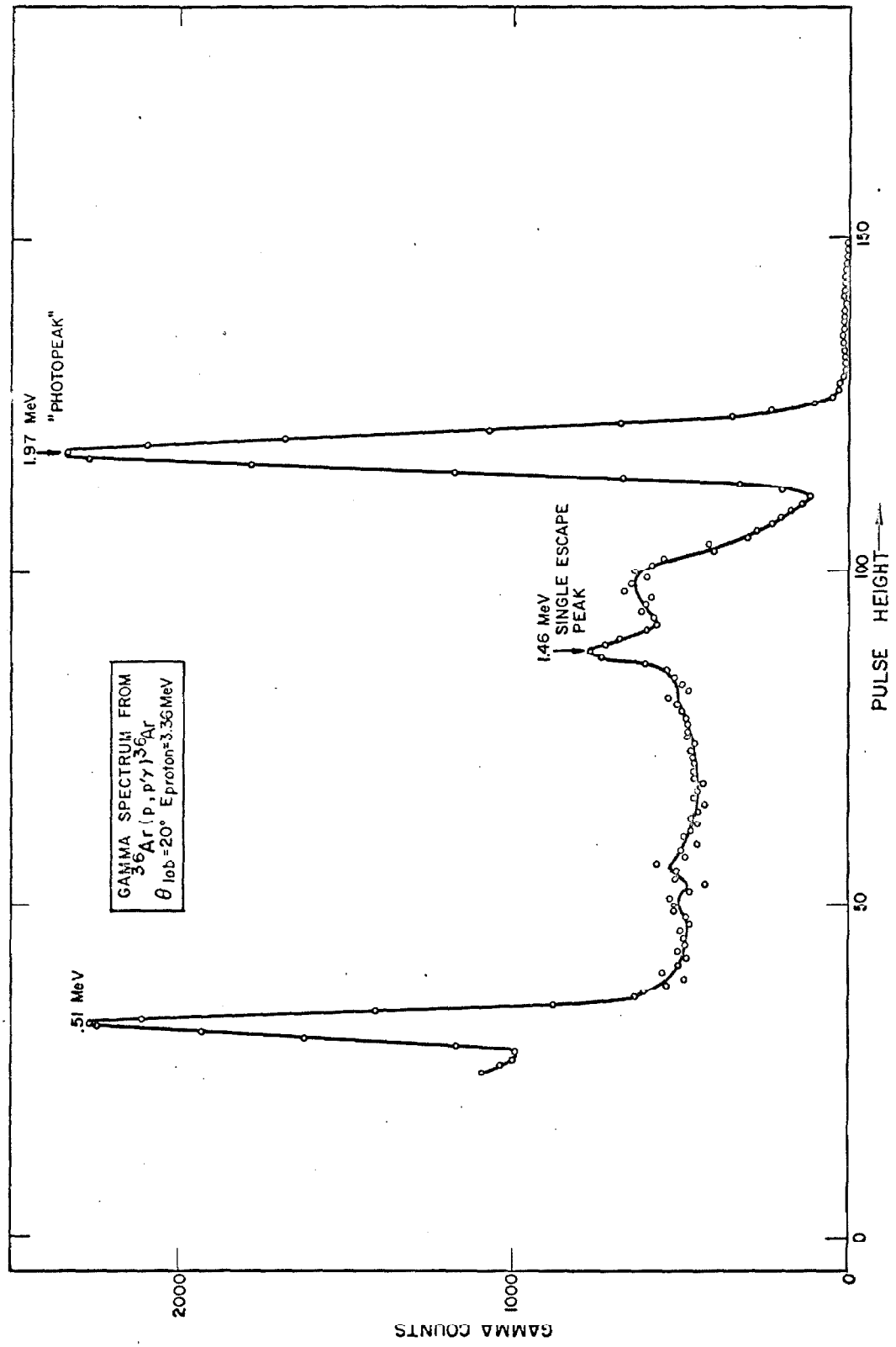
GAMMA SPECTRUM FROM
36Ar(p,p'γ)36Ar
θ lab = 20° Eproton = 3.36 MeV
.51 MeV
1.46 MeV
SINGLE ESCAPE
PEAK
1.97 MeV
"PHOTOPEAK"
GAMMA COUNTS
2000
1000
0
0
50
100
150
PULSE HEIGHT

Figure 9.

The observed angular distribution of 1.97 MeV gamma rays from inelastic scattering through the 5127 keV level in ^{37}K. The error bars are equal to the size of the dots and the solid line is the theoretical angular distribution for $J^{\pi} = 5/2^{-}$ and $j = 3/2$. (page 14)

Figure 9

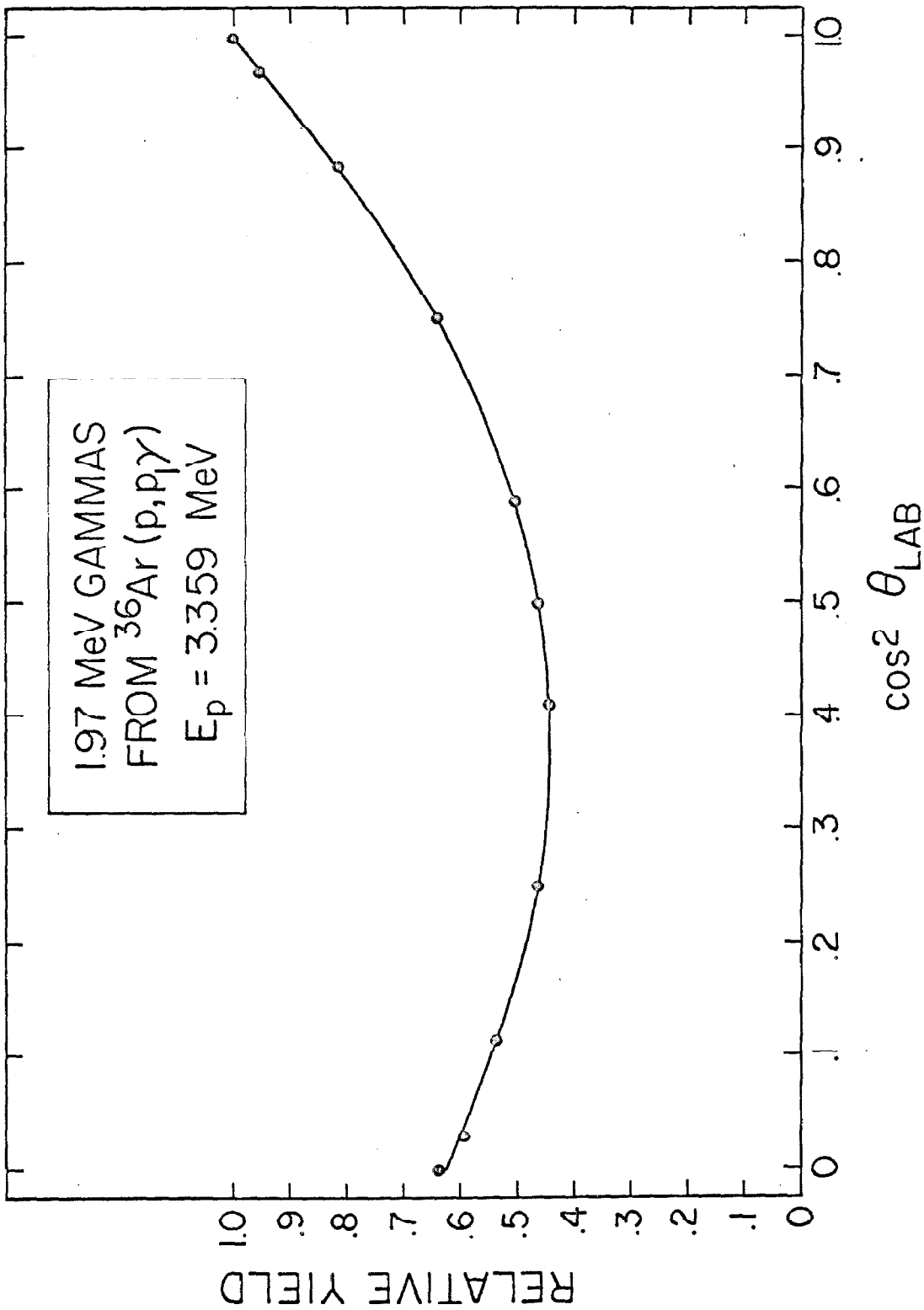
1.97 MeV GAMMAS
FROM ^{36}Ar (p,pγ)
E_p = 3.359 MeV
RELATIVE YIELD
0
.1
.2
.3
.4
.5
.6
.7
.8
.9
1.0
cos² θ_{LAB}
0
.1
.2
.3
.4
.5
.6
.7
.8
.9
1.0

Figure 10.

The observed angular distribution of 1.97 MeV gamma rays from inelastic scattering through the 5258 keV level in ^{37}K. Error bars are about the size of the dots and the solid line is the best fit for $J^{\pi} = 3/2^{-}$. (page 15)

Figure 10

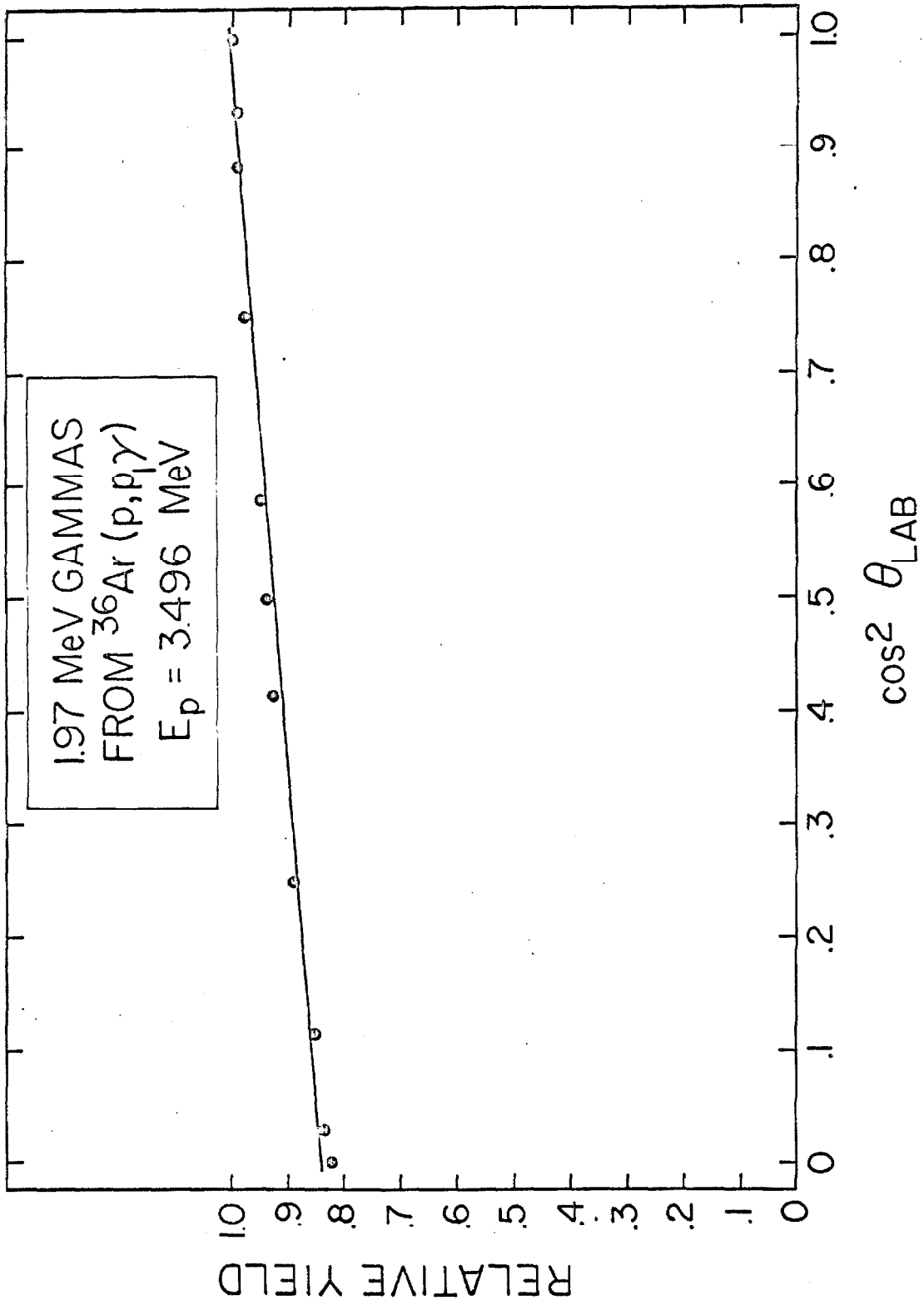
1.97 MeV GAMMAS
FROM ^{36}Ar (p,p$_1\gamma$)
E_p = 3.496 MeV
RELATIVE YIELD
0
.1
.2
.3
.4
.5
.6
.7
.8
.9
1.0
cos^2 θ_{LAB}

Figure 11.

The observed angular distribution of 1.97 MeV gamma rays from inelastic scattering through the 5018 keV level in ^{37}K. The solid line is a fit for $J^{\pi} = 3/2^{+}$ and the dashed line is approximately the best fit for $J^{\pi} = 5/2^{+}$. (page 16)

Figure 11

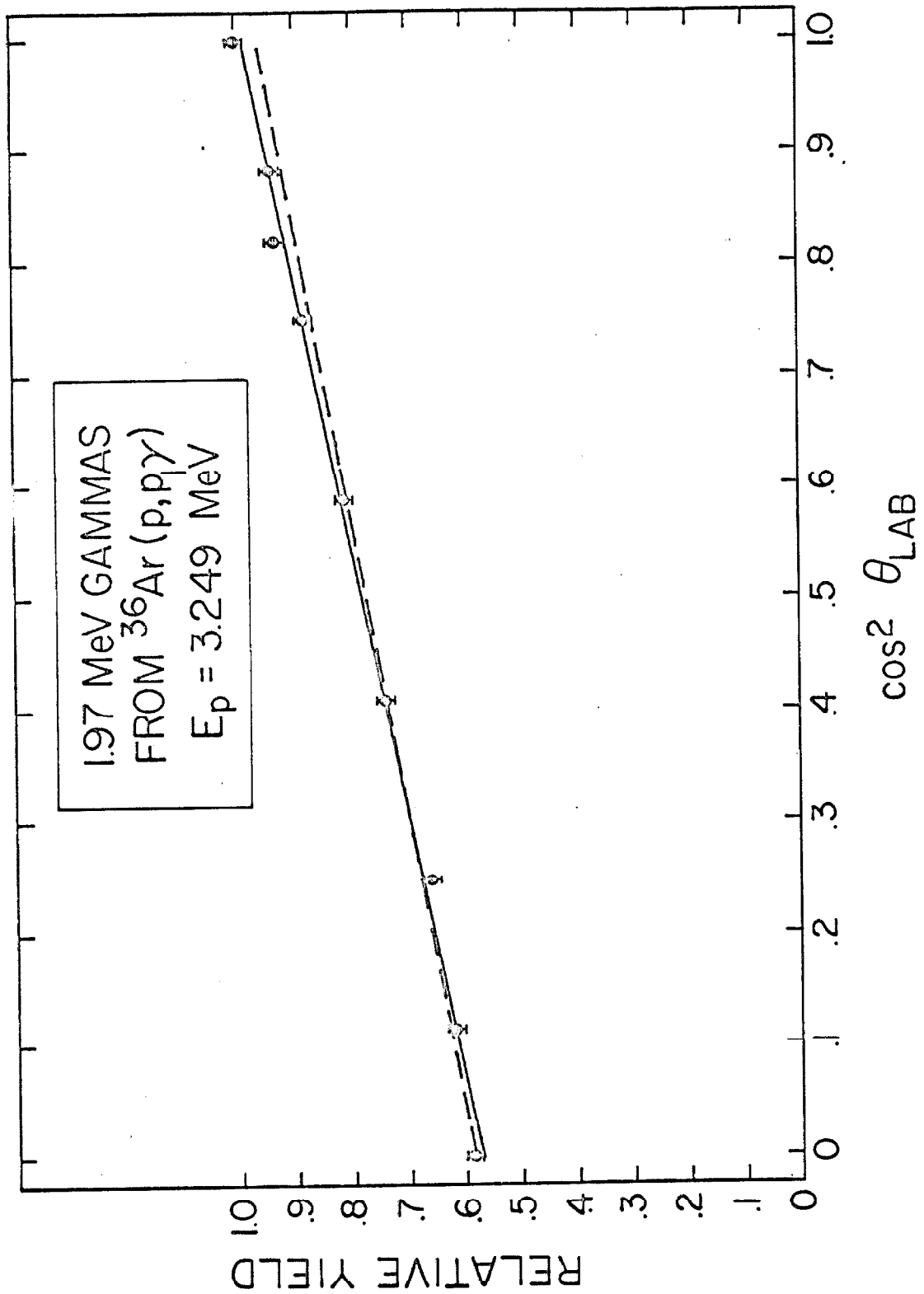
1.97 MeV GAMMAS
FROM ^{36}Ar(p,p$_1\gamma$)
E_p = 3.249 MeV
RELATIVE YIELD
0
.1
.2
.3
.4
.5
.6
.7
.8
.9
1.0
cos^2 θ_{LAB}

Figure 12.

The full width at half maximum of the yield from an infinitely narrow resonance when using a square target thickness and a gaussian beam-straggle profile. The solid curve represents the square target thickness folded into a gaussian straggle, while the dotted curve is the expression

$$\frac{Y}{FWHM} = \frac{(T^2 + FWHM^2)^{1/2}}{FWHM} ,$$

where T is the target thickness and FWHM is the full width at half maximum of the beam-energy profile, and Y is the full width at half maximum of the yield. It is seen that the correct (solid) curve represents a width considerably narrower than that which is simply obtained by taking the square root of the sum of the squares of the two widths. For example, 10 keV of gaussian-beam straggle folded into 15 keV of target thickness results in a curve whose FWHM is 15.7 keV!
(page 19)

Figure 12

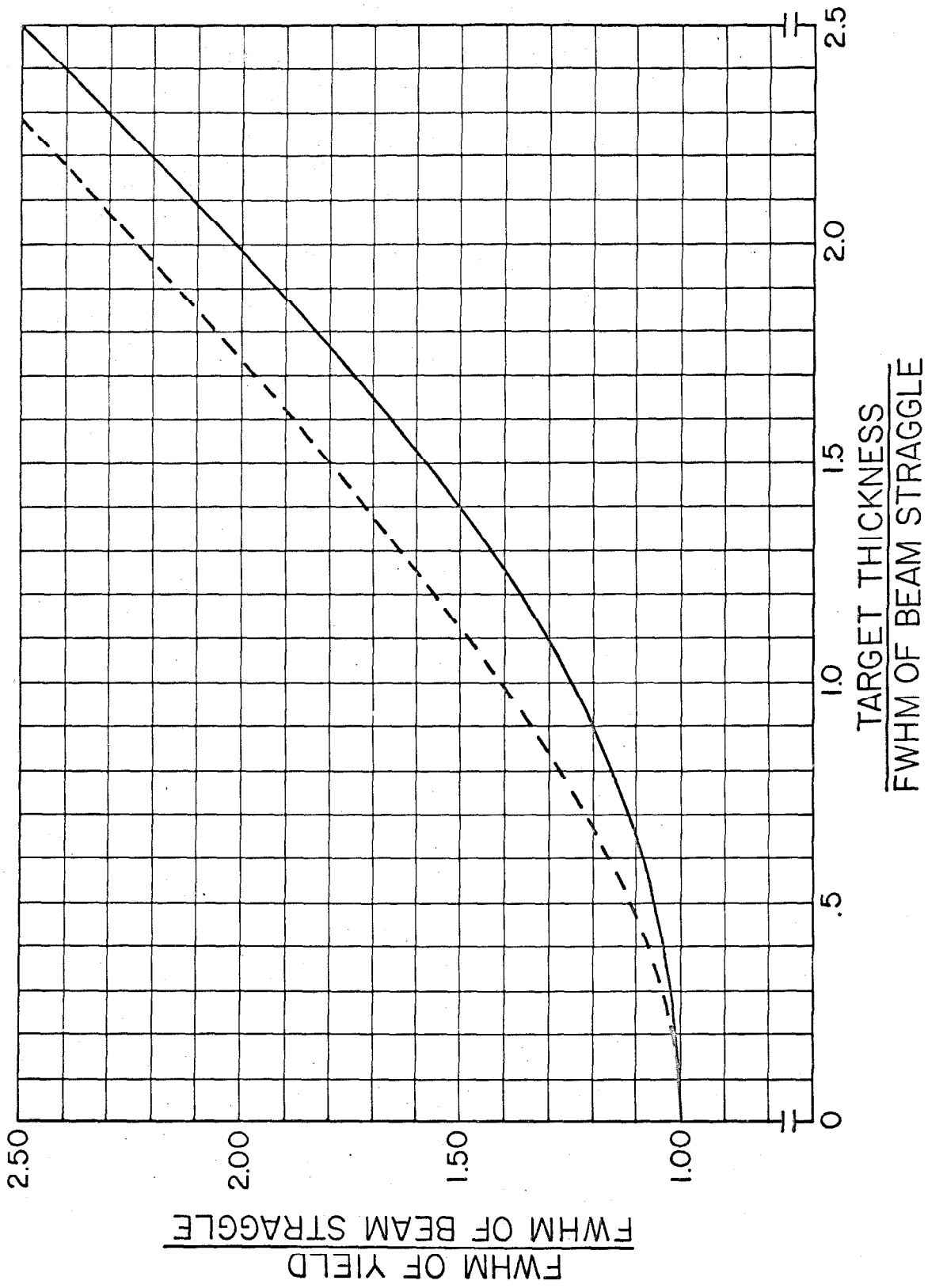
2.50
2.00
1.50
1.00
FWHM OF YIELD / FWHM OF BEAM STRAGGLE
0
.5
1.0
1.5
2.0
2.5
TARGET THICKNESS / FWHM OF BEAM STRAGGLE

Figure 13.

The maximum fraction of the beam that is available for undergoing a reaction through an infinitely narrow resonance as a function of the ratio of the target thickness to the FWHM of the beam-energy profile. The upper curve illustrates the case where this ratio is unity, and shows that when the centroid of the beam-energy profile is at the resonance energy plus one half of the target thickness, about 23% of the beam is never at the correct resonance energy anywhere throughout its passage through the target. (page 21)

Figure 13

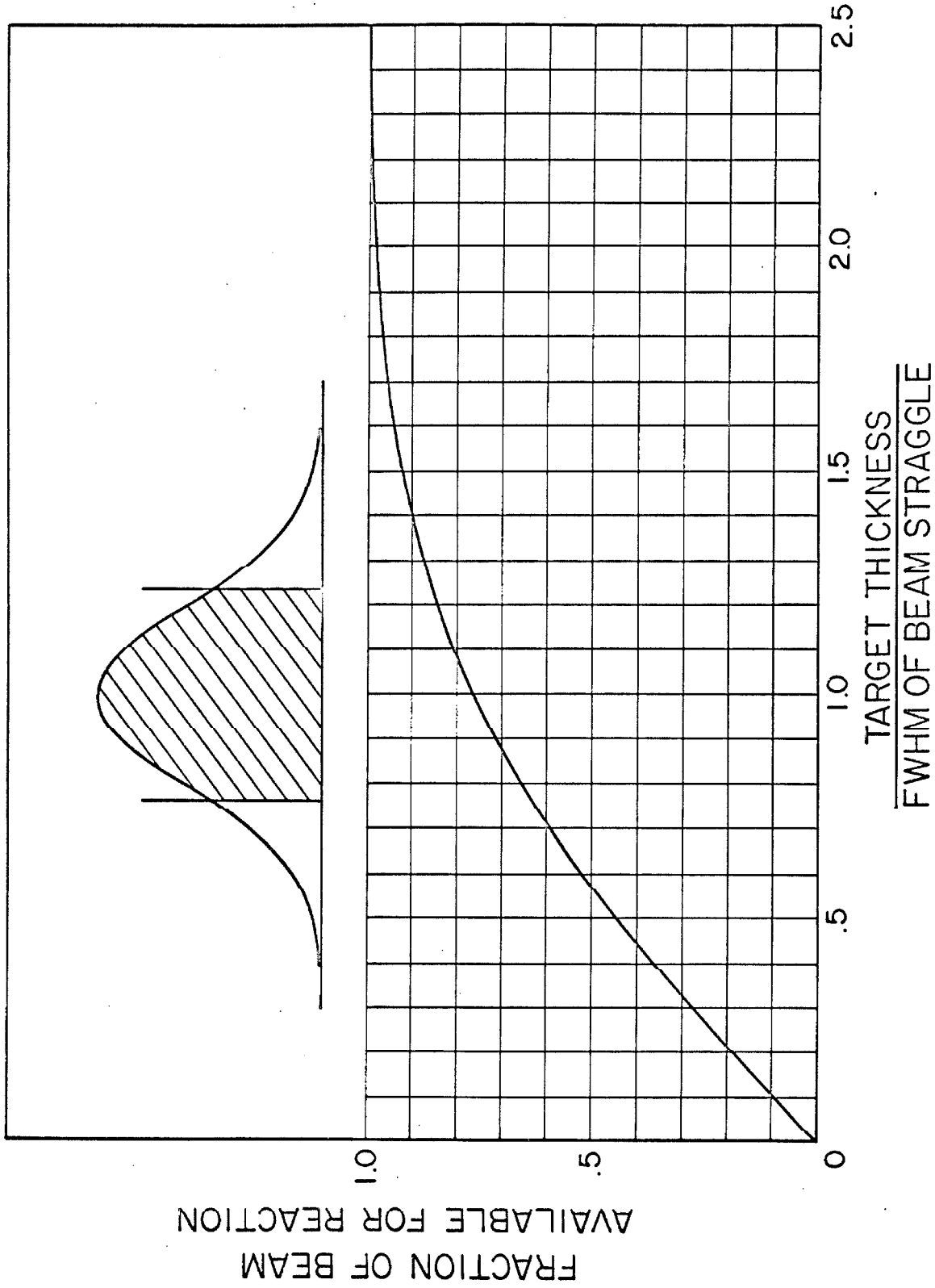
FRACTION OF BEAM
AVAILABLE FOR REACTION
1.0
.5
0
.5
1.0
1.5
2.0
2.5
TARGET THICKNESS
FWHM OF BEAM STRAGGLE

Figure 14.

This figure shows the theoretical elastic-scattering cross section vs. beam energy for a fixed angle for 1.26 MeV protons on ^{36}Ar. The curves on the left are those seen by perfect resolution for $\Gamma = \Gamma_p = 0.5$ keV, $J^\pi = 1/2^+$, and those on the right show the effect of having an experimental resolution of 2.35 keV FWHM. Rutherford scattering is assumed to be the only non-resonant type of scattering. Although this figure and the two to follow are for $E_p = 1.26$ MeV, most of the shapes remain the same for proton energies up to 3.5 MeV. (page 28)

Figure 14

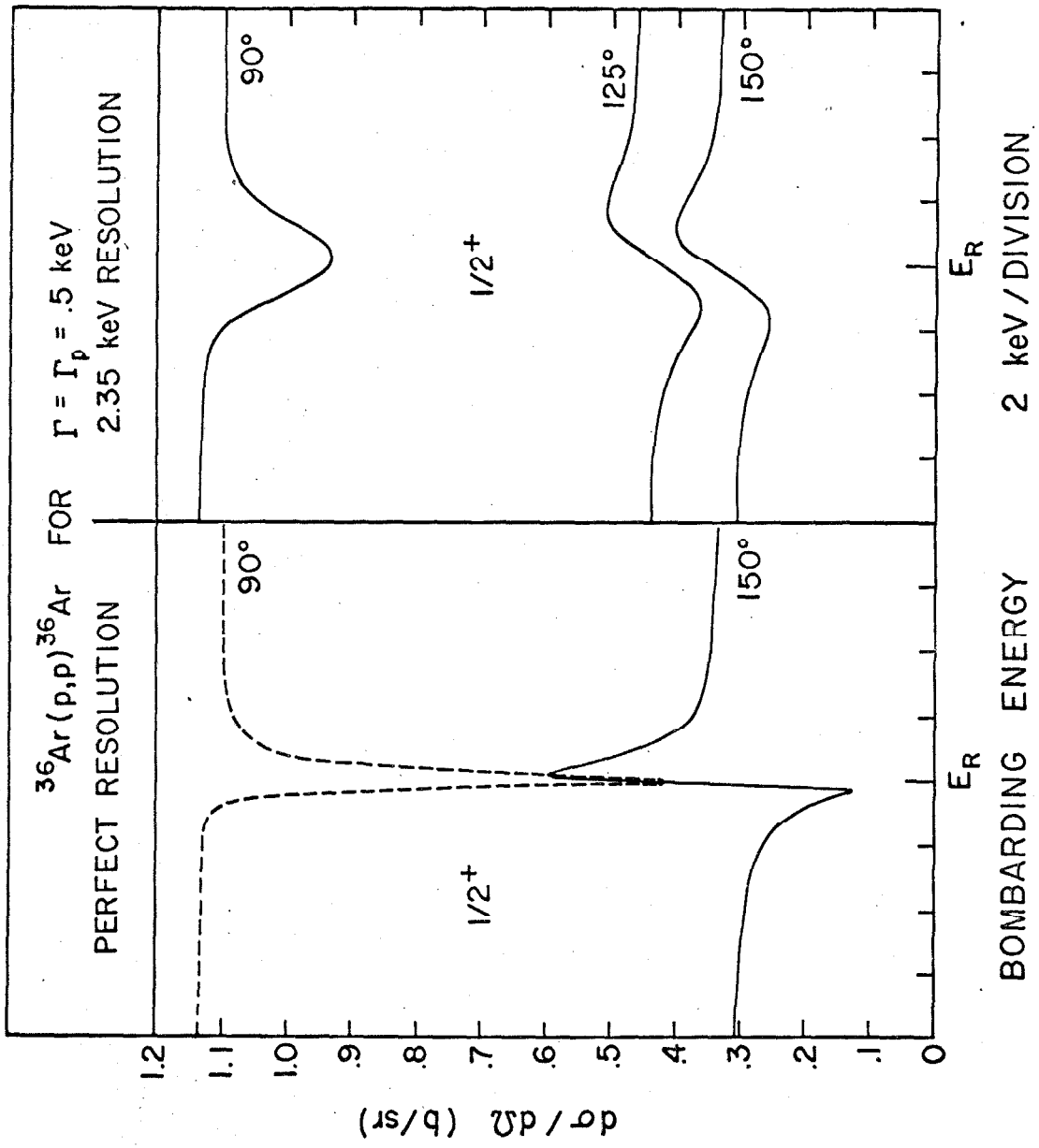
$^{36}Ar(p,p)^{36}Ar$ FOR $\Gamma = \Gamma_p = .5$ keV
2.35 keV RESOLUTION
PERFECT RESOLUTION
90°
125°
150°
$1/2^+$
E_R
2 keV / DIVISION
BOMBARDING ENERGY
$d\sigma/d\Omega$ (b/sr)
0
.1
.2
.3
.4
.5
.6
.7
.8
.9
1.0
1.1
1.2

Figure 15.

The elastic scattering differential cross section vs. beam energy for $\Gamma = \Gamma_p = 0.5$ keV as viewed with 2.35 keV resolution. The spin and parity of the compound level is shown in the center of each graph. Note the slight distinction between the curves for the two values of J allowed for a given value of ℓ. It is seen that the anomaly height divided by the Rutherford background is largest at the back angles, and thus the back angles are the most favorable ones experimentally. (page 28)

Figure 15

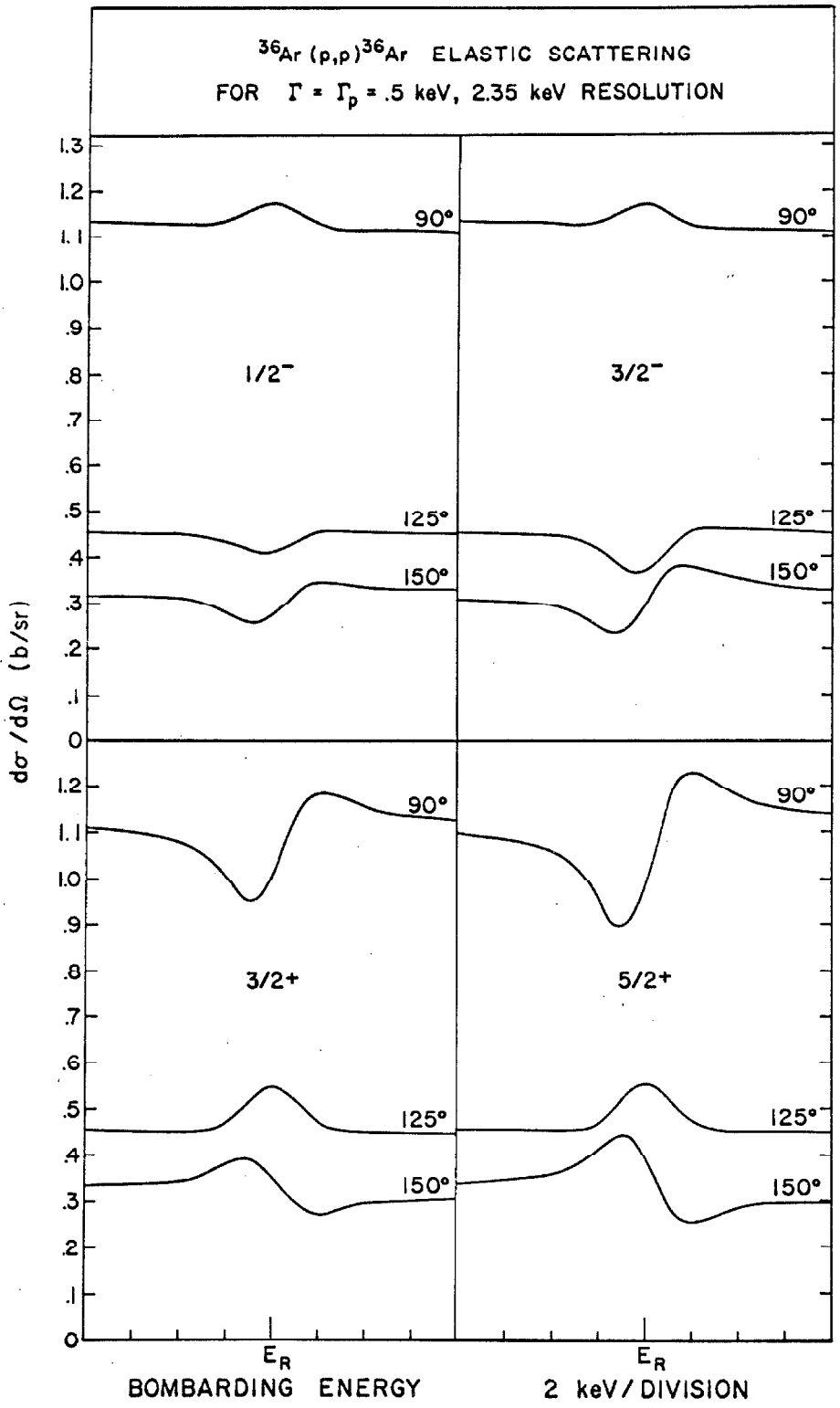
$^{36}Ar\ (p,p)^{36}Ar$ ELASTIC SCATTERING
FOR $\Gamma = \Gamma_p = .5$ keV, 2.35 keV RESOLUTION
1/2⁻
3/2⁻
3/2+
5/2+
90°
125°
150°
dσ/dΩ (b/sr)
E_R
BOMBARDING ENERGY
2 keV/DIVISION

Figure 16.

Elastic-scattering cross sections for $\ell = 3$ and 4. Comparison of figures 14, 15 and 16 reveals that as long as $\Gamma = \Gamma_p$, a measurement of the shape of the anomaly at 90^o and 150^o is sufficient to select the ℓ value if it is less than $\ell = 5$. Sometimes the measurement of the anomaly shape at only one angle will yield a unique value of ℓ. See for example the 150^o anomaly for $\ell = 2$. This is the case for the 5018 and 5048 keV levels in ^{37}K. (page 28)

Figure 16

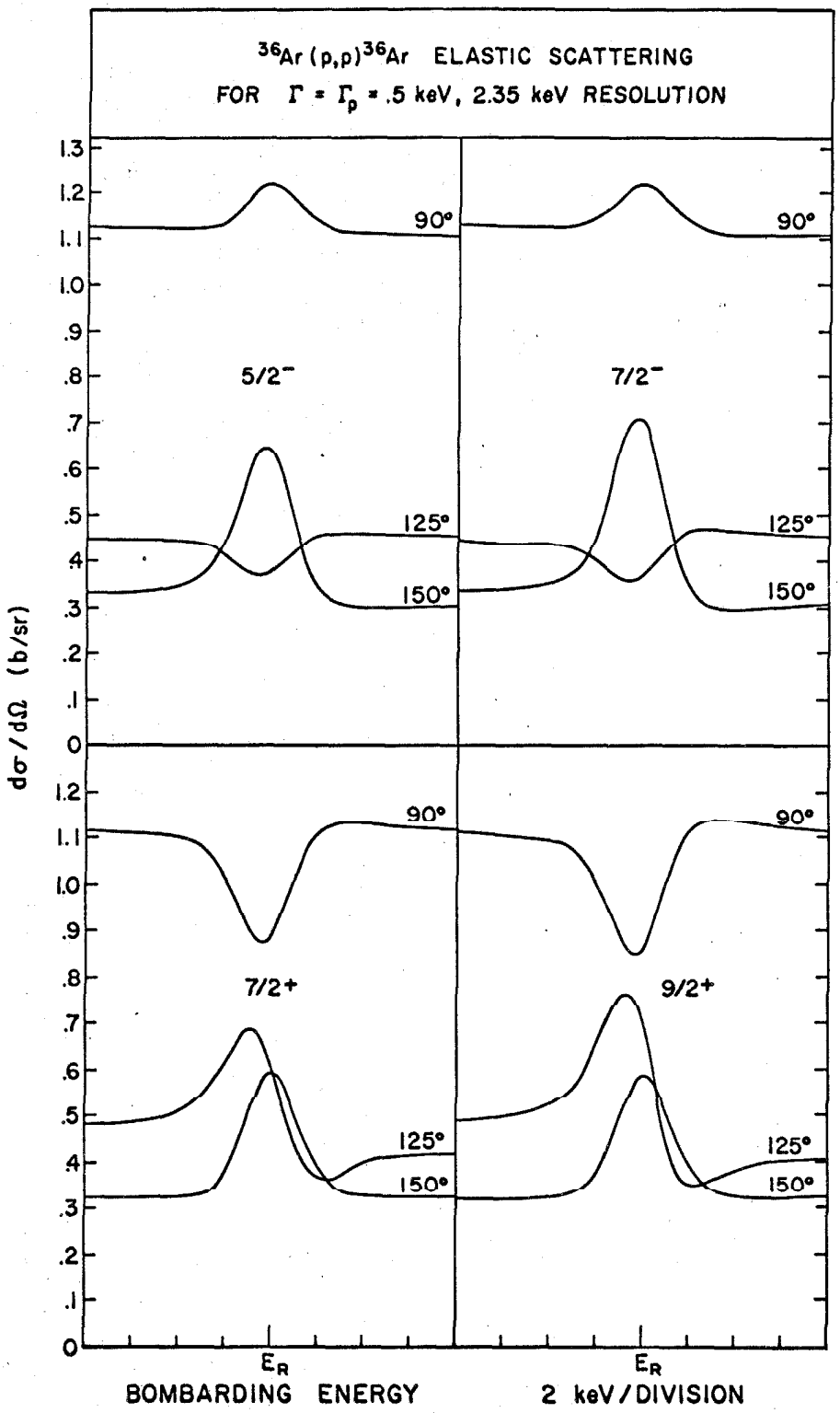
$^{36}Ar(p,p)^{36}Ar$ ELASTIC SCATTERING
FOR $\Gamma = \Gamma_p = .5$ keV, 2.35 keV RESOLUTION
90°
5/2⁻
125°
150°
90°
7/2⁻
125°
150°
90°
7/2+
125°
150°
90°
9/2+
125°
150°
dσ / dΩ (b/sr)
E_R
BOMBARDING ENERGY
E_R
2 keV / DIVISION

Figure 17.

Determination of the spin of the 3311 keV level by elastic scattering. The solid curve on the right is a fit (including the effect of the non-resonant phase shifts taken to be their very small hard-sphere values) for $J^{\pi} = 3/2^{-}$ with $\Gamma = \Gamma_p$ = 2.2 keV and an experimental resolution of 1.6 keV. The dashed curve is a shape for $J^{\pi} = 1/2^{-}$ with perfect resolution. The curve on the left is the width of the proton group seen by the spectrometer off resonance, where the resolution due to dE/dϑ and the slits of the spectrometer was 1.86 keV FWHM. The vertical scale is not calibrated. (page 30)

Figure 17

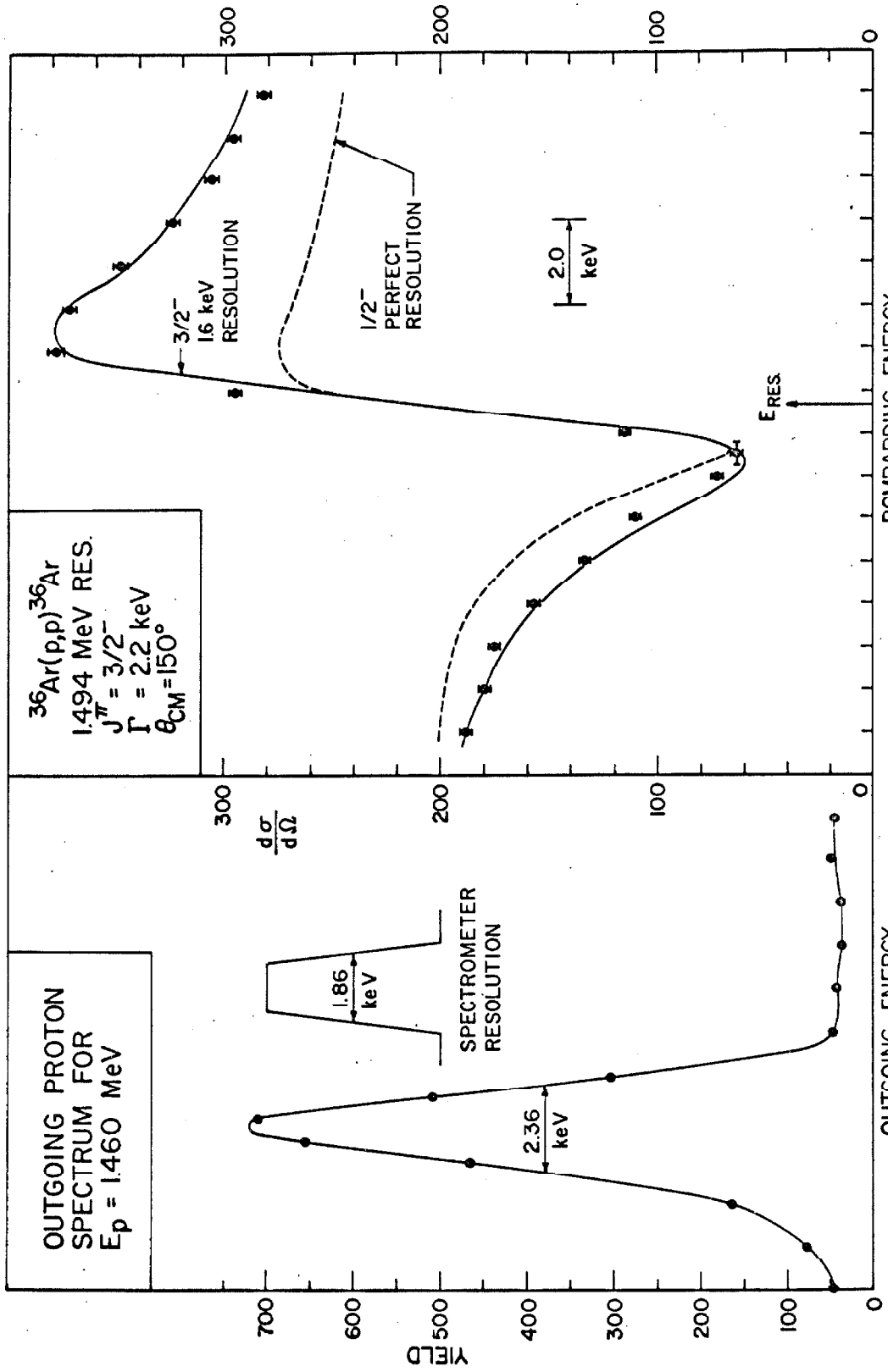
OUTGOING PROTON SPECTRUM FOR E_p = 1.460 MeV
YIELD
OUTGOING ENERGY
2.36 keV
1.86 keV
SPECTROMETER RESOLUTION
$\frac{d\sigma}{d\Omega}$
BOMBARDING ENERGY
$E_{RES.}$
$^{36}Ar(p,p)^{36}Ar$
1.494 MeV RES.
$J^{\pi} = 3/2^-$
Γ = 2.2 keV
θ_{CM}=150°
3/2⁻ 1.6 keV RESOLUTION
1/2⁻ PERFECT RESOLUTION
2.0 keV

Figure 18.

The elastic scattering anomalies for the 5018 and 5048 keV levels taken with the same target. The φ_ℓ have been taken as their small hard-sphere values, but the results are not sensitive to these phase shifts.

The existence of <u>any</u> anomaly at 3280 keV bombarding energy might be questioned after a first glance, but figures 5 and 7 show that there is definitely a resonance 30 ± 3 keV higher than the 3249 keV resonance. The high point on the 3280 keV anomaly is three standard deviations high. If the entire curve on the right were simply a statistical accident, then the probability that any of the seven points in the region 30 ± 3 keV above the 3249 keV resonance would be three standard deviations high is 0.01. It is noted that the separation between maximum and minimum in the 3249 keV anomaly is about 3 keV. Given that the point near 3280 keV is high, the probability that the point 3 keV higher be two standard deviations low is 0.02. Multiplying these two together justifies the existence of this anomaly. This anomaly was run with another target and the high and low points were again separated by 3 keV. (page 31)

Figure 18

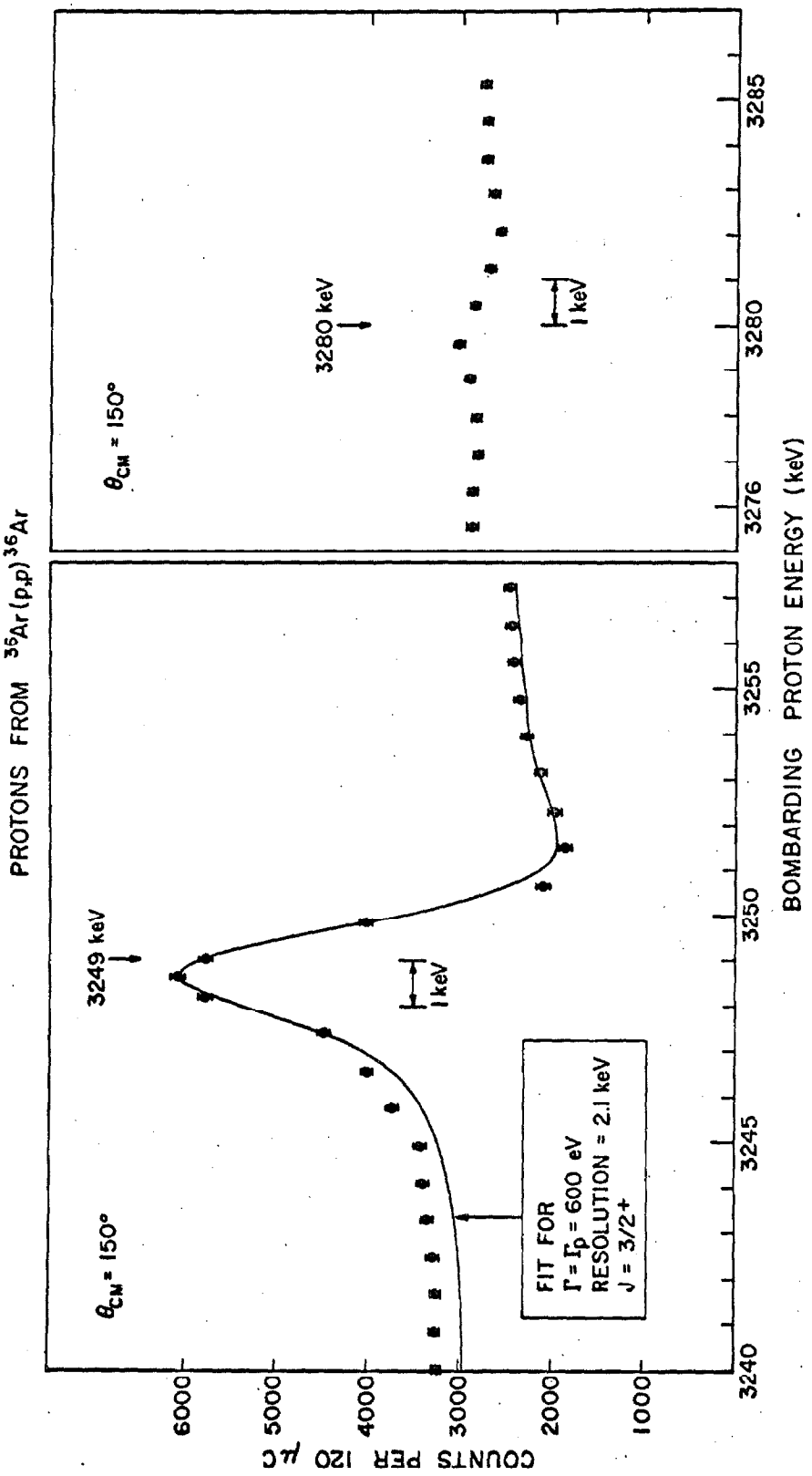
PROTONS FROM $^{35}Ar(p,p)^{35}Ar$
θ_{CM} = 150°
3249 keV
1 keV
FIT FOR
Γ = Γp = 600 eV
RESOLUTION = 2.1 keV
J = 3/2+
θ_{CM} = 150°
3280 keV
1 keV
COUNTS PER 120 μC
BOMBARDING PROTON ENERGY (keV)

Figure 19.

The elastic scattering cross section near the 1260 keV resonance. The resolution measurement before and after runs A and B is shown in figure 20. The expected shape of the anomaly for various spins and parities is given by figures 14-16. An upper limit of 430 counts is taken for the magnitude of any anomaly in this figure. (page 33)

Figure 19

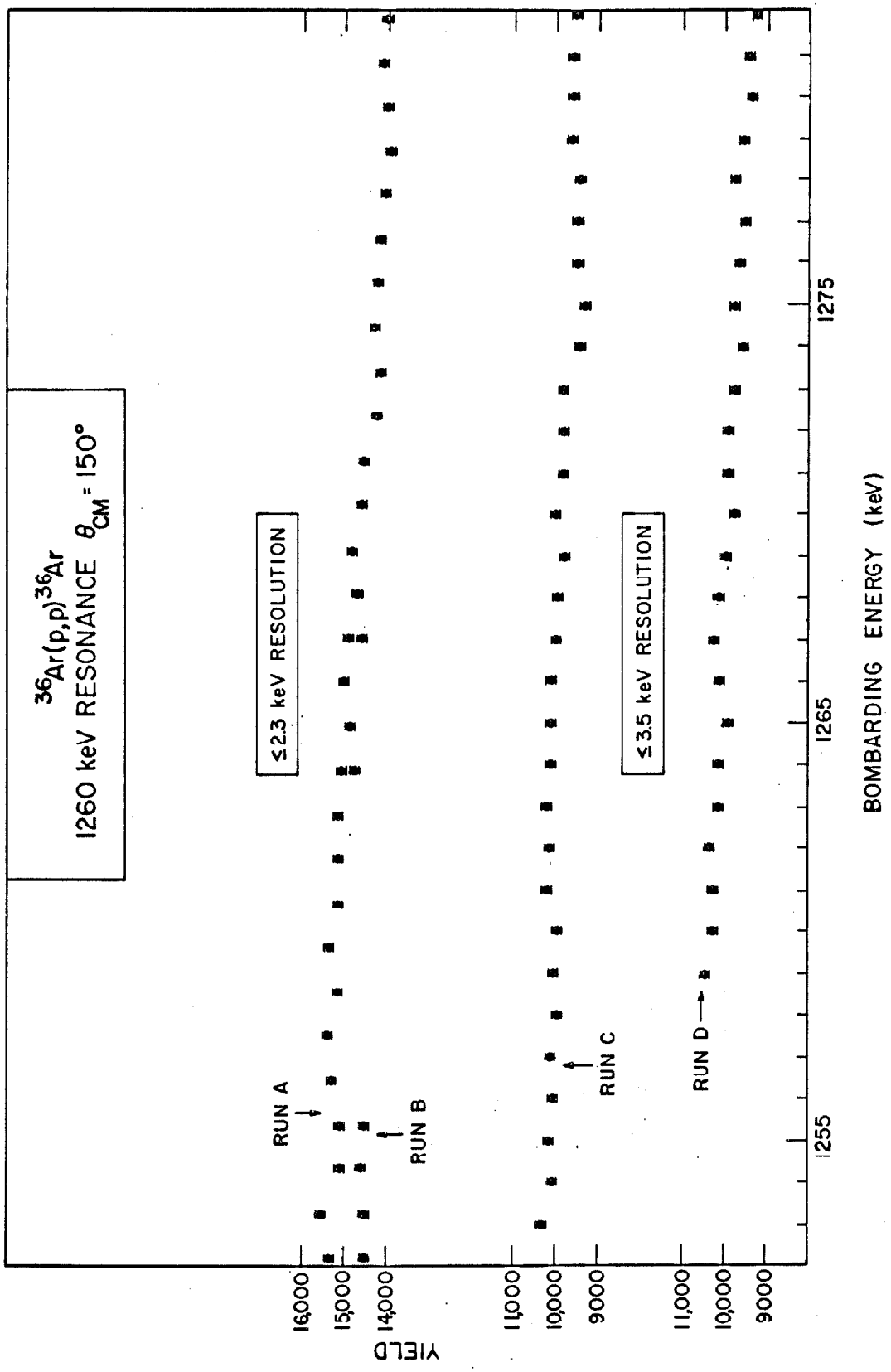
$^{36}Ar(p,p)^{36}Ar$
1260 keV RESONANCE $\theta_{CM} = 150°$
≤2.3 keV RESOLUTION
≤3.5 keV RESOLUTION
RUN A
RUN B
RUN C
RUN D
YIELD
16000
15000
14000
11000
10000
9000
11000
10000
9000
1255
1265
1275
BOMBARDING ENERGY (keV)

Figure 20.

The outgoing proton energy spectra before and after Run B of figure 19 was taken. Unfolding the spectrometer resolution for both curves gives an initial resolution of the target and beam of 2.1 keV and a final one of 2.5 keV. The background under the left curve is mostly due to a 0.1% iron contaminant in the beryllium. (page 33)

Figure 20

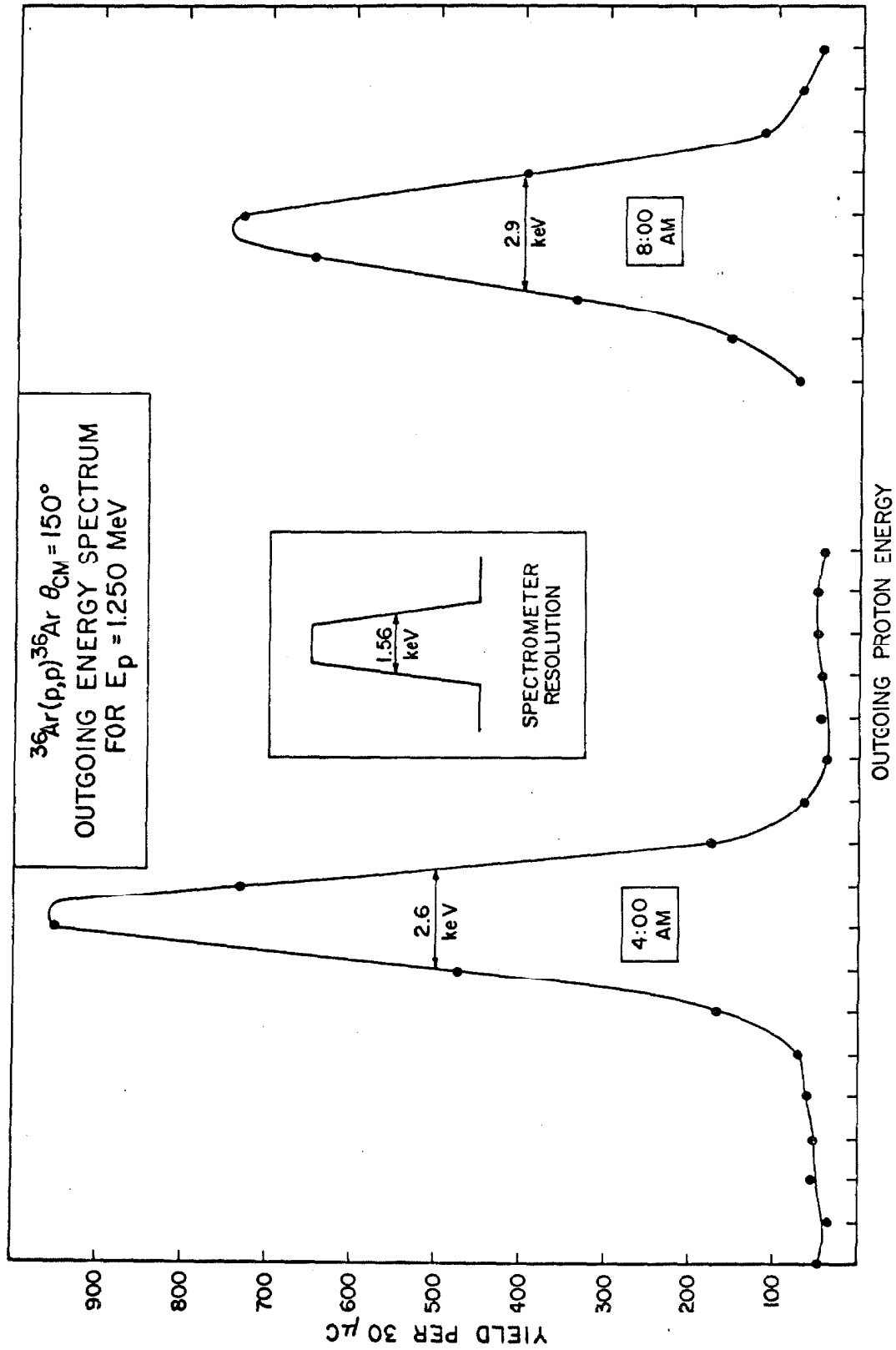
$^{36}Ar(p,p)^{36}Ar$ $\theta_{CM} = 150°$
OUTGOING ENERGY SPECTRUM
FOR E_p = 1.250 MeV
SPECTROMETER RESOLUTION
1.56 keV
2.6 keV
4:00 AM
2.9 keV
8:00 AM
YIELD PER 30 μC
OUTGOING PROTON ENERGY
900
800
700
600
500
400
300
200
100

Figure 21.

Measurement of the resolution of the beam in the foil-less gas cell as measured by a well-known $^{40}Ar(p,\gamma)^{41}K$ resonance. The doppler broadening is 35 eV and the target thickness is 120 eV. The horizontal scale is the beam energy as read by the 90^{o} analyzing magnet calibration curve. (page 34)

Figure 21

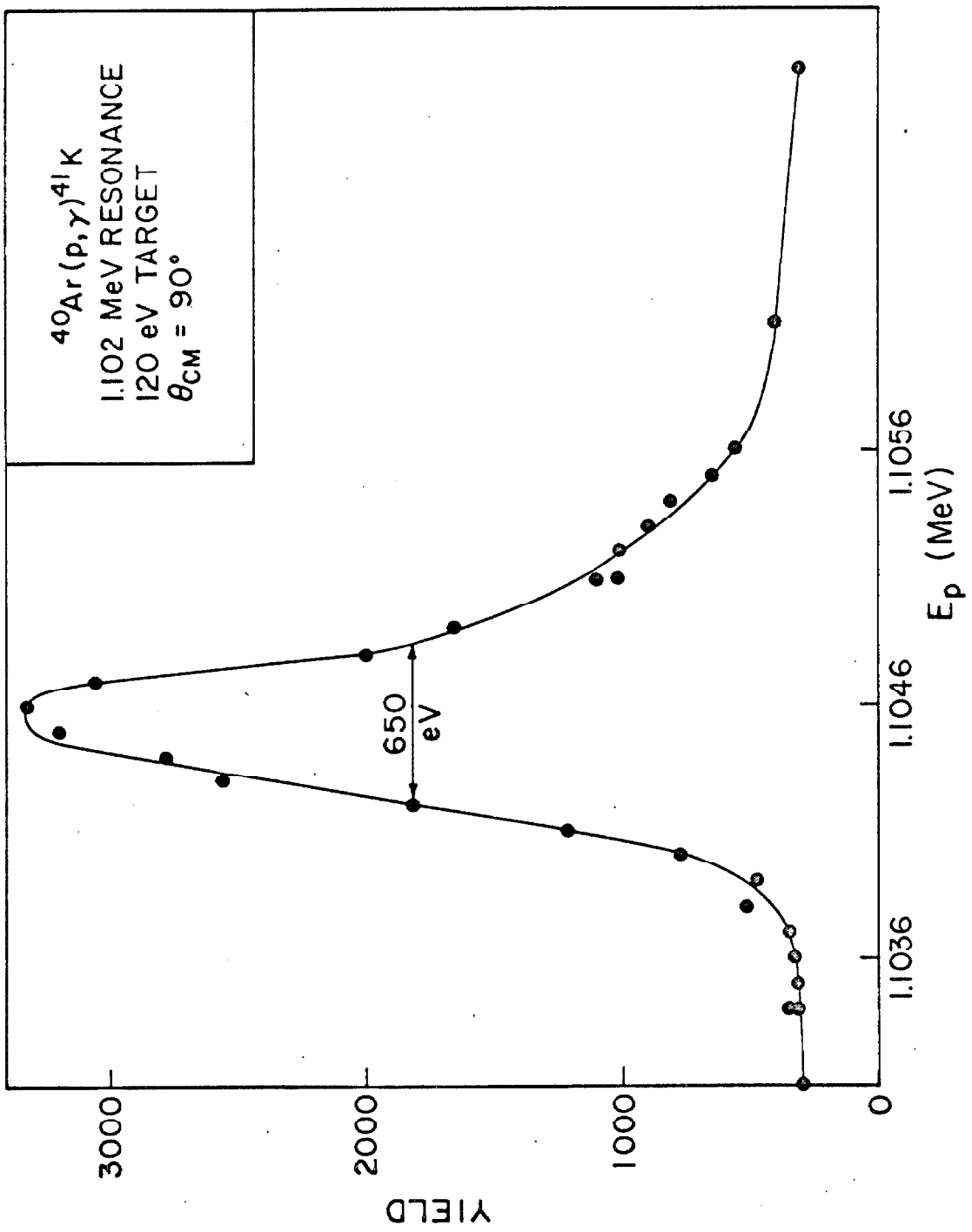
$^{40}Ar(p,\gamma)^{41}K$
1.102 MeV RESONANCE
120 eV TARGET
$\theta_{CM} = 90°$
650 eV
YIELD
3000
2000
1000
0
1.1036
1.1046
1.1056
E_p (MeV)

Figure 22.

The yield of elastically scattered protons near the 1260 keV resonance as seen in the foil-less gas cell. The slope of the curves is due to a gradual decrease in target gas pressure via leakage through the beam entrance hole. The runs proceeded in the order: run A, left to right; run B, left to right; and run C, right to left. The dip near 1262 keV in run A is seen to disappear in run B.
(page 34)

Figure 22

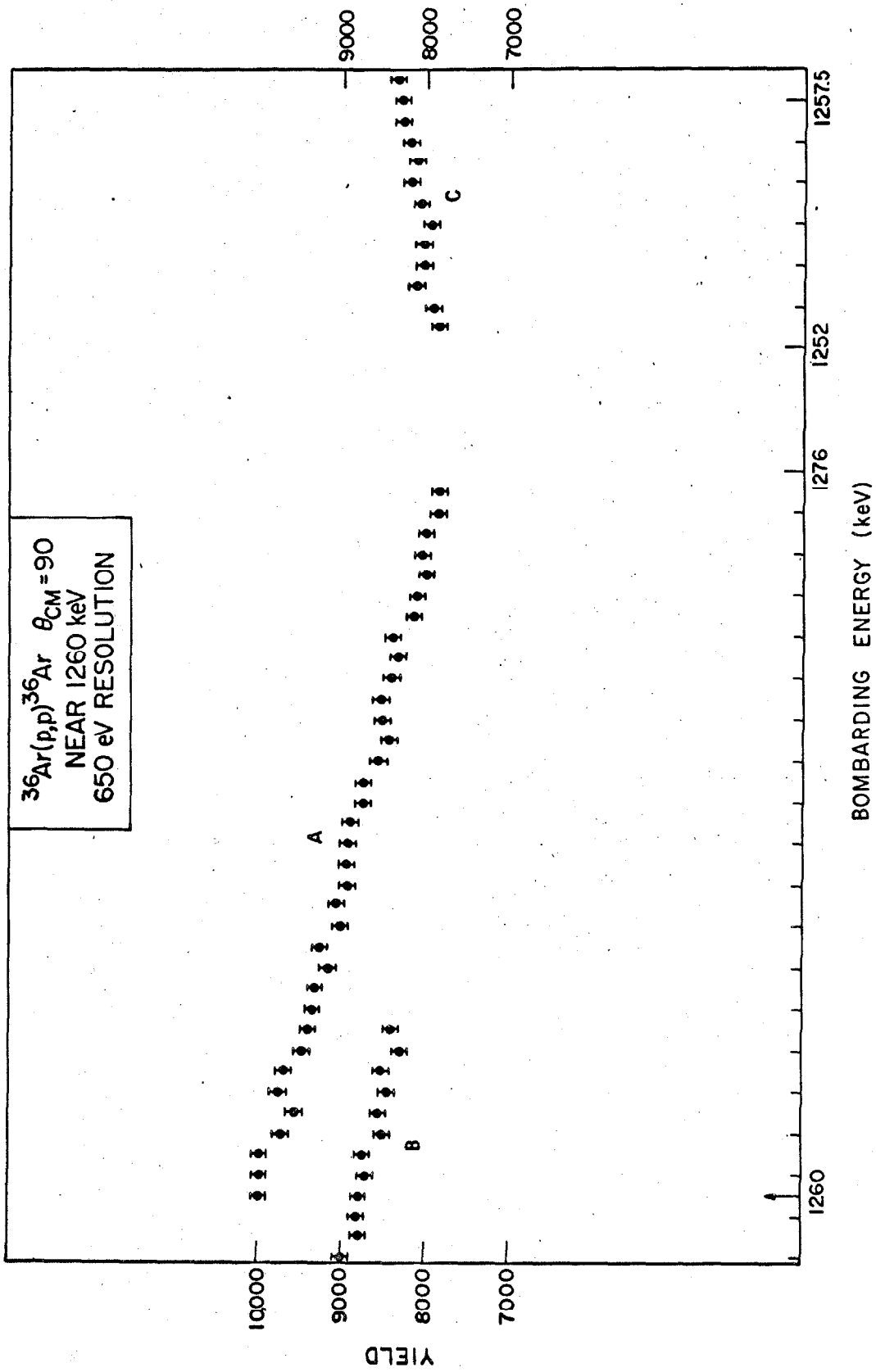
$^{36}Ar(p,p)^{36}Ar$ $\theta_{CM}=90$
NEAR 1260 keV
650 eV RESOLUTION
A
B
C
YIELD
10000
9000
8000
7000
9000
8000
7000
1260
1276
1252
1257.5
BOMBARDING ENERGY (keV)

Figure 23.

The alpha-particle spectrum at three angles from the proton bombardment of ^{40}Ca. The numbers are excitation energies in MeV. The peak at "X" is an impurity. The peak at 1.37 MeV excitation is shown in part X to be a doublet. (page 37)

Figure 23

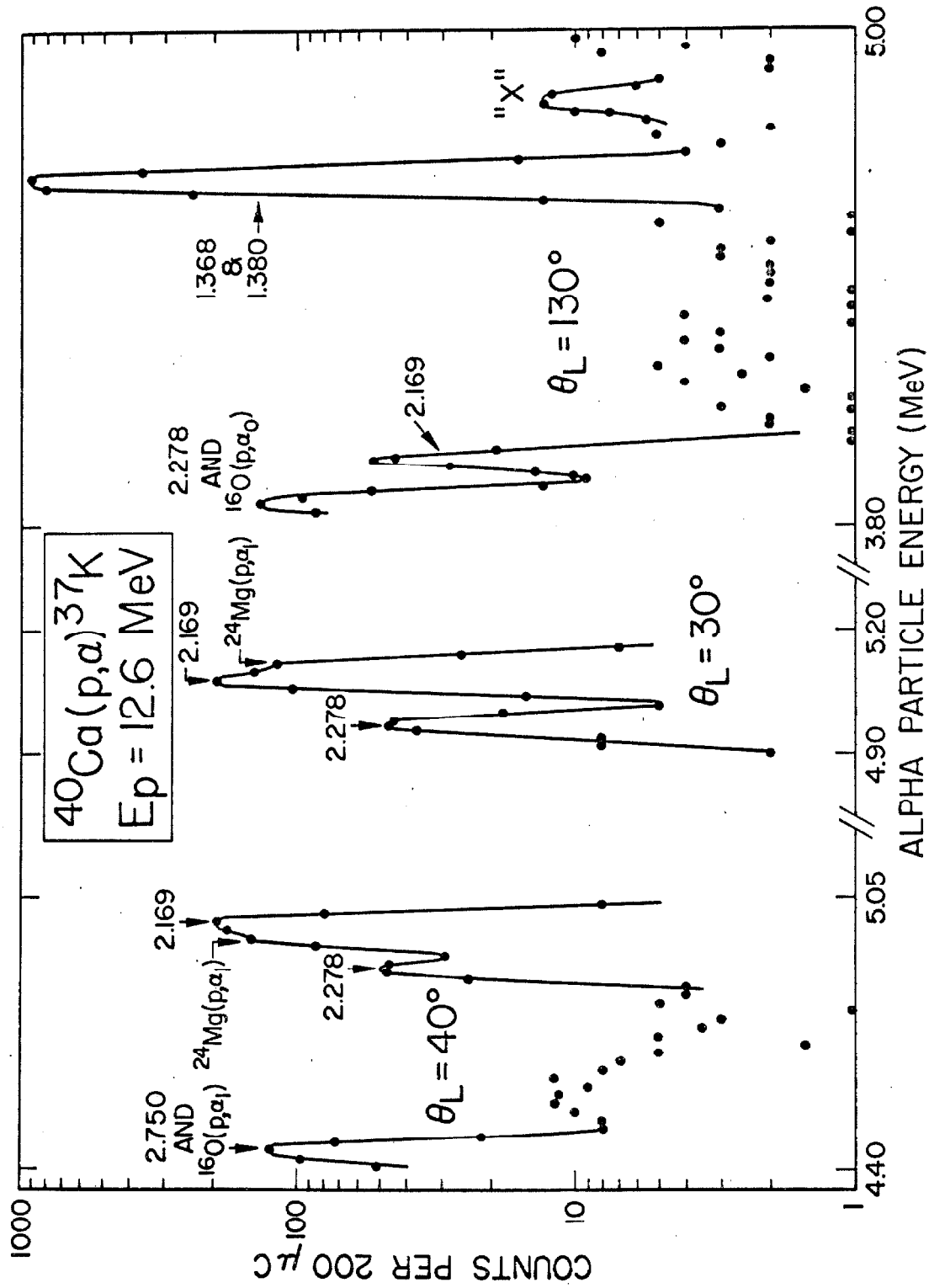
$^{40}Ca(p,\alpha)^{37}K$
Ep = 12.6 MeV
2.750 AND $^{16}O(p,\alpha_1)$
2.169
$^{24}Mg(p,\alpha_1)$
2.278
$\theta_L = 40°$
2.169
$^{24}Mg(p,\alpha_1)$
2.278
$\theta_L = 30°$
2.278 AND $^{16}O(p,\alpha_0)$
2.169
$\theta_L = 130°$
1.368 & 1.380
"X"
COUNTS PER 200 μC
1000
100
10
1
4.40
5.05
4.90
5.20
3.80
5.00
ALPHA PARTICLE ENERGY (MeV)

Figure 24.

The ground state and the doublet near 1.37 MeV excitation as seen with 12 keV resolution. The number "1.373" MeV comes from the spectrometer calibration constant. (page 37)

Figure 24

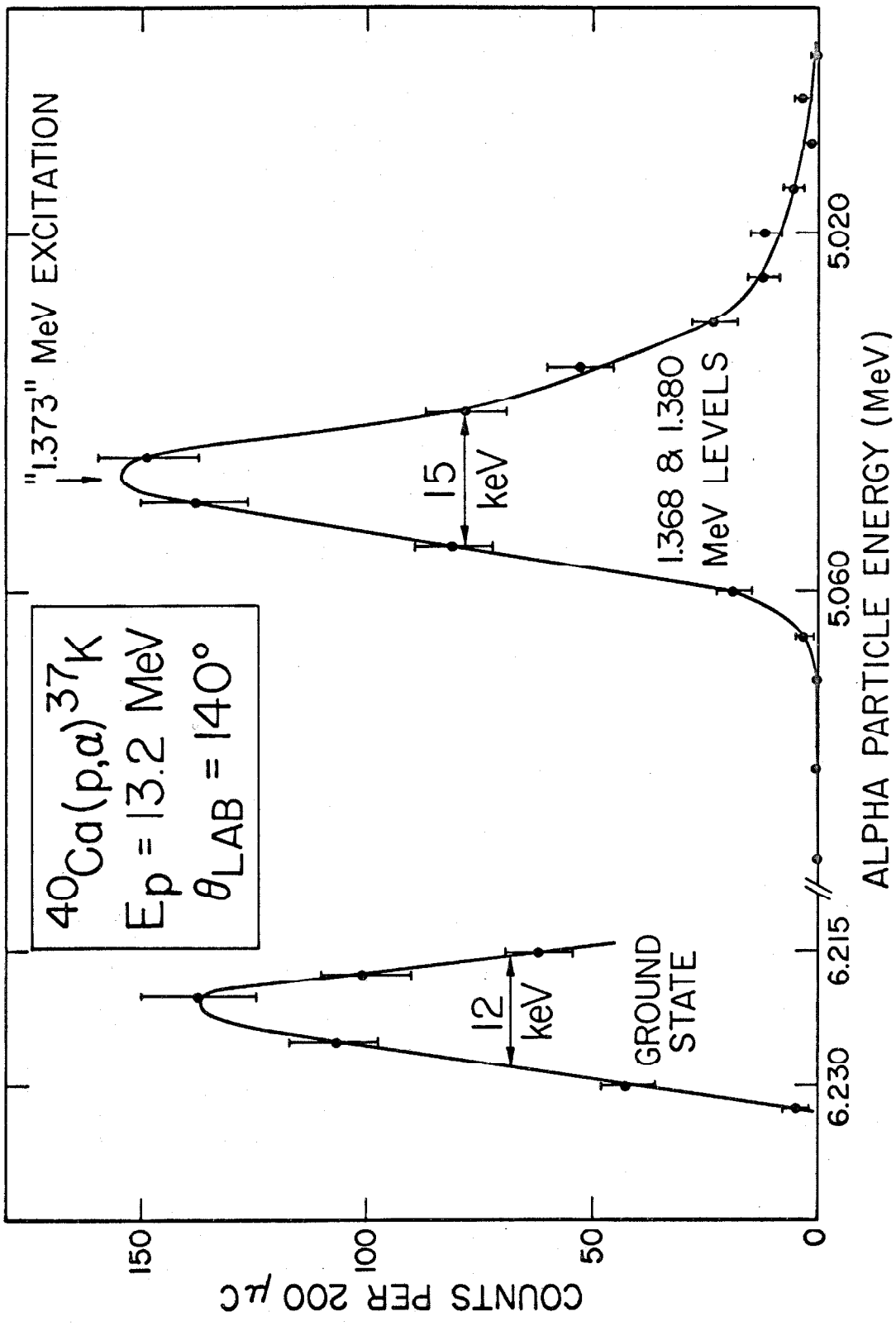
$^{40}Ca(p,\alpha)^{37}K$
E_p = 13.2 MeV
θ_{LAB} = 140°
"1.373" MeV EXCITATION
15 keV
12 keV
1.368 & 1.380 MeV LEVELS
GROUND STATE
6.230
6.215
5.060
5.020
ALPHA PARTICLE ENERGY (MeV)
COUNTS PER 200 μC
0
50
100
150

Figure 25.

The alpha-particle spectra showing the 2.169 and 2.278 MeV levels. The curve on the right is the calibration of the 2.278 MeV level and the two curves demonstrate that it arises from a mass-40 target. (page 37)

Figure 25

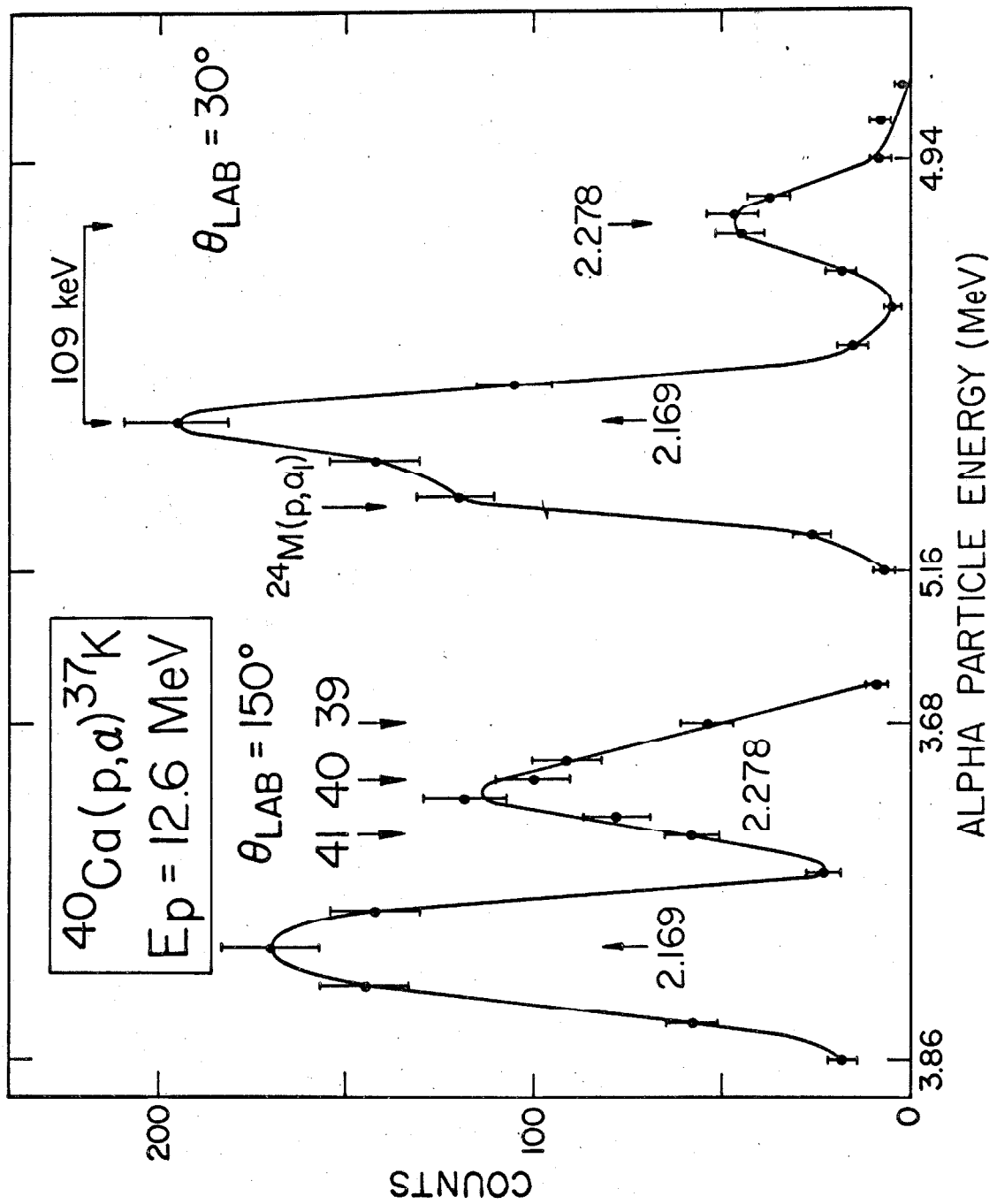
$^{40}Ca(p,\alpha)^{37}K$
Ep = 12.6 MeV
θ_{LAB} = 150°
θ_{LAB} = 30°
109 keV
41 40 39
$^{24}M(p,\alpha_1)$
2.169
2.278
2.169
2.278
COUNTS
200
100
0
3.86
3.68
5.16
4.94
ALPHA PARTICLE ENERGY (MeV)

Figure 26.

The pulse-height spectrum in a silicon surface-barrier detector from the neutrons produced by the deuteron bombardment of ^{36}Ar. A sheet of tantalum 0.5 mm thick prevented any charged particles from entering the counter. The dashed curve is the response of the counter to an 8.17 MeV neutron group and the solid curve is the pulse-height spectrum with ^{36}Ar in the cell. The symbols are explained on page 39.

Figure 26

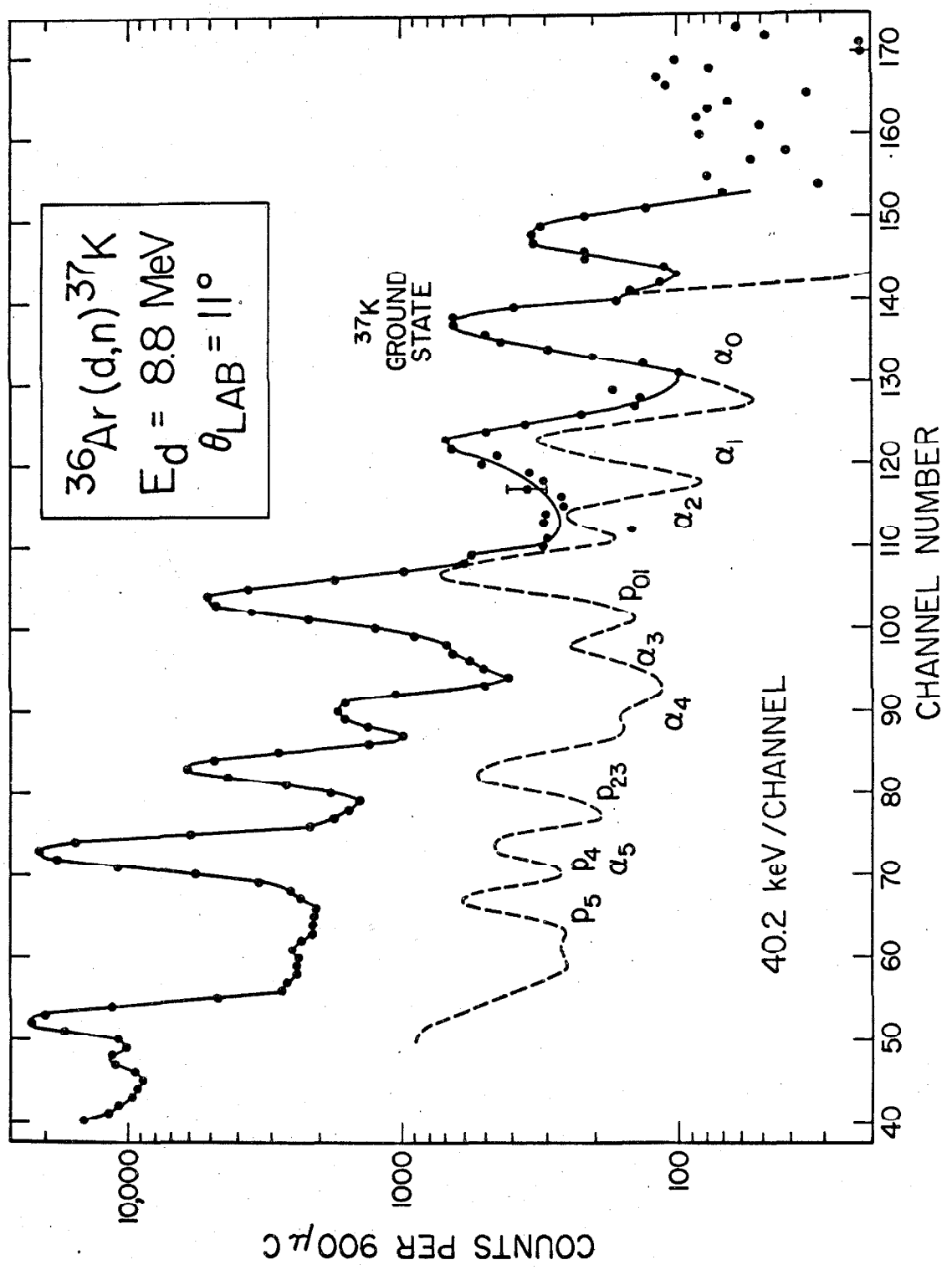
$^{36}Ar(d,n)^{37}K$
E_d = 8.8 MeV
θ_{LAB} = 11°
^{37}K GROUND STATE
α_0
α_1
α_2
p_{01}
α_3
α_4
p_{23}
p_4
α_5
p_5
40.2 keV/CHANNEL
CHANNEL NUMBER
COUNTS PER 900 μC
10,000
1000
100
40
50
60
70
80
90
100
110
120
130
140
150
160
170

Figure 27.

The neutron pulse-height spectrum after subtraction of the ground-state response function. Singly-primed symbols arise from the response to neutrons populating the doublet at 1.37 MeV excitation, and doubly-primed ones to the 2.169 MeV level. (page 40)

Figure 27

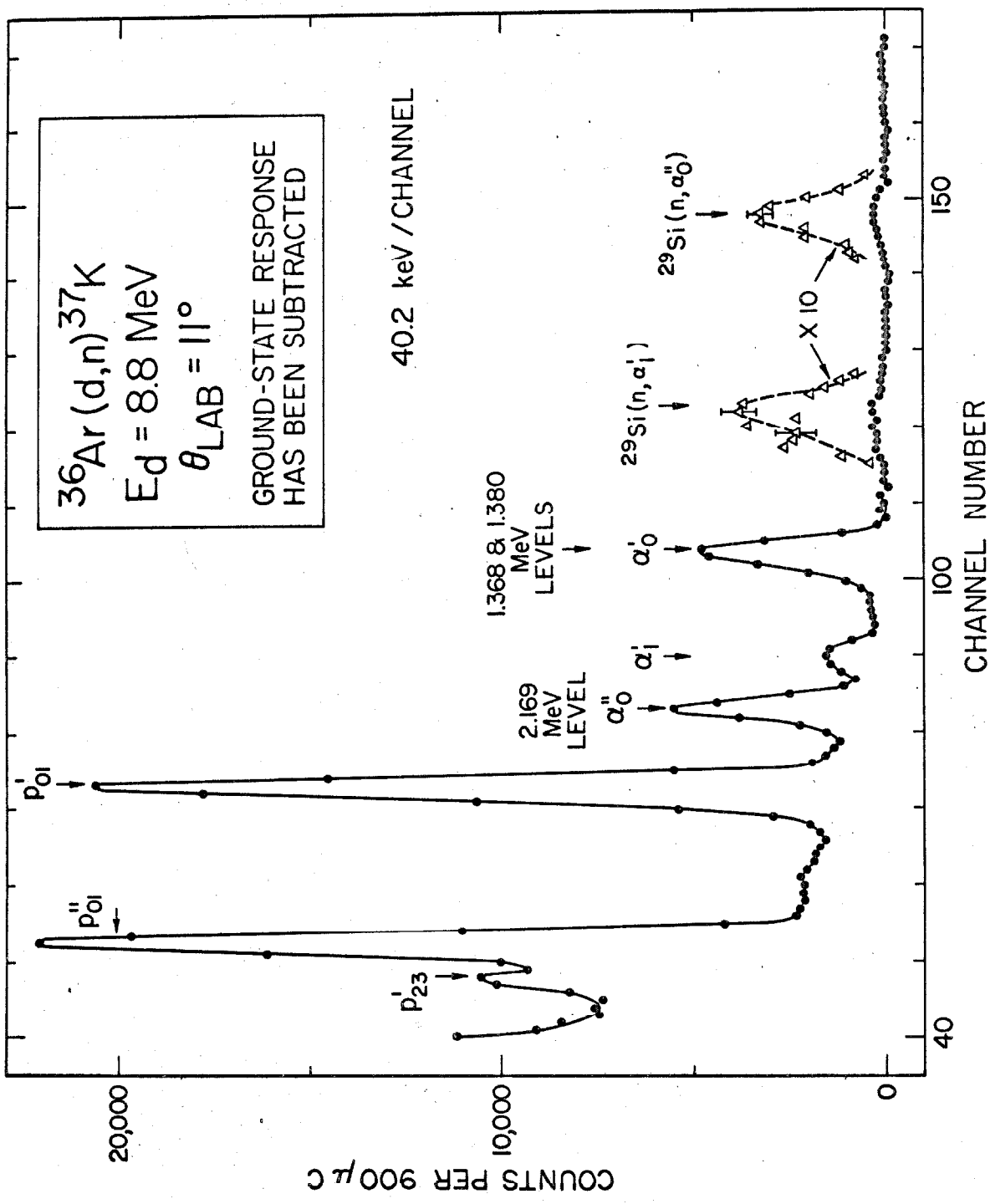
$^{36}Ar(d,n)^{37}K$
$E_d = 8.8$ MeV
$\theta_{LAB} = 11°$
GROUND-STATE RESPONSE HAS BEEN SUBTRACTED
40.2 keV / CHANNEL
p'_{01}
p''_{01}
p'_{23}
1.368 & 1.380 MeV LEVELS
2.169 MeV LEVEL
α''_0
α'_1
α'_0
$^{29}Si(n,\alpha'_1)$
$^{29}Si(n,\alpha''_0)$
X 10
COUNTS PER 900 μC
20,000
10,000
0
40
100
150
CHANNEL NUMBER

Figure 28.

The pulse-height spectrum after subtraction of the ground state and 1.37 MeV level response functions. The peak and dip labeled "X" and "Y" are the result of slight gain shifts. The three remaining peaks are due to the response function of the neutrons populating the 2.169 MeV level. (page 41)

Figure 28

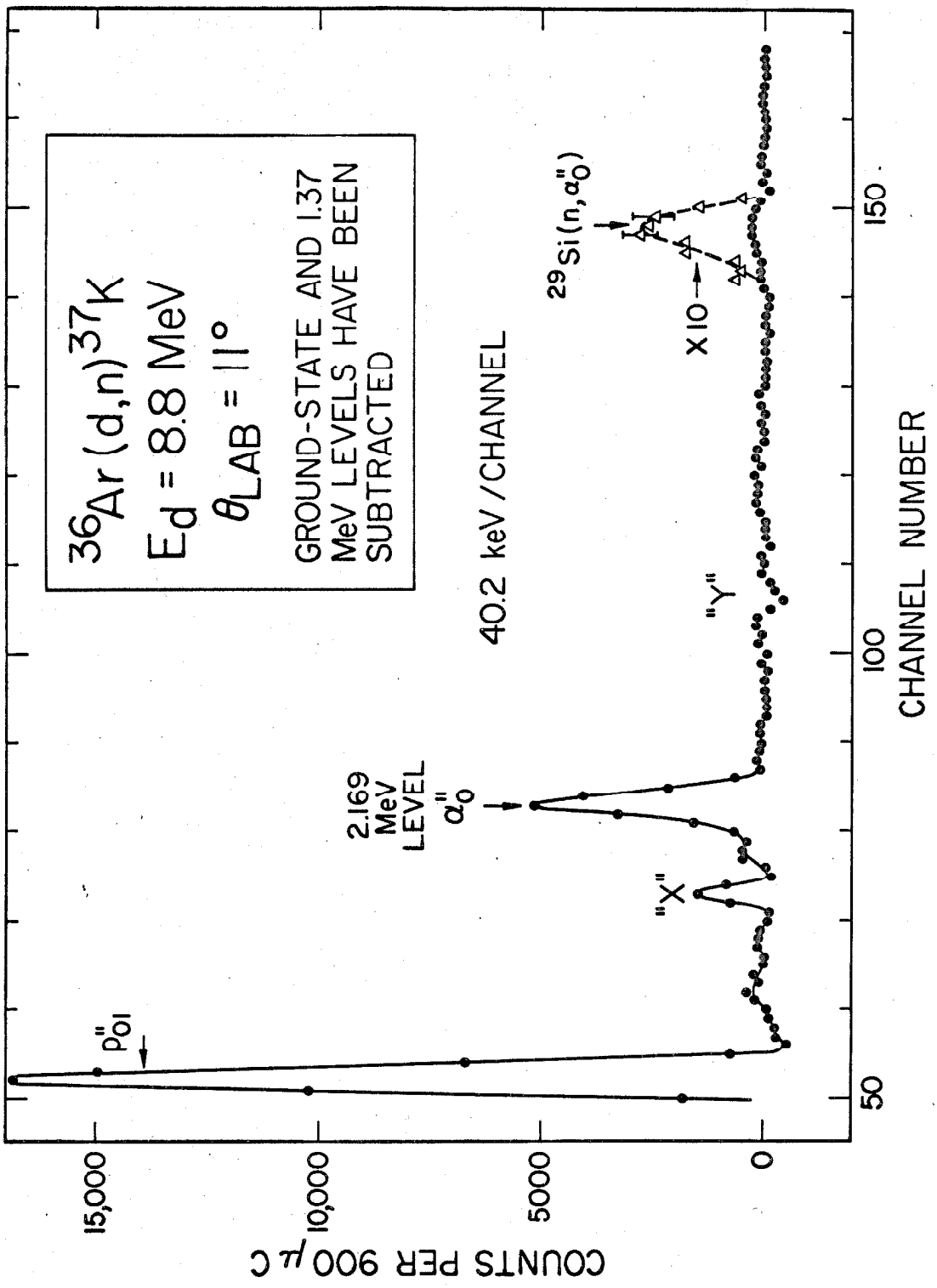
$^{36}Ar(d,n)^{37}K$
$E_d = 8.8$ MeV
$\theta_{LAB} = 11°$
GROUND-STATE AND 1.37 MeV LEVELS HAVE BEEN SUBTRACTED
40.2 keV/CHANNEL
p''_{01}
2.169 MeV LEVEL α''_0
"X"
"Y"
$^{29}Si(n,\alpha''_0)$
X10
COUNTS PER 900 μC
15,000
10,000
5000
0
50
100
150
CHANNEL NUMBER

Figure 29.

The gas cell arrangement used to study the $^{36}Ar(^{3}He, d)^{37}K$ reaction. With the beam entering through foil A, θ can be varied from zero to 65^{o}, and when the beam enters through foil B, from 60^{o} to 122^{o}. The black area shows the extreme parts of the target gas which can emit particles into the spectrometer when the latter is set at 30^{o}. (page 42)

Figure 29

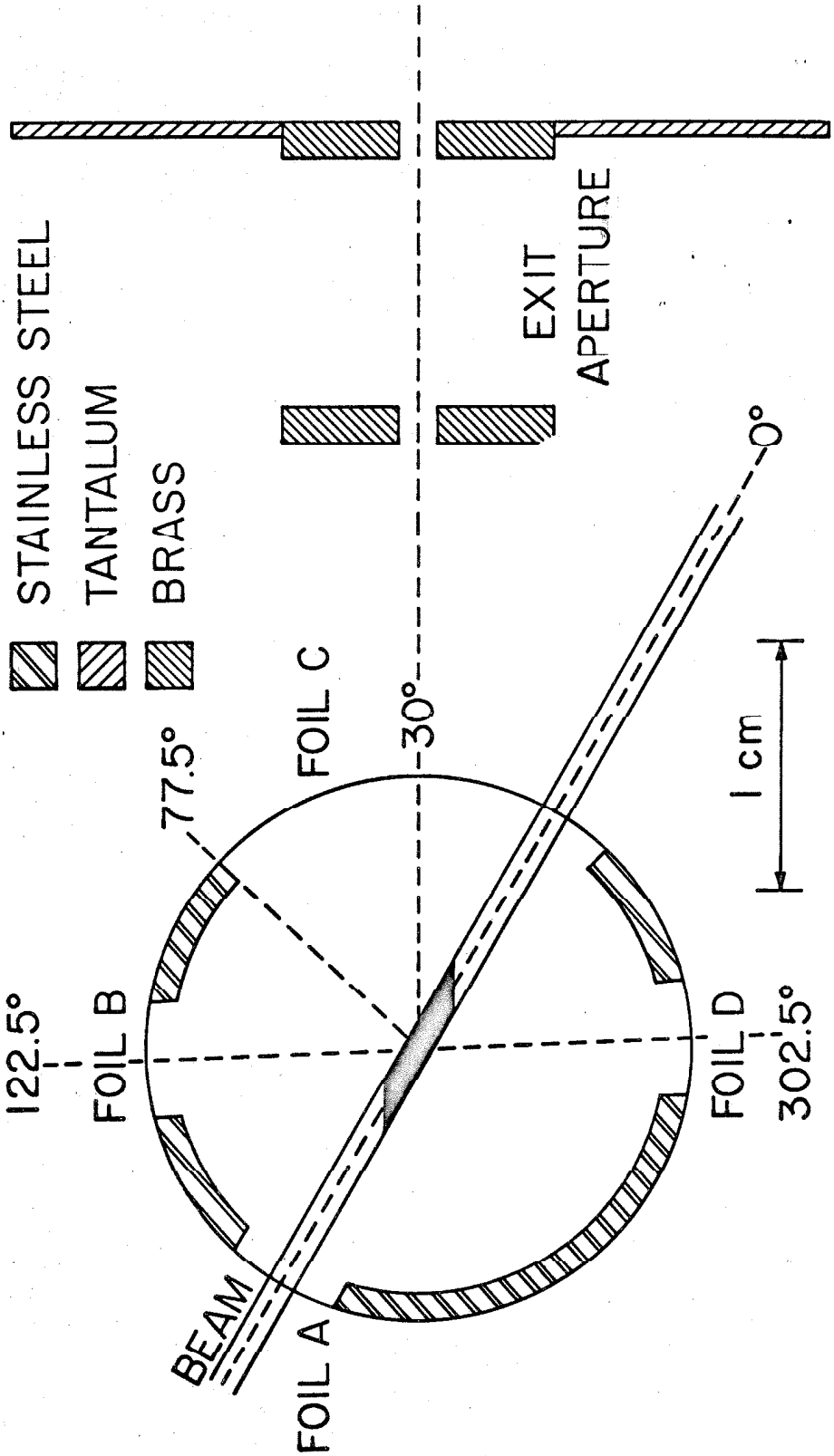
STAINLESS STEEL
TANTALUM
BRASS
EXIT APERTURE
0°
30°
77.5°
FOIL C
1 cm
122.5°
FOIL B
FOIL D
302.5°
BEAM
FOIL A

Figure 30.

Deuteron spectrum from the ^{3}He bombardment of ^{36}Ar. The deuteron momentum is in units of NMR frequency for the spectrometer magnet. Oxygen, nitrogen and carbon impurities are apparent. Deuterons leading to the 3.311 MeV level are not shown here but at $\theta_{Lab} = 30^{o}$ appear twice as strong as those leading to the 2.750 MeV level. (page 43)

Figure 30

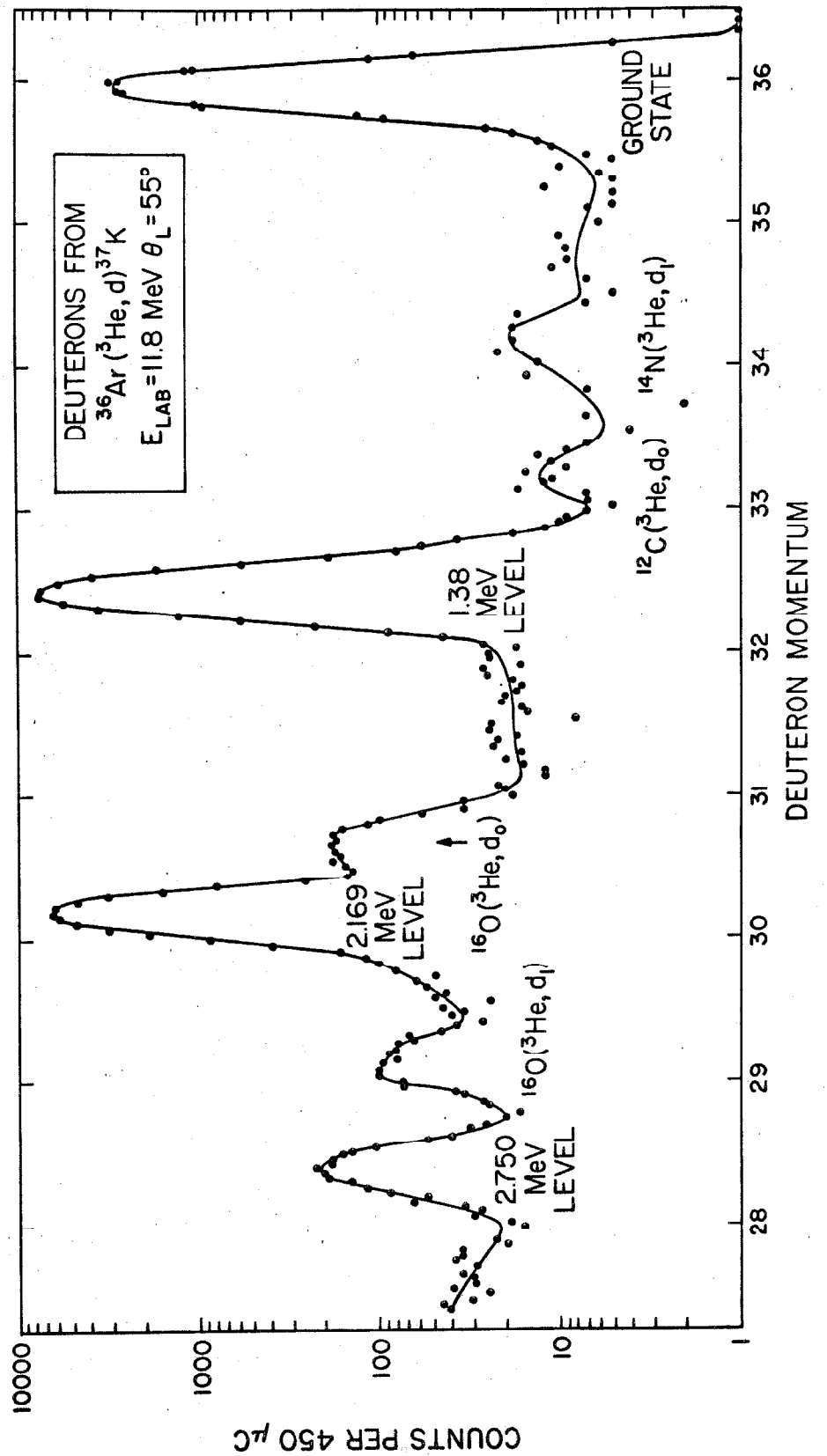
DEUTERONS FROM
$^{36}Ar(^3He, d)^{37}K$
E_{LAB}=11.8 MeV θ_L=55°
GROUND STATE
$^{14}N(^3He, d_1)$
$^{12}C(^3He, d_0)$
1.38 MeV LEVEL
$^{16}O(^3He, d_0)$
2.169 MeV LEVEL
$^{16}O(^3He, d_1)$
2.750 MeV LEVEL
COUNTS PER 450 μC
DEUTERON MOMENTUM
10000
1000
100
10
1
28
29
30
31
32
33
34
35
36

Figure 31.

Deuteron spectrum from a 13.63 MeV ^{3}He beam on ^{36}Ar. Part of the peak labeled 2.169 MeV is due to ^{16}O. (page 43)

Figure 31

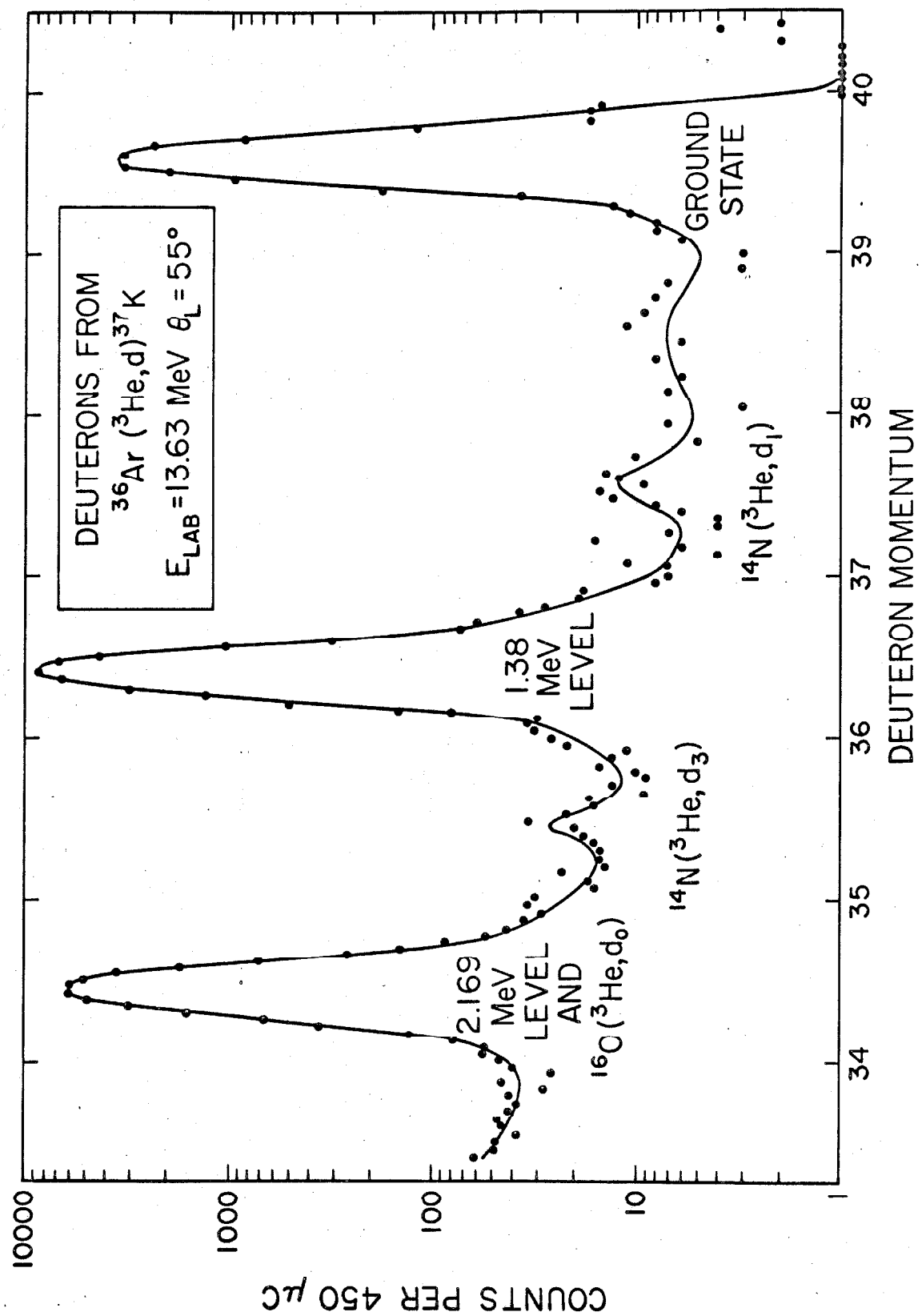
DEUTERONS FROM
^{36}Ar (^3He,d)^{37}K
E_{LAB}=13.63 MeV θ_L=55°
GROUND STATE
^{14}N (^3He, d_1)
1.38 MeV LEVEL
^{14}N(^3He, d_3)
2.169 MeV LEVEL AND ^{16}O(^3He, d_0)
COUNTS PER 450 μC
10000
1000
100
10
1
34
35
36
37
38
39
40
DEUTERON MOMENTUM

Figure 32.

The experimental angular distribution of deuterons leading to the ground state of ^{37}K. The solid line is an optical-model prediction for $\ell_p = 2$, and the predictions for $\ell_p = 1$ and 3 are shown as dashed curves. The cross sections are in the CM system and the error on the vertical scale is $\pm$ 20%. (page 44)

Figure 32

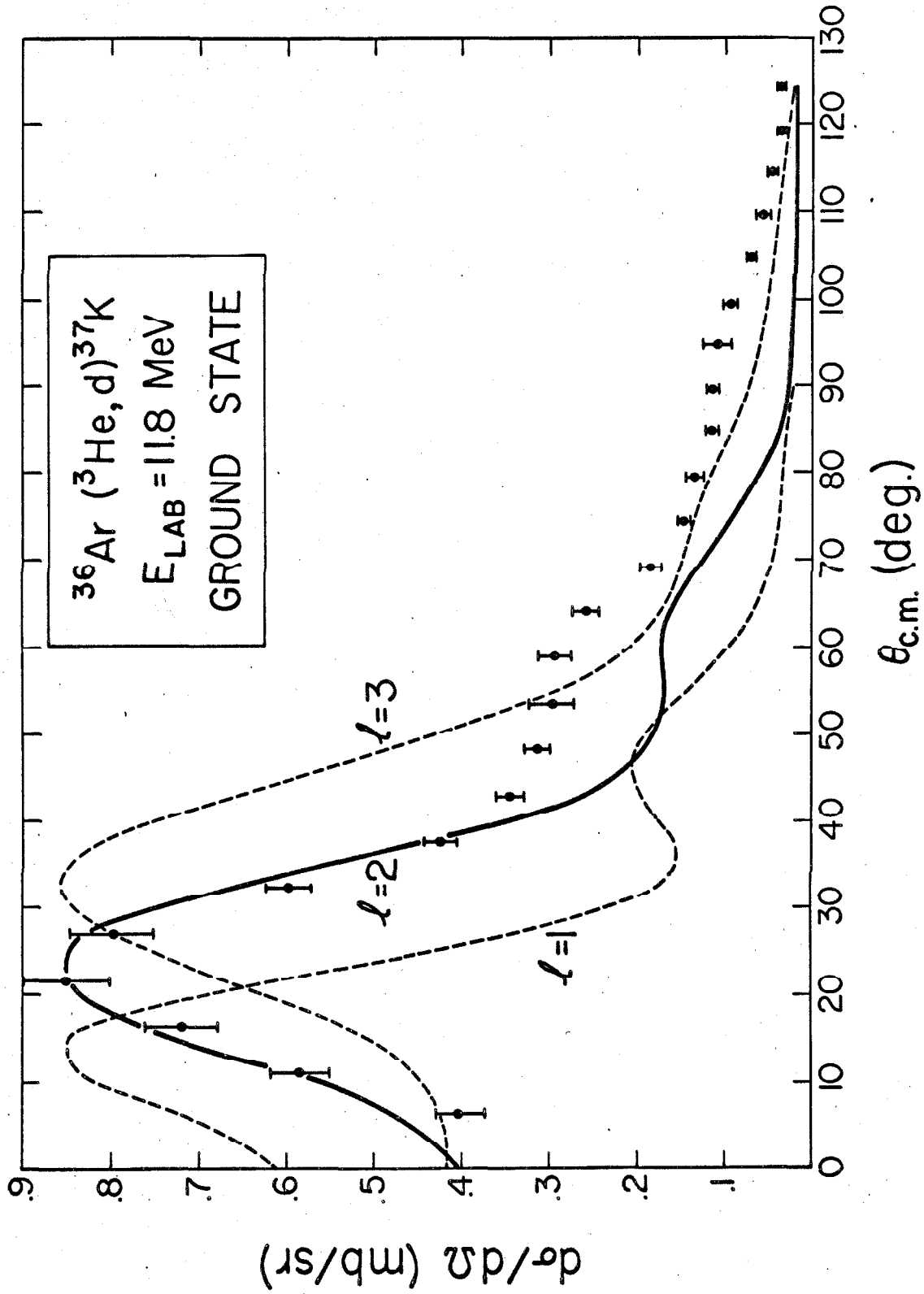
^{36}Ar (^{3}He, d)^{37}K
E_{LAB} = 11.8 MeV
GROUND STATE
ℓ=3
ℓ=2
ℓ=1
dσ/dΩ (mb/sr)
$\theta_{c.m.}$ (deg.)
0
10
20
30
40
50
60
70
80
90
100
110
120
130
.1
.2
.3
.4
.5
.6
.7
.8
.9

Figure 33.

The center-of-mass angular distribution of deuterons leading to the 1.38 MeV level. The ℓ_p = 2, 3 and 4 optical-model predictions are shown. The error on the vertical scale is ± 20%. (page 46)

Figure 33

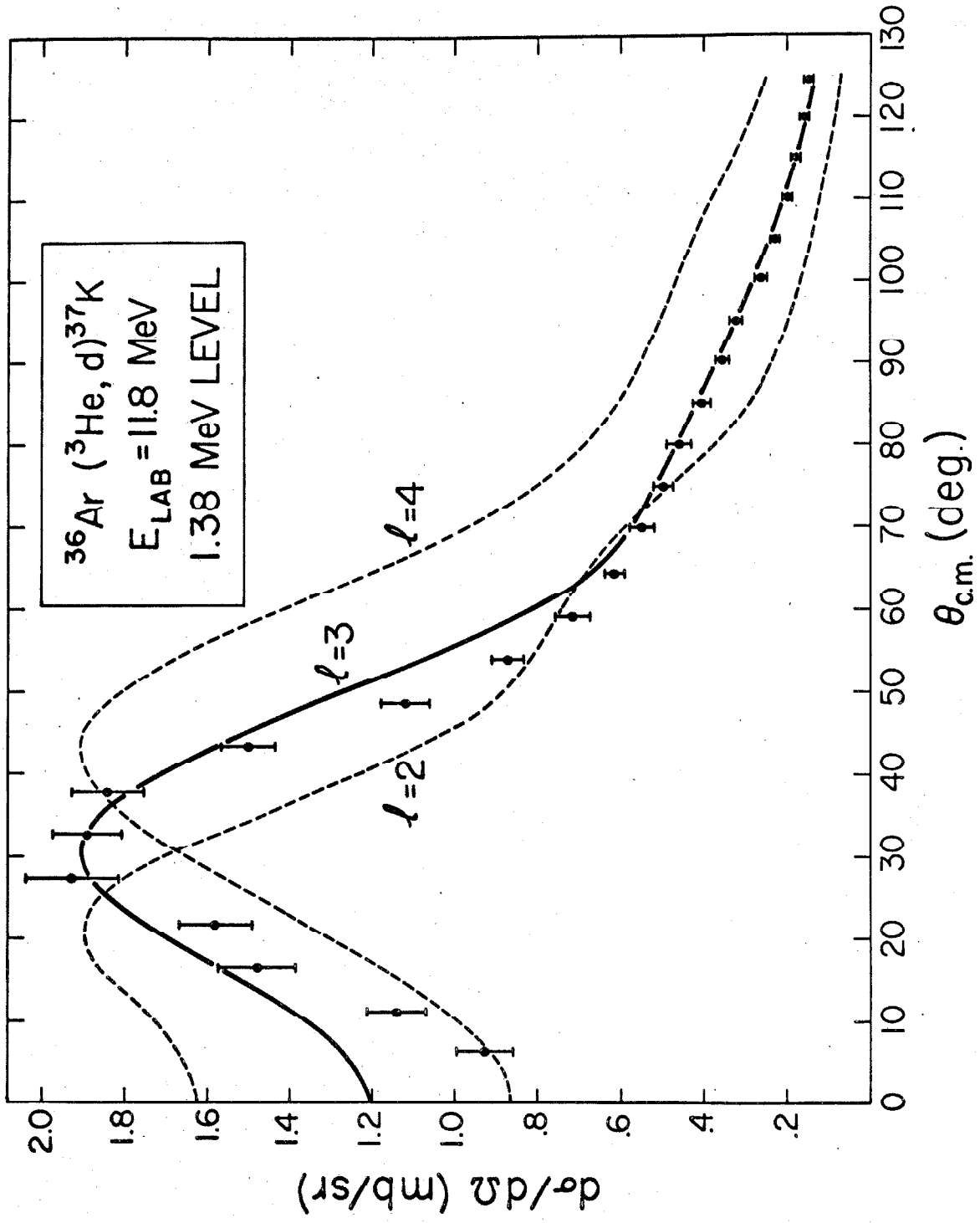
^{36}Ar (^{3}He, d)^{37}K
E_{LAB} = 11.8 MeV
1.38 MeV LEVEL
ℓ=4
ℓ=3
ℓ=2
dσ/dΩ (mb/sr)
θc.m. (deg.)
0
10
20
30
40
50
60
70
80
90
100
110
120
130
.2
.4
.6
.8
1.0
1.2
1.4
1.6
1.8
2.0

Figure 34.

The center-of-mass angular distribution of deuterons leading to the 2.169 MeV level in ^{37}K. This level is unbound by 312 keV, and the three optical-model curves show the effect of changing the binding energy from 0.68 MeV to 0.02 MeV for $\ell_p = 1$. The error on the vertical scale is $\pm$ 20%. (page 46)

Figure 34

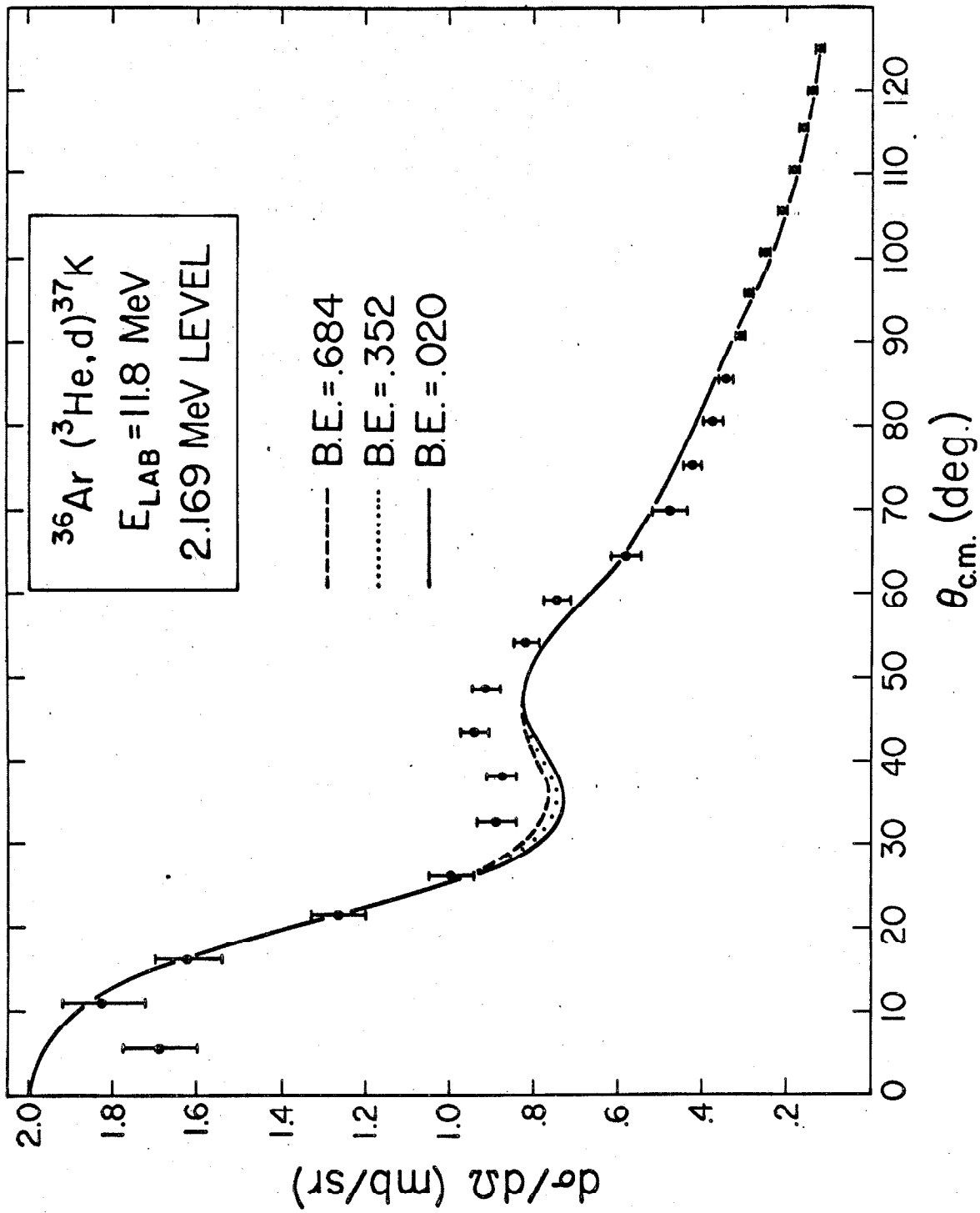
^{36}Ar (^{3}He,d)^{37}K
E_{LAB}=11.8 MeV
2.169 MeV LEVEL
B.E.=.684
B.E.=.352
B.E.=.020
dσ/dΩ (mb/sr)
$\theta_{c.m.}$ (deg.)
0
10
20
30
40
50
60
70
80
90
100
110
120
.2
.4
.6
.8
1.0
1.2
1.4
1.6
1.8
2.0

Figure 35.

The CM angular distribution of deuterons leading to the 2.169 MeV level with ℓ_p = 0, 1 and 2 optical-model predictions. The diffuseness a' in the exit channel is 0.6 fm. (page 47)

Figure 35

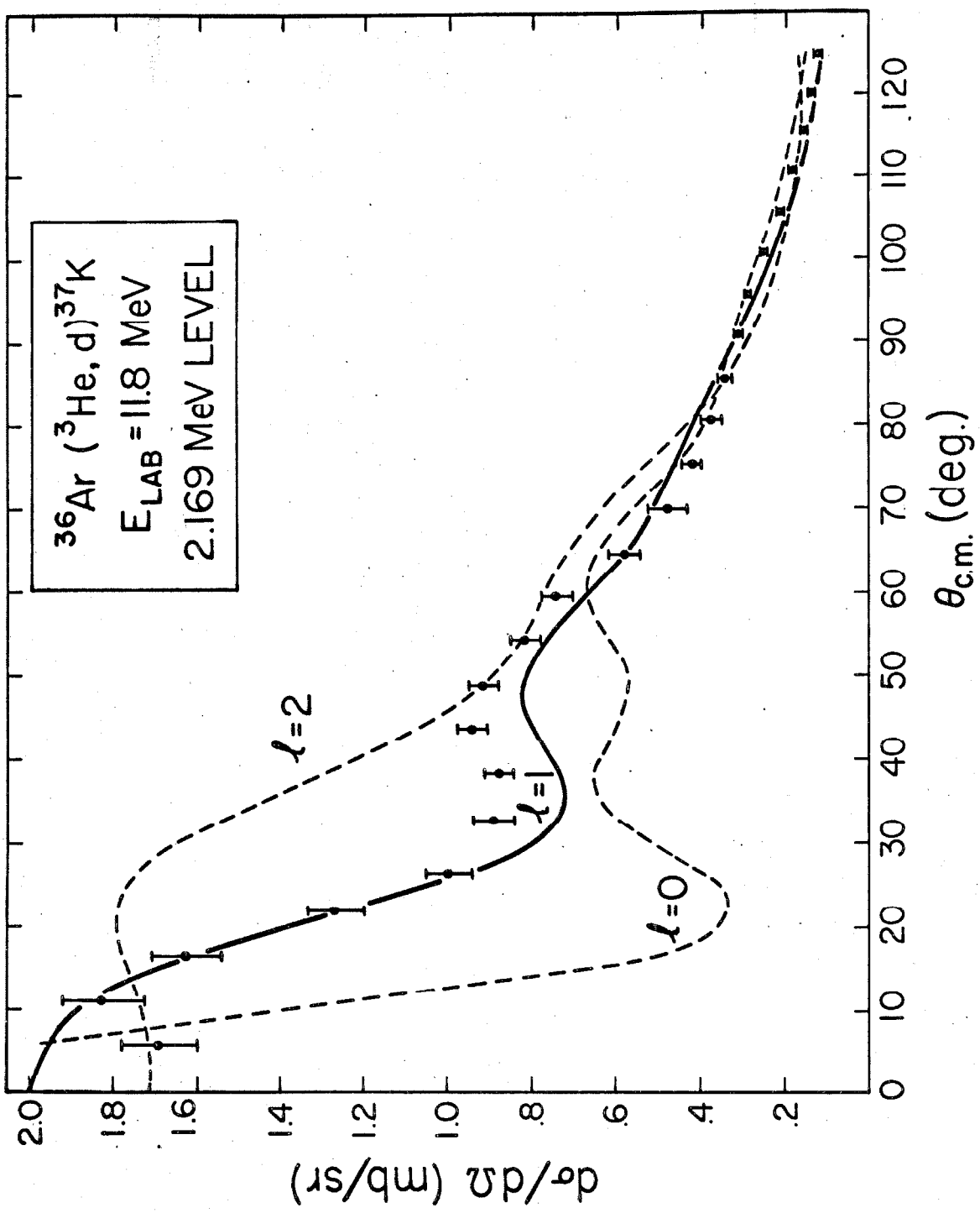
^{36}Ar (^{3}He, d)^{37}K
E_{LAB} = 11.8 MeV
2.169 MeV LEVEL
ℓ=2
ℓ=1
ℓ=0
dσ/dΩ (mb/sr)
θc.m. (deg.)
2.0
1.8
1.6
1.4
1.2
1.0
.8
.6
.4
.2
0
10
20
30
40
50
60
70
80
90
100
110
120

Figure 36.

The CM angular distribution of deuterons leading to the 2.169 MeV level with $\ell_p = 0$, 1 and 2 optical-model predictions with a' = 0.5 fm. Comparison with figure 35 shows the effect of changing a'. (page 47)

Figure 36

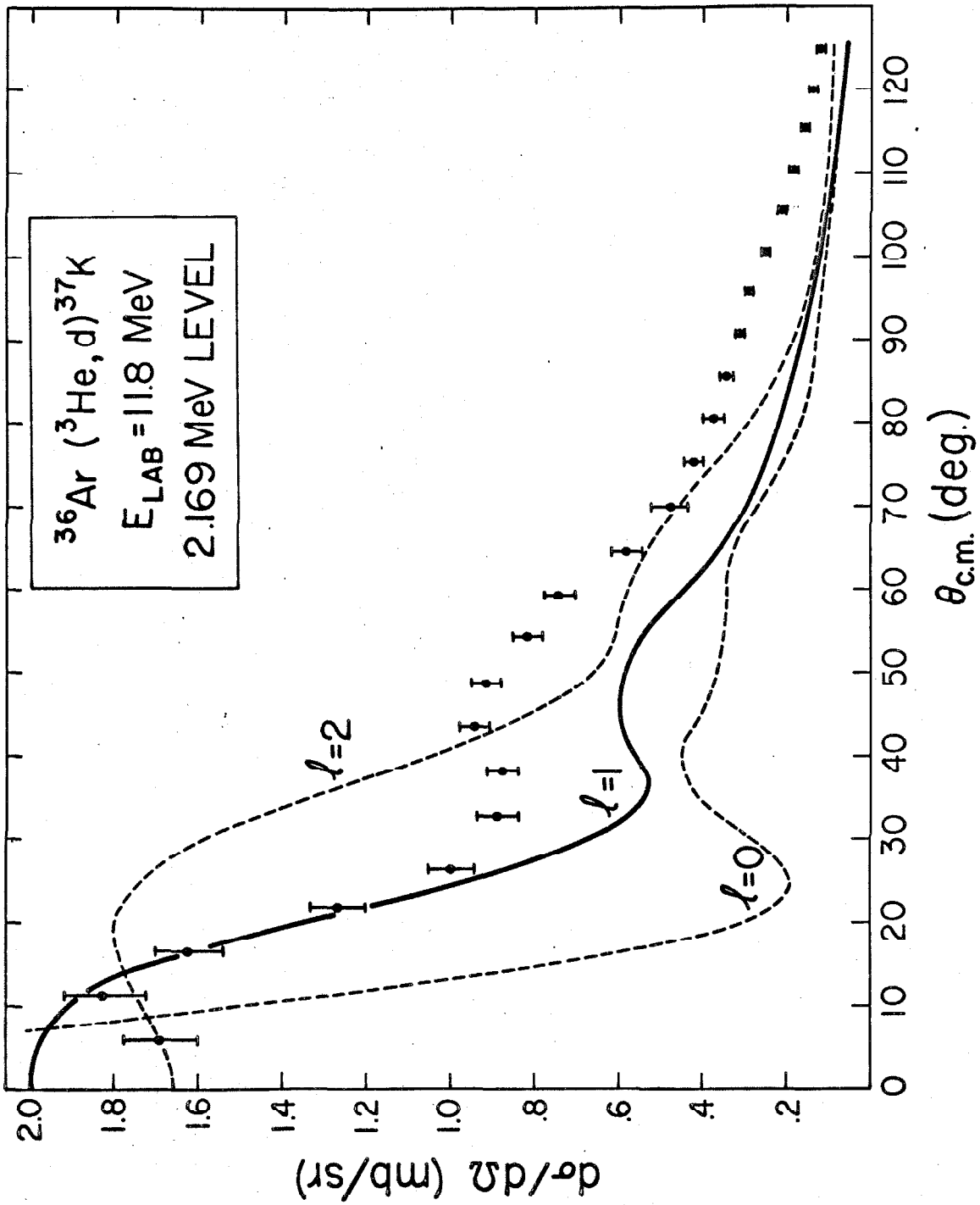
^{36}Ar (^{3}He, d)^{37}K
E_{LAB}=11.8 MeV
2.169 MeV LEVEL
ℓ=2
ℓ=1
ℓ=0
dσ/dΩ (mb/sr)
$\theta_{c.m.}$ (deg.)
0
10
20
30
40
50
60
70
80
90
100
110
120
.2
.4
.6
.8
1.0
1.2
1.4
1.6
1.8
2.0

Figure 37.

Gamma rays from the 4.417 MeV level as seen by a 12.7 by 10.2 cm NaI(Tl) crystal about 9 mm away from the center of the target. The ground-state transition and one cascade are evident. The 1.976 MeV gamma ray arises from inelastic scattering. The rising part above channel 180 is due to 6 MeV gamma rays from ^{19}F impurities. (page 49)

Figure 37

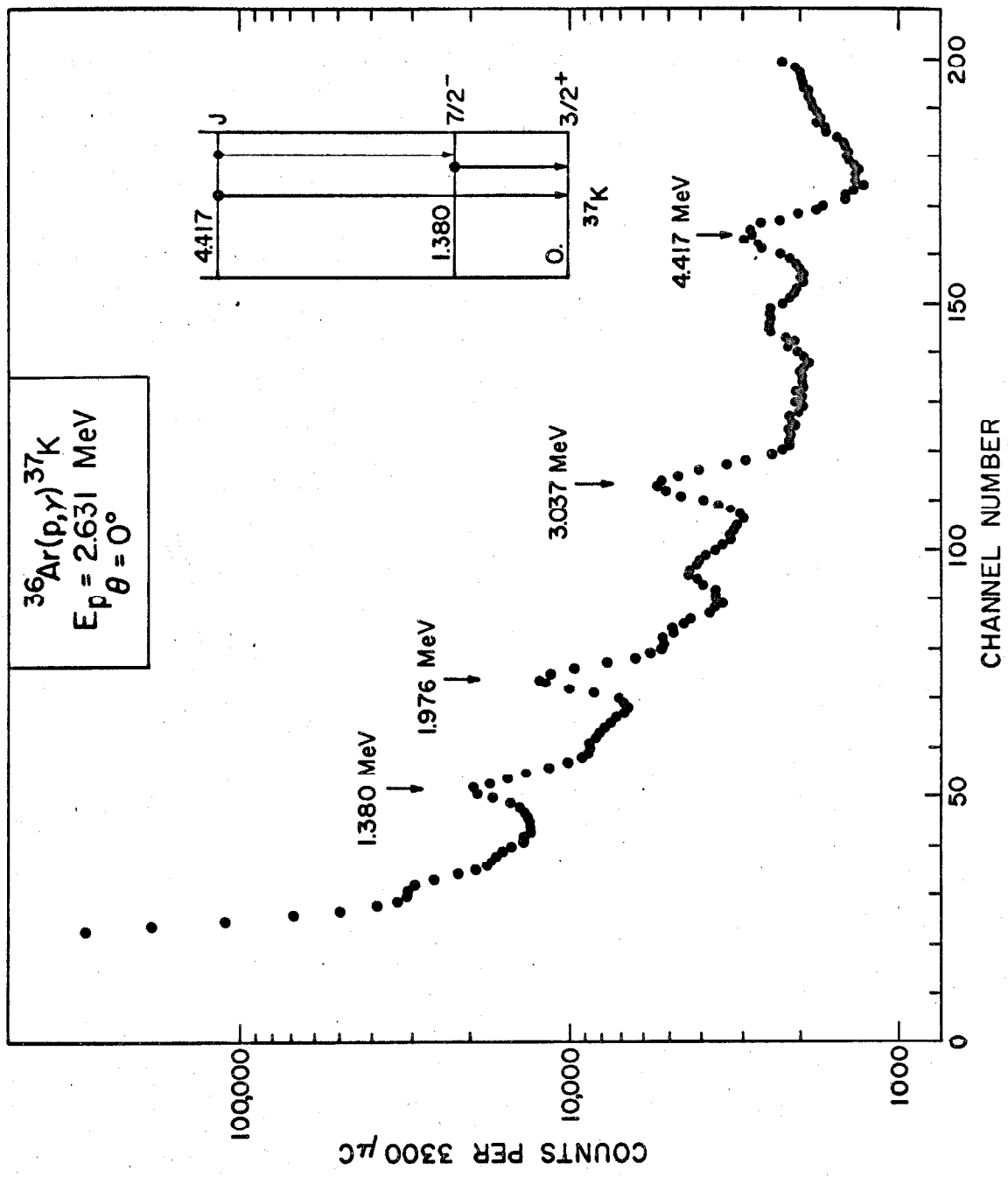
$^{36}Ar(p,\gamma)^{37}K$
$E_p = 2.631$ MeV
$\theta = 0°$
1.380 MeV
1.976 MeV
3.037 MeV
4.417 MeV
J
7/2⁻
3/2⁺
4.417
1.380
0.
^{37}K
COUNTS PER 3300 μC
100,000
10,000
1000
0
50
100
150
200
CHANNEL NUMBER

Figure 38.

The gamma-ray spectrum from the 4.417 MeV level as seen by a 4 cm^3 Ge(Li) counter at 90^o to the beam. No background has been subtracted and the 0.549 MeV gamma ray is an impurity. It is seen that the gamma rays of figure 37 above 2 MeV appear mostly as double escape peaks 1.022 MeV below the appropriate gamma-ray energy. The appearance of the pair peak at 3.40 MeV indicates that the ground-state transition is real and not due to summing of the cascades, because the efficiencies are too low in this detector for such summing to be seen. (page 49)

Figure 38

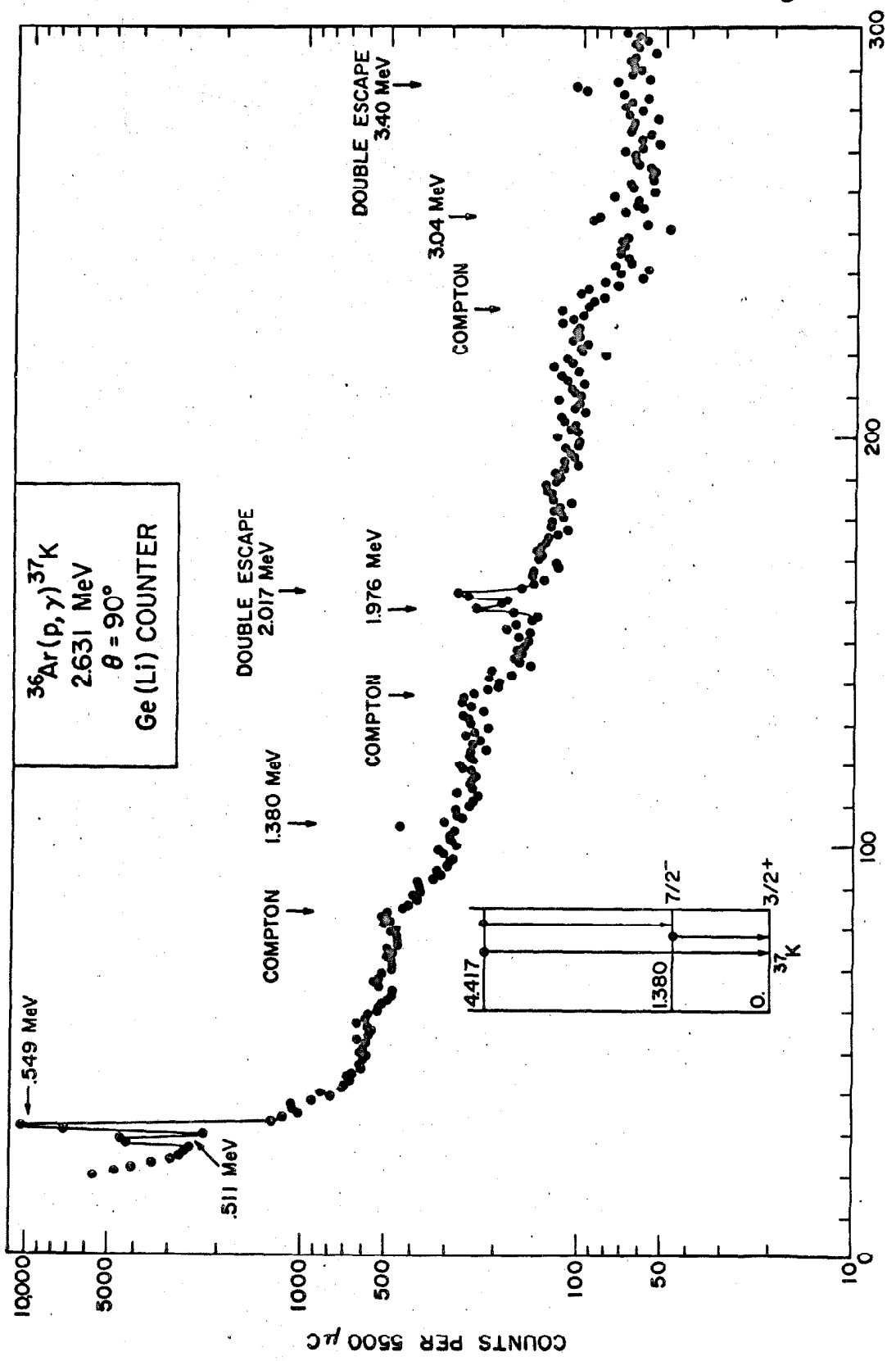
$^{36}Ar(p,\gamma)^{37}K$
2.631 MeV
θ = 90°
Ge (Li) COUNTER
.549 MeV
.511 MeV
COMPTON
1.380 MeV
DOUBLE ESCAPE
2.017 MeV
COMPTON
1.976 MeV
COMPTON
304 MeV
DOUBLE ESCAPE
340 MeV
4.417
1.380
0.
7/2⁻
3/2⁺
^{37}K
COUNTS PER 5500 μC
CHANNEL NUMBER
10,000
5000
1000
500
100
50
10
0
100
200
300

Figure 39.

The calibration curve used in determining the gamma-ray energies of the peaks in figure 38. (page 49)

Figure 39

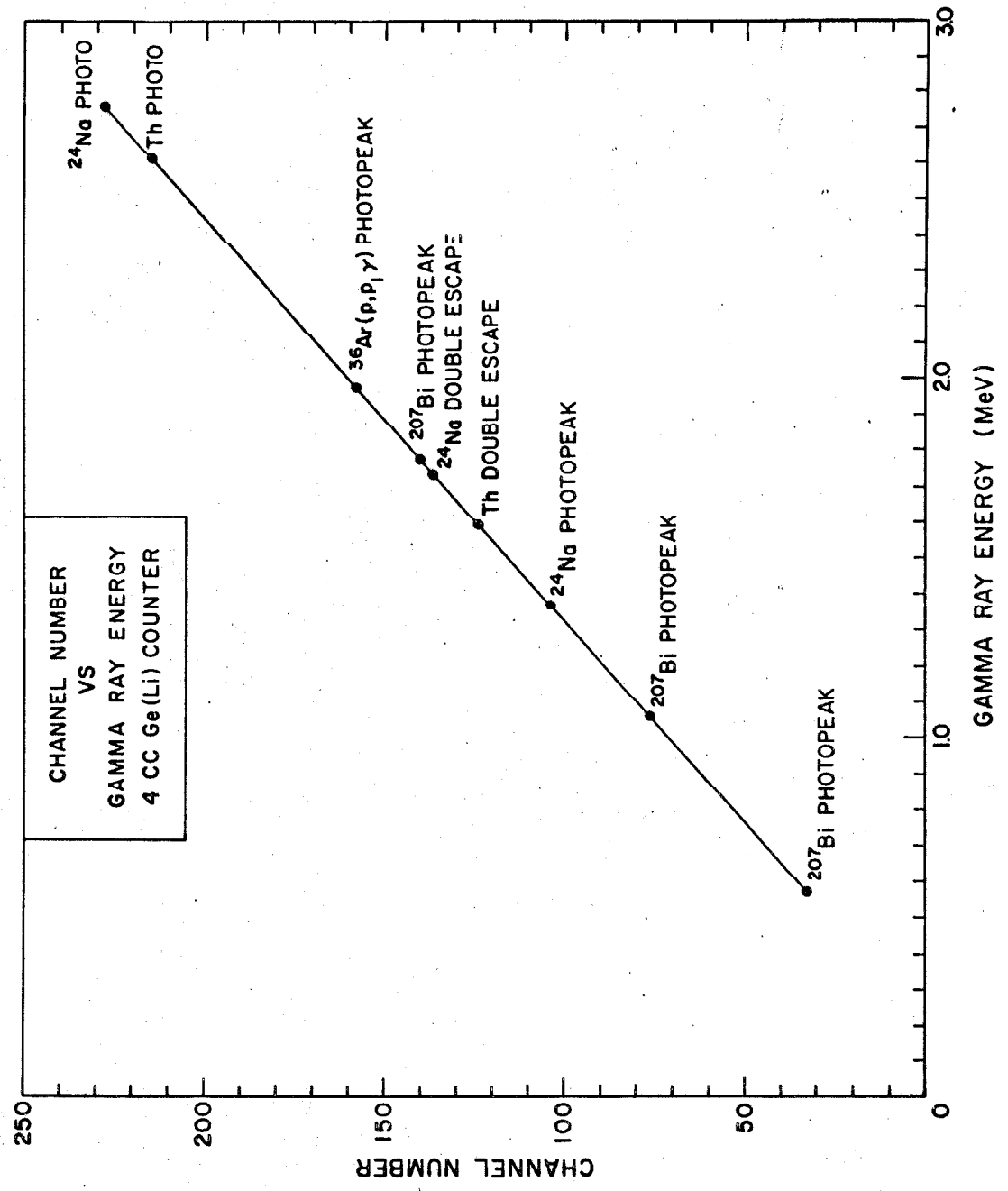
CHANNEL NUMBER
VS
GAMMA RAY ENERGY
4 CC Ge(Li) COUNTER
^{24}Na PHOTO
Th PHOTO
^{36}Ar(p,p$_1$ γ) PHOTOPEAK
^{207}Bi PHOTOPEAK
^{24}Na DOUBLE ESCAPE
Th DOUBLE ESCAPE
^{24}Na PHOTOPEAK
^{207}Bi PHOTOPEAK
^{207}Bi PHOTOPEAK
CHANNEL NUMBER
250
200
150
100
50
0
1.0
2.0
3.0
GAMMA RAY ENERGY (MeV)

Figure 40.

The block diagram of the electronics used to measure the lifetime of the 1.380 MeV level. The shaded square is the target chamber. The photomultipliers are RCA 8575 and the anode signals provide the inputs to the fast amplifiers. The discriminators pass pulses whose heights correspond to greater than 0.7 and 1.5 MeV, respectively. If pulses from all three inputs to the analyzer occur within 2 microseconds, the analyzer stores a count in a horizontal channel number corresponding to the pulse height from the start crystal and in a vertical channel corresponding to the time delay between the start and stop pulses. (page 50)

Figure 40

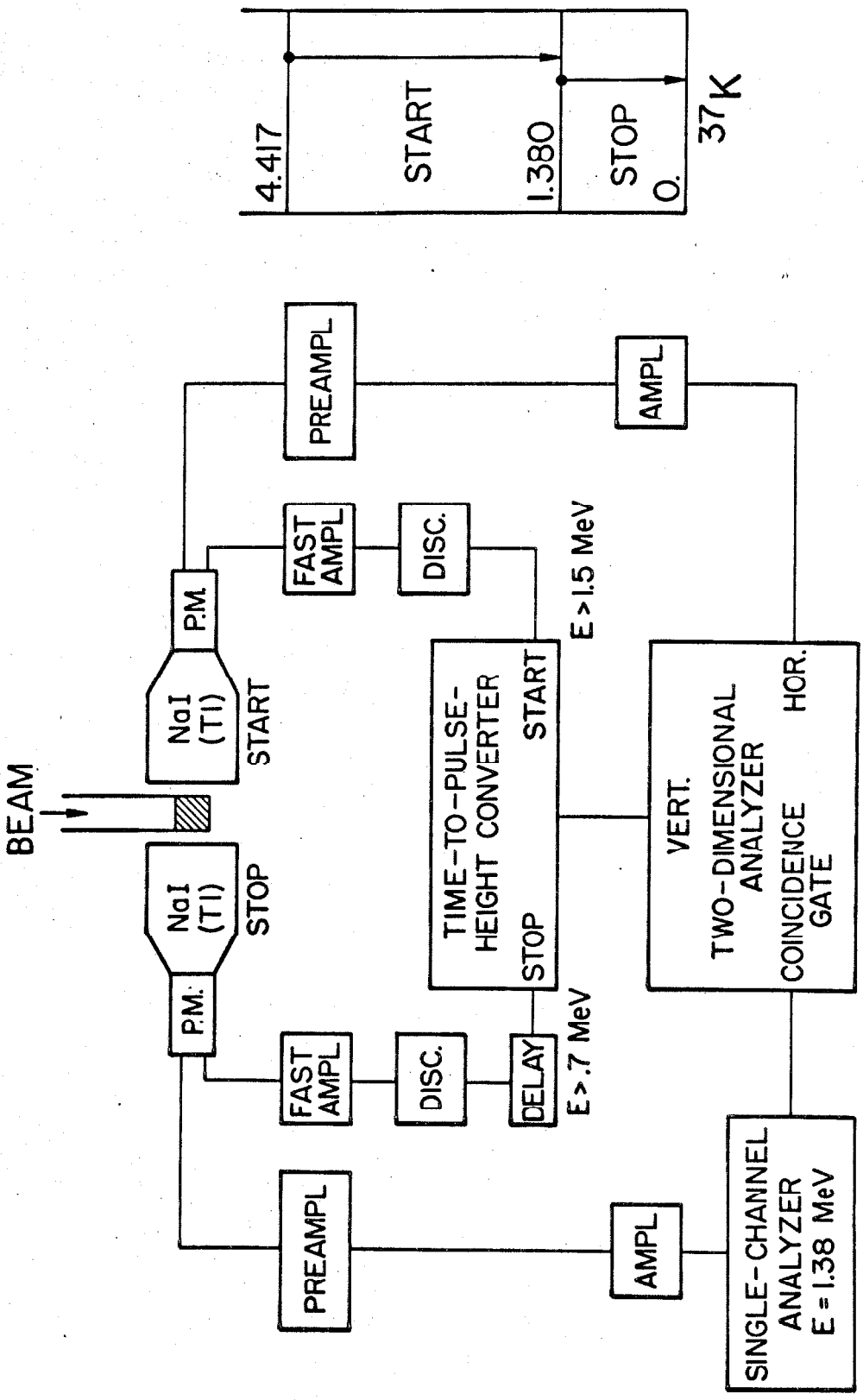
4.417
START
1.380
STOP
0.
37K
BEAM
NaI (Tl)
P.M.
START
NaI (Tl)
P.M.
STOP
PREAMPL
FAST AMPL
DISC.
E > 1.5 MeV
TIME-TO-PULSE-HEIGHT CONVERTER
START
STOP
FAST AMPL
DISC.
DELAY
E > .7 MeV
PREAMPL
AMPL
AMPL
VERT.
TWO-DIMENSIONAL ANALYZER
HOR.
COINCIDENCE GATE
SINGLE-CHANNEL ANALYZER E = 1.38 MeV

Figure 41.

This figure shows part of the analyzer output with ^{36}Ar in the cell. The numbers ranging from 21 to 37 in the top row denote horizontal channel number and also the gamma-ray pulse height in units of 100 keV. Since the start gamma ray has an energy of 3.04 MeV, the photopeak of this gamma ray is in column 30. The slow amplifier on the start side was saturating at 3.4 MeV, creating a fictitious peak in column 34.

The numbers running vertically from zero to 40 represent the time delay between start and stop pulses in units of 1.08 ± 0.1 nanoseconds per channel. Time delay increases downward and a delay inserted into the stop circuit causes the zero of time to be near row 15. Time slewing in the amplifiers causes a gradual slope in the zero of time. To partially correct for this, the channels are summed at an angle. For example, the sum of all of the boxed numbers is taken as the yield for zero time delay.

It is seen that there are tails extending down past time channel number 33 for columns 21 to 30, but no tails exist for columns 31-34 (other than those due to resolution). This is to be expected, since the photopeak of the start gamma ray is in column 30. (page 51)

Figure 41

	21	22	23	24	25	26	27	28	29	30	31	32	33	34	35	36	37
0	0	0	0	0	0	0	0	0	0	0	0	0	0	0	0	0	0
1	0	0	0	0	0	0	0	0	0	0	0	0	0	0	0	0	0
2	0	0	0	0	0	0	0	0	0	0	0	0	0	0	0	0	0
3	0	0	0	0	0	0	0	0	0	0	0	0	0	0	0	0	0
4	0	0	0	0	0	0	0	0	0	0	0	0	0	0	0	0	0
5	0	0	0	0	0	0	0	0	0	0	0	0	0	0	0	0	0
6	0	0	0	0	0	0	0	0	0	0	0	0	0	0	0	0	0
7	0	0	0	0	0	0	0	0	0	0	0	0	0	0	0	0	0
8	0	0	0	0	0	0	0	0	0	0	0	0	0	0	0	0	0
9	0	0	0	0	0	0	0	0	0	0	0	0	0	0	0	0	0
10	0	0	0	0	0	0	0	0	0	0	0	0	1	0	0	0	0
11	0	0	0	0	0	0	0	0	0	0	0	0	0	0	0	0	0
12	3	1	0	1	0	0	0	0	0	0	0	0	0	0	0	0	0
13	30	6	13	2	2	0	1	1	0	0	1	0	0	0	0	0	0
14	83	86	54	50	47	20	26	13	10	7	5	1	2	0	0	0	0
15	38	47	49	69	69	71	56	56	58	68	62	95	77	73	1	0	0
16	14	18	20	11	30	30	33	28	36	48	46	67	159	428	1	1	0
17	11	6	12	14	12	14	11	8	18	23	12	12	40	284	4	0	0
18	6	9	9	10	15	16	11	4	14	14	5	6	17	61	3	0	0
19	6	8	5	10	9	12	5	3	9	7	4	2	10	18	0	0	0
20	1	6	11	15	7	5	6	3	9	12	0	2	2	2	1	0	0
21	3	2	7	7	6	4	8	1	6	12	2	0	2	0	0	0	0
22	8	1	4	6	9	2	7	3	8	6	1	1	0	0	0	0	0
23	3	3	5	2	1	8	3	4	4	6	3	0	0	1	0	0	0
24	3	5	8	3	2	6	7	2	3	7	0	0	0	0	0	0	0
25	3	3	5	4	7	1	1	3	3	4	0	0	0	1	0	0	0
26	2	4	2	1	5	2	0	1	1	3	0	1	0	0	0	0	0
27	3	2	3	1	3	0	3	3	2	5	0	0	1	0	0	0	0
28	1	3	2	3	2	4	1	1	0	5	0	0	0	0	0	0	0
29	1	1	2	0	1	1	1	0	3	2	0	0	0	1	0	0	0
30	2	1	2	0	1	0	2	2	1	0	0	0	0	0	0	0	0
31	0	1	3	1	2	0	2	1	1	0	0	0	0	0	0	0	0
32	0	0	3	2	2	0	0	1	2	1	0	0	0	0	0	0	0
33	0	1	1	3	3	1	0	0	1	3	0	0	0	0	0	0	0
34	0	0	0	1	1	0	0	0	1	1	1	0	0	0	0	0	0
35	2	0	0	1	0	1	0	0	0	1	0	0	0	0	0	0	0
36	0	0	0	0	2	0	0	0	0	0	0	0	0	0	0	0	0
37	0	0	1	2	0	0	0	0	0	1	0	0	0	0	0	0	0
38	0	0	0	0	0	0	1	0	1	0	0	0	0	0	0	0	0
39	0	1	0	0	0	1	0	0	0	0	1	0	0	0	0	0	0
40	0	1	0	0	0	1	0	0	0	0	0	0	0	0	0	0	0

Figure 42.

This is the same spectrum as in figure 41 except that the target gas was replaced by helium as a background run. Because of charge normalization, this run must be multiplied by 1.7 before comparison with figure 41. (page 52)

Figure 42

	21	22	23	24	25	26	27	28	29	30	31	32	33	34	35	36	37
0	0	0	0	0	0	0	0	0	0	0	0	0	0	0	0	0	0
1	0	0	0	0	0	0	0	0	0	0	0	0	0	0	0	0	0
2	0	0	0	0	0	0	0	0	0	0	0	0	0	0	0	0	0
3	0	0	0	0	0	0	0	0	0	0	0	0	0	0	0	0	0
4	0	0	0	0	0	0	0	0	0	0	0	0	1	0	0	0	0
5	0	0	0	0	0	0	0	0	0	0	0	0	0	0	0	0	0
6	0	0	0	0	0	0	0	0	0	0	0	0	0	0	0	0	0
7	0	0	0	0	0	0	0	0	0	0	0	0	0	0	0	0	0
8	0	0	0	0	0	0	0	0	0	0	0	0	0	0	0	0	0
9	0	0	0	0	0	0	0	0	0	0	0	0	0	0	0	0	0
10	0	0	0	0	0	0	0	0	0	0	0	0	0	0	0	0	0
11	0	0	0	0	0	0	0	0	0	0	0	0	0	0	0	0	0
12	0	0	0	0	0	0	0	0	0	0	0	0	0	1	0	0	0
13	13	5	3	2	0	1	0	0	0	0	0	0	0	0	0	0	0
14	31	31	21	20	17	13	10	7	2	2	1	0	1	0	0	0	0
15	13	9	19	25	22	23	26	22	17	27	29	40	35	25	1	0	0
16	5	3	4	6	4	9	11	7	9	14	34	41	84	230	0	0	0
17	0	2	2	3	4	1	1	3	4	3	3	10	26	159	1	0	0
18	0	1	0	0	2	2	0	2	1	1	1	4	2	34	1	0	0
19	0	1	1	0	0	0	1	0	0	0	3	0	5	12	0	0	0
20	0	0	1	0	0	0	0	0	1	1	0	1	1	4	0	0	0
21	0	0	0	0	0	0	0	0	0	0	0	1	0	1	0	0	0
22	0	0	0	0	0	0	0	0	0	0	0	0	0	0	0	0	0
23	0	0	0	0	0	0	0	0	0	0	0	0	0	0	0	0	0
24	0	0	0	0	0	0	0	0	0	0	1	0	1	0	0	0	0
25	0	0	0	0	0	0	0	0	0	0	0	0	0	0	0	0	0
26	0	0	0	0	0	0	0	0	0	0	0	0	0	0	0	0	0
27	0	0	0	0	0	0	0	0	0	0	0	0	0	0	0	0	0
28	0	0	0	0	0	0	0	0	0	0	0	0	0	0	0	0	0
29	0	0	0	0	0	0	0	0	0	0	0	0	0	0	0	0	0
30	0	0	0	0	0	0	0	0	0	0	0	0	0	0	0	0	0
31	0	0	0	0	0	0	0	0	0	0	0	0	0	0	0	0	0
32	0	0	0	0	0	0	0	0	0	0	0	0	0	0	0	0	0
33	0	0	0	0	0	0	0	0	0	0	0	0	0	0	0	0	0
34	0	0	0	0	0	0	0	0	0	0	0	0	0	0	0	0	0
35	0	0	0	0	0	0	0	0	0	0	0	0	0	0	0	0	0
36	0	0	0	0	0	0	0	0	0	0	0	0	0	0	0	0	0
37	0	0	0	0	0	0	0	0	0	0	0	0	0	0	0	0	0
38	0	0	0	0	0	0	0	0	0	0	0	0	0	0	0	0	0
39	0	0	0	0	0	0	0	0	0	0	0	0	0	1	0	0	0
40	0	0	0	0	0	0	0	0	0	0	0	0	0	0	0	0	0

Figure 43.

The resolution check on the electronics by use of the two coincident gamma rays from the decay of ^{24}Na. This was a particularly good calibrator because of the similarity of these gamma-ray energies with those of figure 40. The resolution measured is 3.2 nanoseconds FWHM. (page 52)

Figure 43

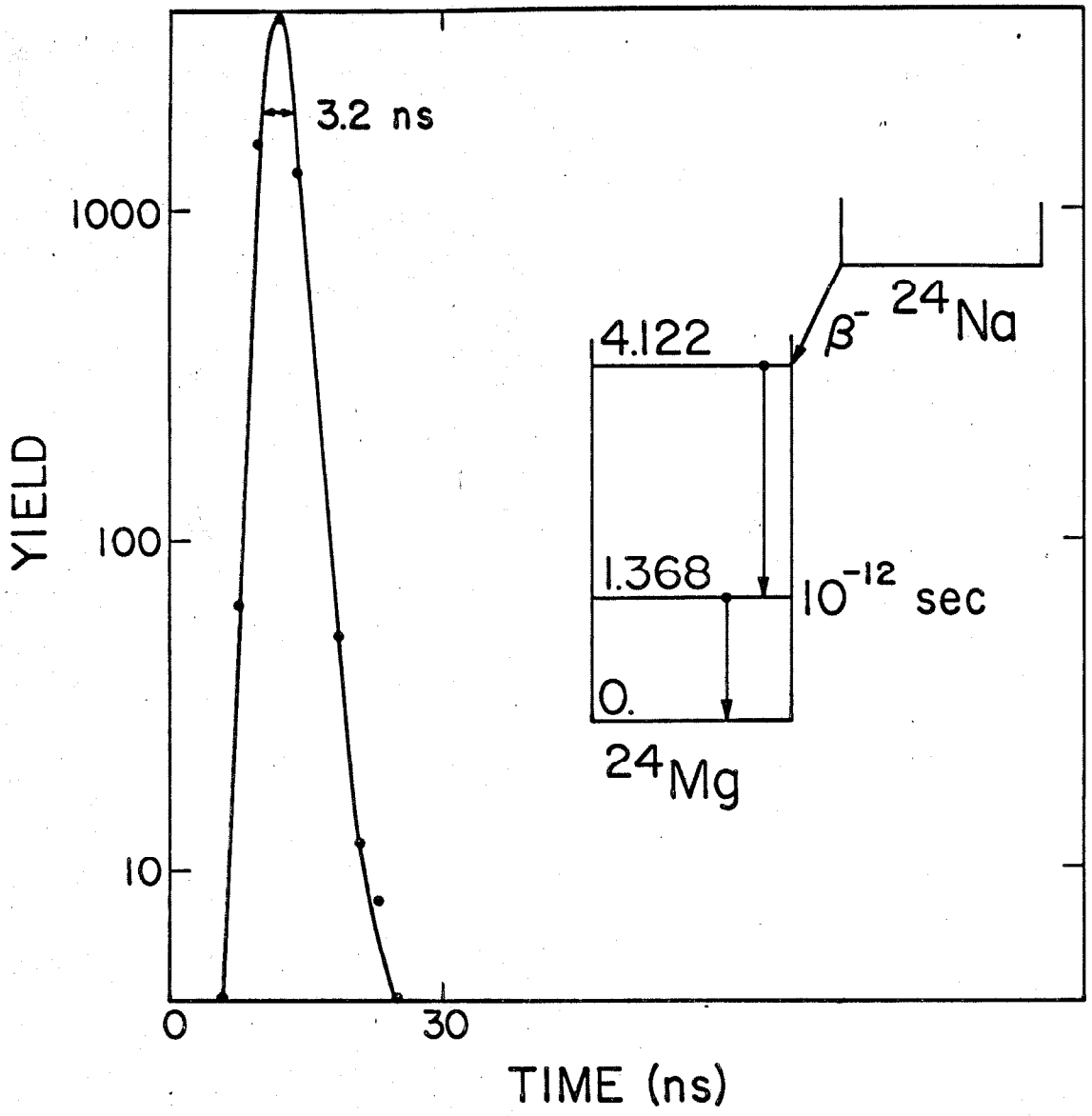
3.2 ns
1000
100
10
YIELD
0
30
TIME (ns)
4.122
β⁻ ²⁴Na
1.368
10⁻¹² sec
0.
²⁴Mg

Figure 44.

The result for the half-life of the 1.380 MeV level in ^{37}K. The background with helium in the cell at the original beam energy has been subtracted and the vertical scale is the number of counts in a given time-delay interval for start energy pulse heights between 2.1 and 3.0 MeV. As long as one stays two full-widths of the time resolution away from the peak of this curve, the observed curve falls with the same time constant as it would if seen with perfect time resolution.(page 52)

Figure 44

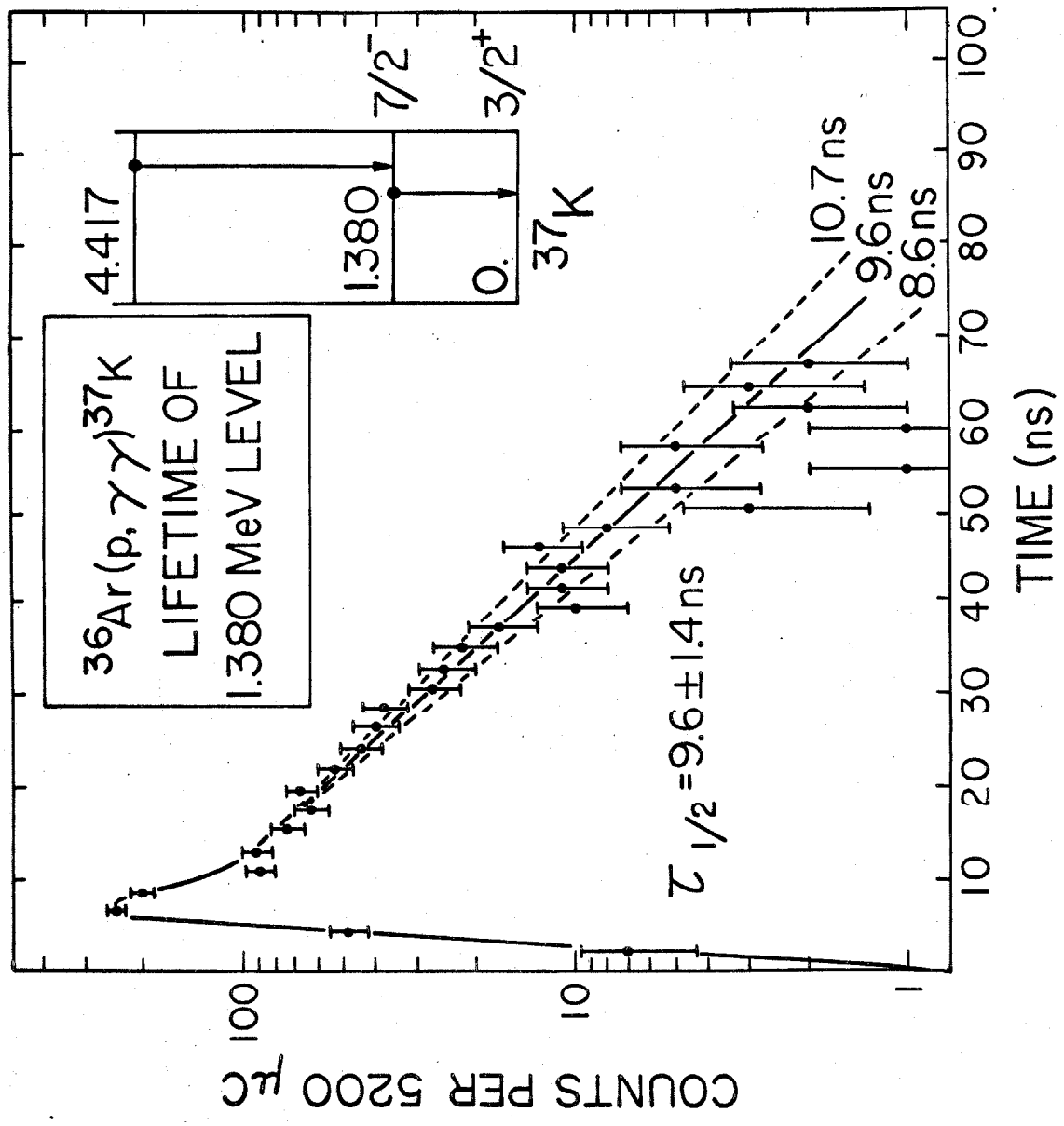
$^{36}Ar(p,\gamma\gamma)^{37}K$
LIFETIME OF
1.380 MeV LEVEL
4.417
1.380
0.
^{37}K
$7/2^-$
$3/2^+$
10.7ns
9.6ns
8.6ns
$\tau_{1/2}$=9.6±1.4ns
COUNTS PER 5200 μC
TIME (ns)

Figure 45.

The experimental setup for the 90^{o} run on the gamma-ray decay of the 3311 keV level. The beam enters from the top of the diagram and the target is a line 9 mm long and 1.5 mm wide. The lead collimator was used to shield the front face of the NaI(Tl) crystal from room background, but was not used in the measurements at the other resonances reported in this work. (page 57)

Figure 45

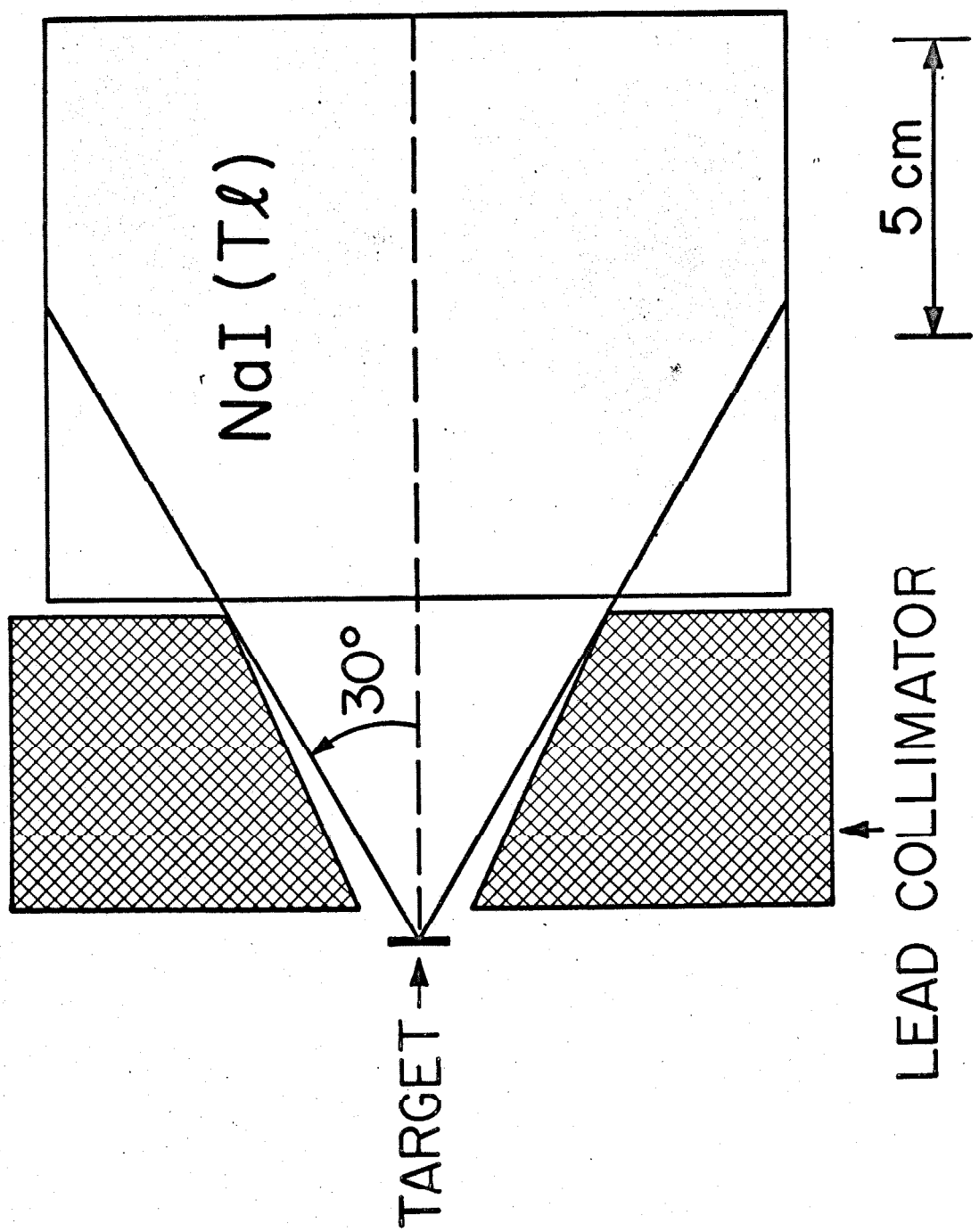

Figure 46.

The gamma-ray spectra at 0^{o} and 90^{o} from the 3.311 MeV level with the geometry shown in figure 45. The scale on the left is for the upper curve and the one on the right for the lower curve. The shaded areas represent the estimated photopeaks. The on-resonance background with helium in the gas cell has been subtracted. The 0.511 MeV peaks which appear in this and other figures are due to the pair-annihilation quanta from positrons emitted in the beta decay of ^{37}K.

(page 57)

Figure 46

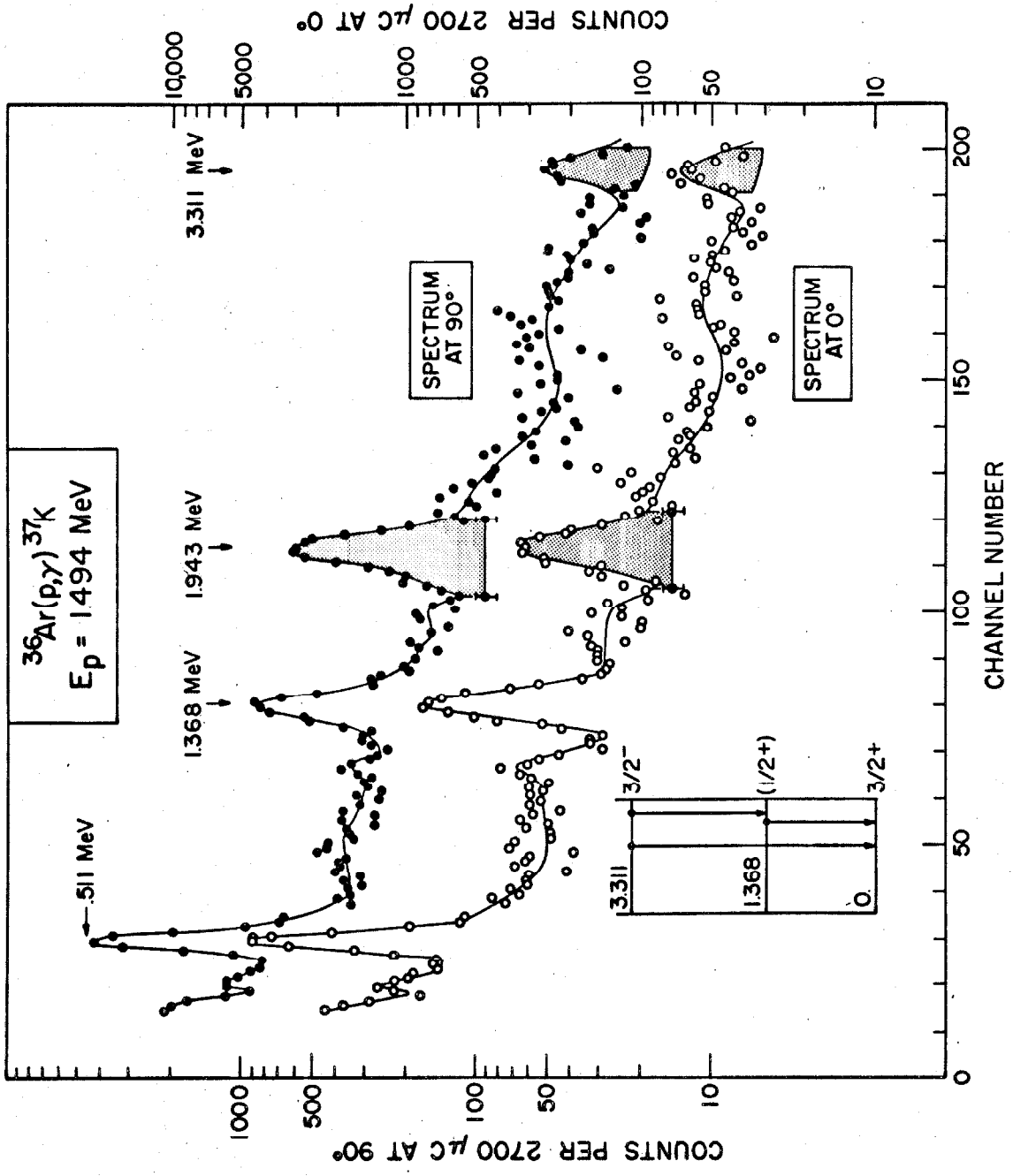
$^{36}Ar(p,\gamma)^{37}K$
E_p = 1.494 MeV
.511 MeV
1.368 MeV
1.943 MeV
3.311 MeV
SPECTRUM AT 90°
SPECTRUM AT 0°
3/2⁻
(1/2⁺)
3/2⁺
3.311
1.368
0
COUNTS PER 2700 μC AT 90°
COUNTS PER 2700 μC AT 0°
CHANNEL NUMBER

Figure 47.

The gamma rays from the 3.311 MeV level as seen at 90^{o} to the beam with a 4 cm^{3} Ge(Li) counter. No background has been subtracted, and the peak at 0.31 MeV is an impurity. The pair peak due to the ground-state gamma ray would be in channel 252 but would only be four counts high. (page 57)

Figure 47

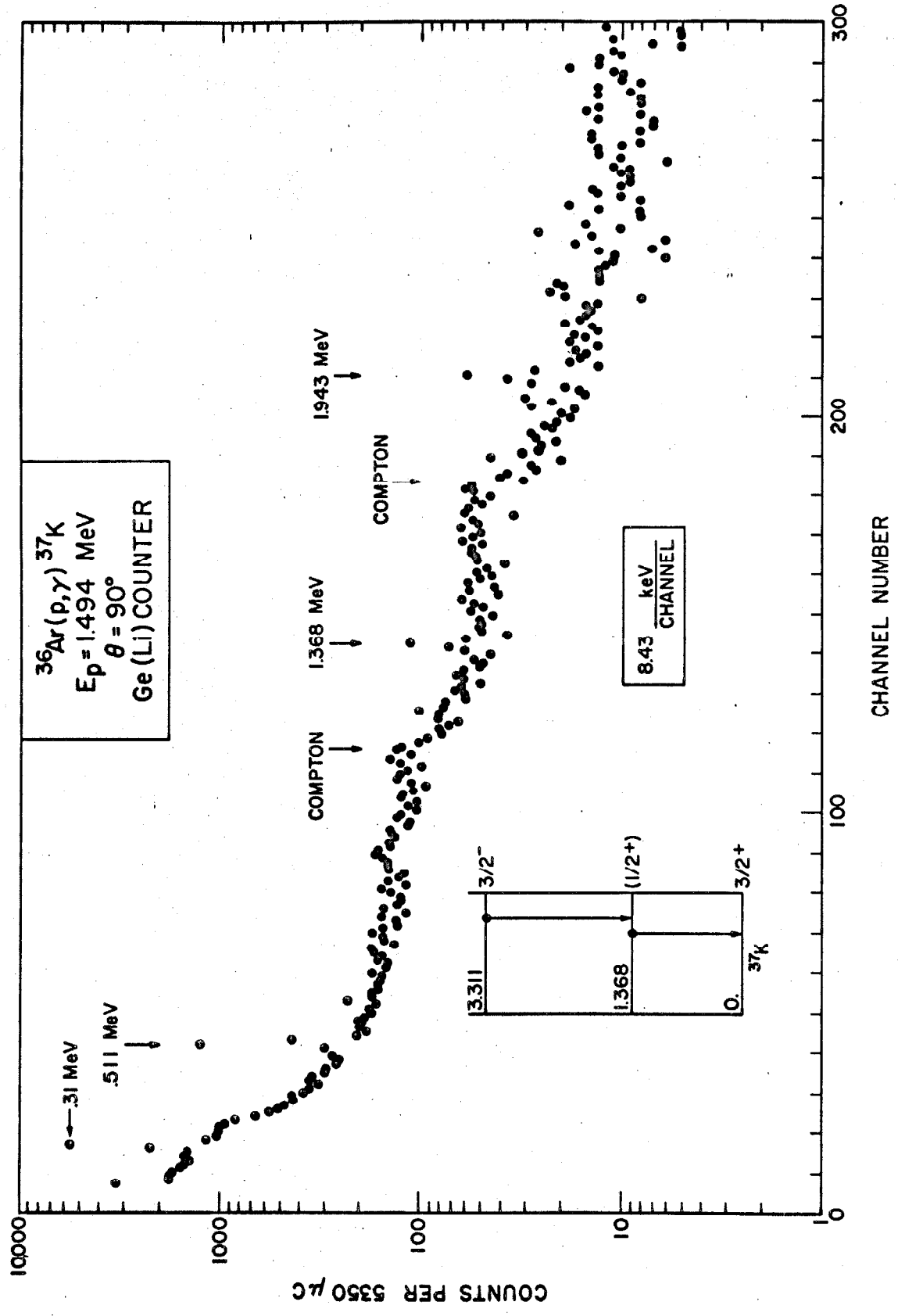
$^{36}Ar(p,\gamma)^{37}K$
E_p = 1.494 MeV
θ = 90°
Ge(Li) COUNTER
.31 MeV
.511 MeV
COMPTON
1.368 MeV
COMPTON
1.943 MeV
8.43 keV/CHANNEL
3/2⁻
(1/2⁺)
3/2⁺
3.311
1.368
0.
^{37}K
COUNTS PER 5350 μC
CHANNEL NUMBER
10000
1000
100
10
1
0
100
200
300

Figure 48.

The gamma-ray spectrum from the decay of the 2.750 MeV level as seen by a 7.6 by 7.6 cm NaI(Tl) crystal at 0^{o}. The dominant decay is to the ground state, but a few percent decays through the doublet at 1.37 MeV. The on-resonance background with helium in the cell has been subtracted. The peak at 0.68 MeV is a backscatter peak due to summing in the crystal of one annihilation quantum and a backscattered quantum which has 0.17 MeV of energy. (page 59)

Figure 48

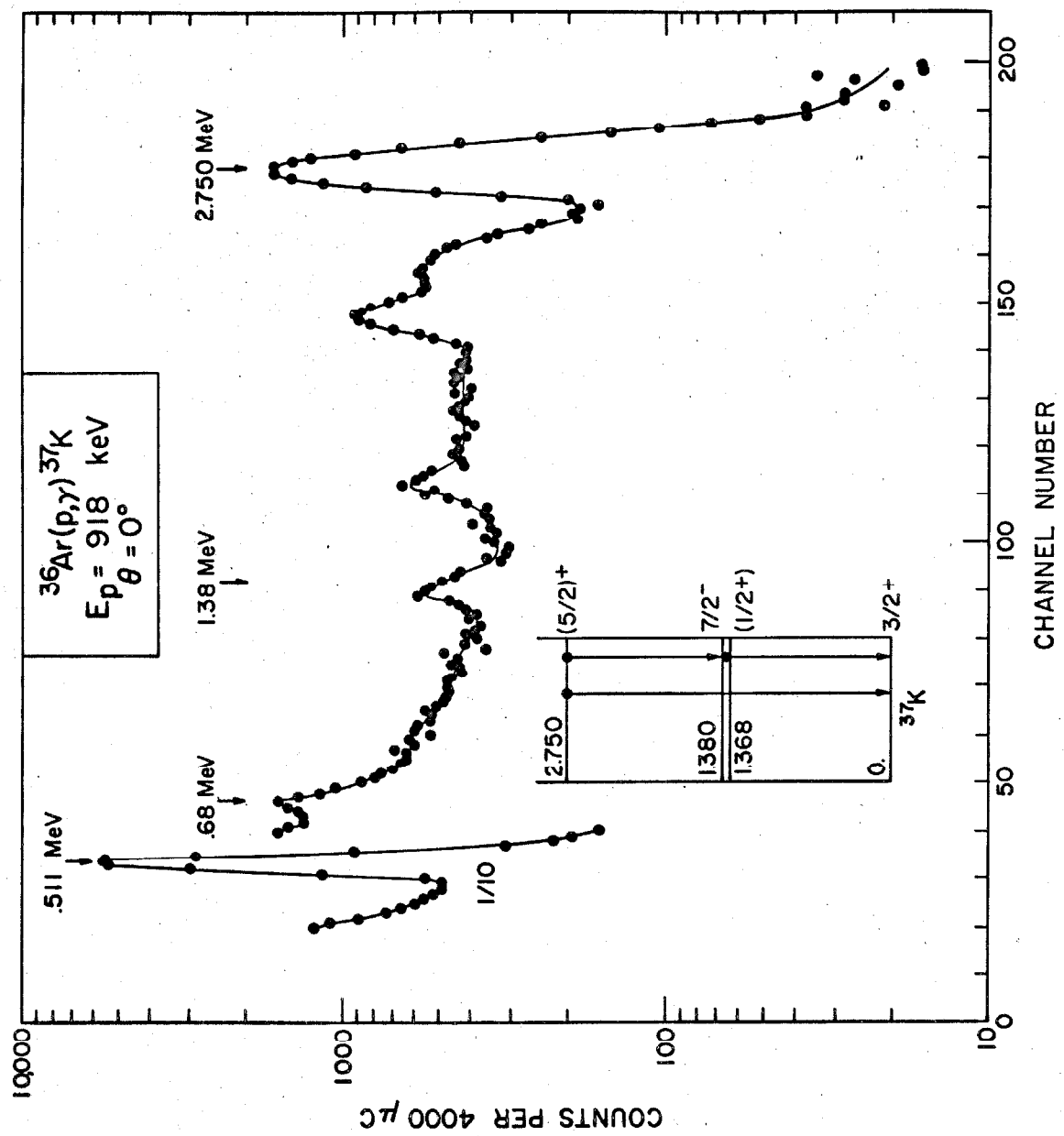
$^{36}Ar(p,\gamma)^{37}K$
E_p = 918 keV
θ = 0°
.511 MeV
.68 MeV
1.38 MeV
2.750 MeV
1/10
(5/2)+
7/2−
(1/2+)
3/2+
2.750
1380
1368
0.
^{37}K
COUNTS PER 4000 μC
CHANNEL NUMBER
10000
1000
100
10
0
50
100
150
200

Figure 49.

The observed angular distribution of the ground-state gamma ray from the 2.750 MeV level, as seen in a 7.6 by 7.6 cm NaI(Tl) crystal 5.2 cm from the target center. The angular attenuation factors were $Q_2 = 0.83$ and $Q_4 = 0.52$ as calculated by the code BAZKJL. Small background corrections for impurities and room background have been measured and taken into account. The order of the angles taken was 90^o, 0^o, 80^o, 10^o, 70^o, 20^o, 60^o, 30^o, 50^o, 40^o, 90^o, 0^o, 80^o, and 10^o.

The solid line is a theoretical fit for $5/2^+$ to $3/2^+$ by 1.5% E2 and the dashed lines are fits for $3/2^+$ to $3/2^+$ with various M1-E2 admixtures. For the dashed lines it is seen that 62% E2 is an extremum because the anisotropy is closer to unity if the mixing is changed in either direction from 62%. (page 60)

Figure 49

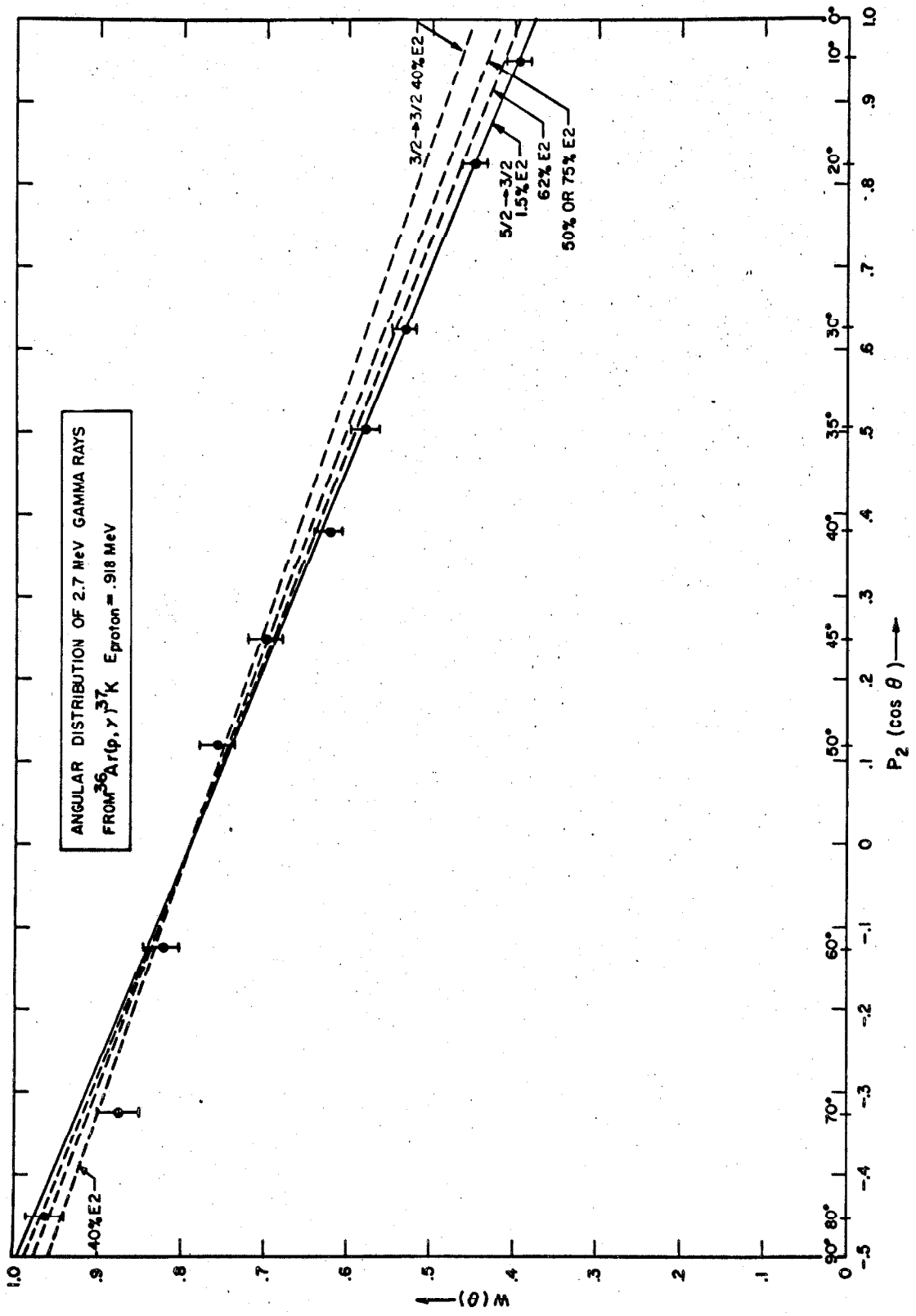
ANGULAR DISTRIBUTION OF 2.7 MeV GAMMA RAYS
FROM $^{36}Ar(p,\gamma)^{37}K$ E_{proton} = .918 MeV
3/2→3/2 40% E2
5/2→3/2 1.5% E2
62% E2
50% OR 75% E2
40% E2
W(θ)
P_2 (cos θ)

Figure 50.

The gamma-ray spectra at 0^{o} and 90^{o} from the 3.083 MeV level as seen by a 12.7 by 10.2 cm NaI(Tl) crystal one centimeter from the target center. On-resonance background with helium has been subtracted. Decays through the 1.38 and 2.169 MeV levels are evident. After corrections for summing in the crystal are taken into account, the ground-state branch is about 10%. (page 62)

Figure 50

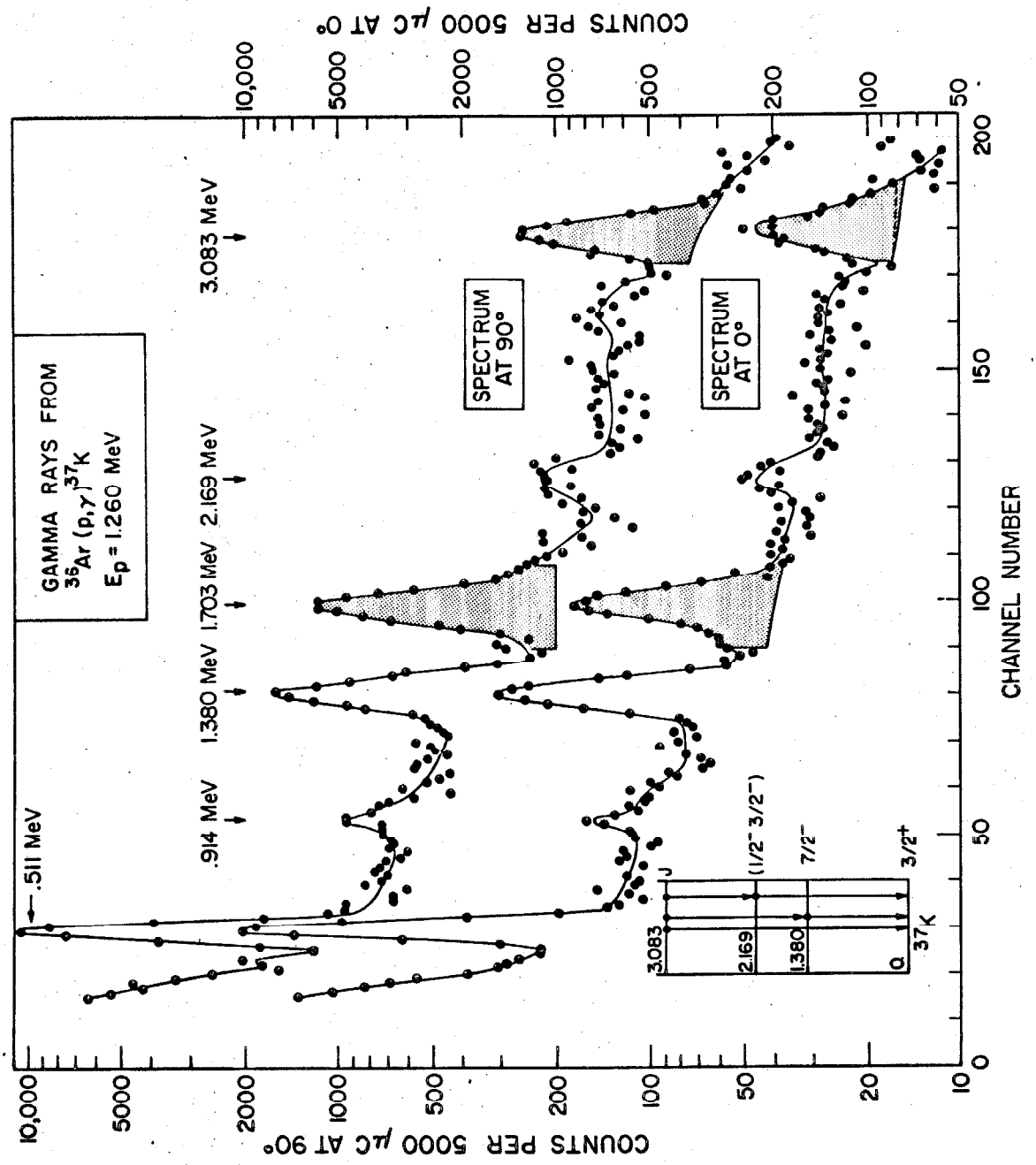
GAMMA RAYS FROM
$^{36}Ar(p,\gamma)^{37}K$
E_p = 1.260 MeV
.511 MeV
.914 MeV
1.380 MeV
1.703 MeV
2.169 MeV
3.083 MeV
SPECTRUM AT 90°
SPECTRUM AT 0°
COUNTS PER 5000 μC AT 90°
COUNTS PER 5000 μC AT 0°
CHANNEL NUMBER
J
(1/2⁻ 3/2⁻)
7/2⁻
3/2⁺
3.083
2.169
1.380
0
37K

Figure 51.

The gamma-ray spectrum at 90^{o} from the decay of the 3.083 MeV level as seen by a 20 cm^{3} Ge(Li) counter. No background subtraction has been made. The decay through the 1.380 MeV level is evident through the 1.380 and 1.703 MeV photopeaks. The first gamma ray in the cascade through the 2.169 MeV level is the 0.914 MeV bump, but the 2.169 MeV gamma ray is lost in background. The pair peak of the ground-state gamma ray should appear at 2.061 MeV, but is swamped by background. The peak at 2.614 MeV is presumably due to radiothorium and the peak at 1.462 MeV due to ^{40}K in the concrete walls of the tandem target room. The peak at 1.275 MeV is due to ^{22}Na nuclei which had been embedded into the target chamber walls by the reaction $^{20}Ne(^{3}He, p)^{22}Na$ in an earlier experiment, the peak at 0.511 MeV is due to annihilation quanta, and the peak at 0.478 MeV is due to a ^{7}Be source situated about 14 feet from the counter during the course of the run (Hensley, 1966). (page 62)

Figure 51

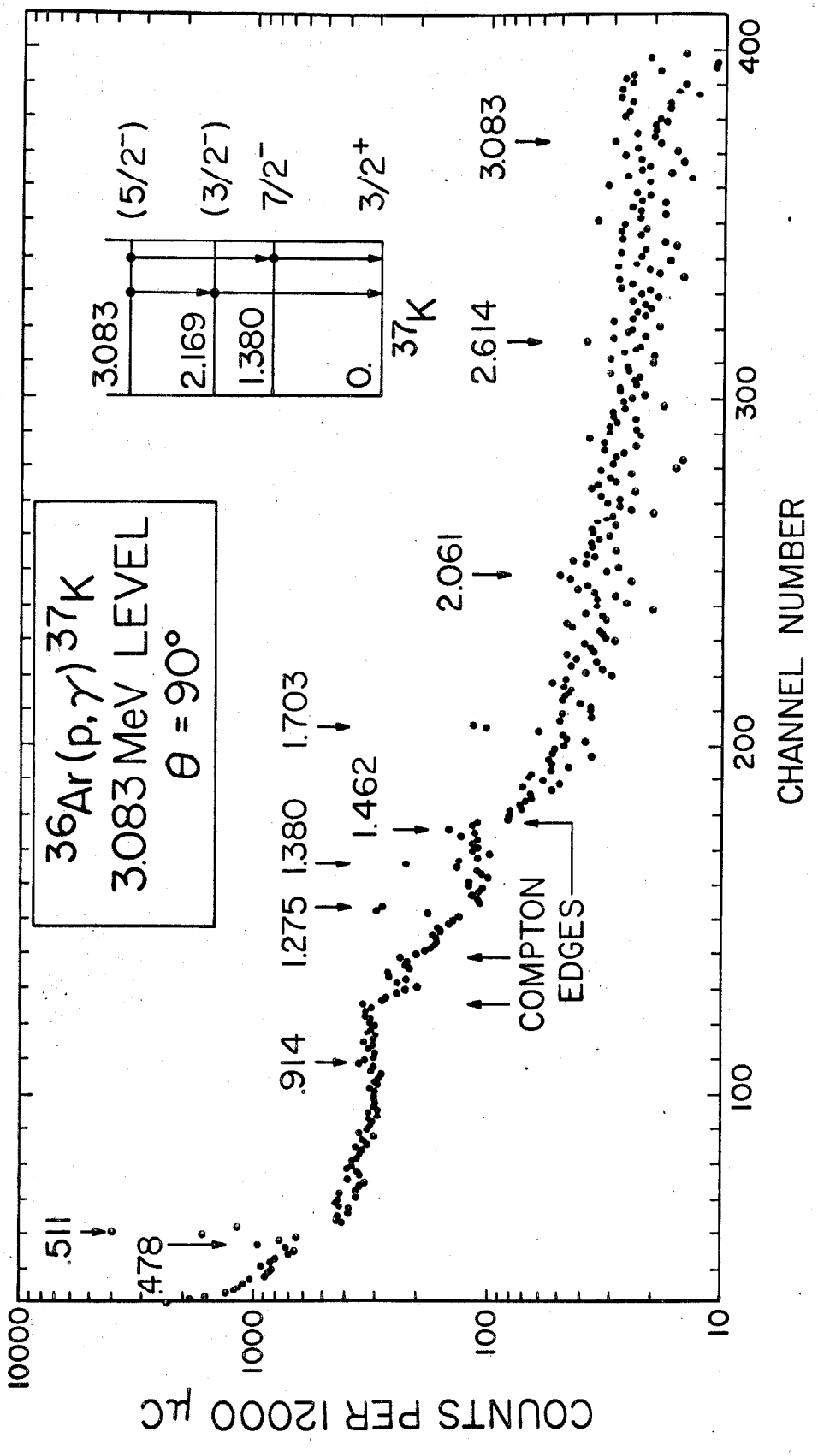
$^{36}Ar(p,\gamma)^{37}K$
3.083 MeV LEVEL
θ = 90°
3.083
2.169
1.380
0.
^{37}K
(5/2⁻)
(3/2⁻)
7/2⁻
3/2⁺
.511
.478
.914
1.275
1.380
1.462
1.703
2.061
2.614
3.083
COMPTON EDGES
COUNTS PER 12000 μC
CHANNEL NUMBER
10000
1000
100
10
100
200
300
400

Figure 52.

Gamma rays at 0^{o} and 90^{o} from the decay of the 3.083 MeV level seen by a NaI(Tl) crystal with better angular resolution than that used in figure 50. On-resonance background with helium in the chamber as well as room-background has been subtracted. The ratio of the shaded areas under part of the photopeak of the 1.703 MeV gamma ray was used to determine the experimental anisotropy. The shaded areas represent only a fraction of the photopeak because the uncertainty in the background (shown with error bars) under the 1.703 MeV photopeak makes the statistical uncertainty in the anisotropy larger if the entire photopeak is used. About 8% of the number of 1.703 MeV gamma rays which lose their entire energy in the detector do not appear in the photopeak due to summing with the 1.380 MeV gamma ray. Since this effect is nearly the same for both the 0^{o} and 90^{o} spectra, the effect on the anisotropy is negligible. The 1.380 MeV gamma ray is nearly isotropic, but this information does not eliminate any of the spin assignments made in part X. (page 63)

Figure 52

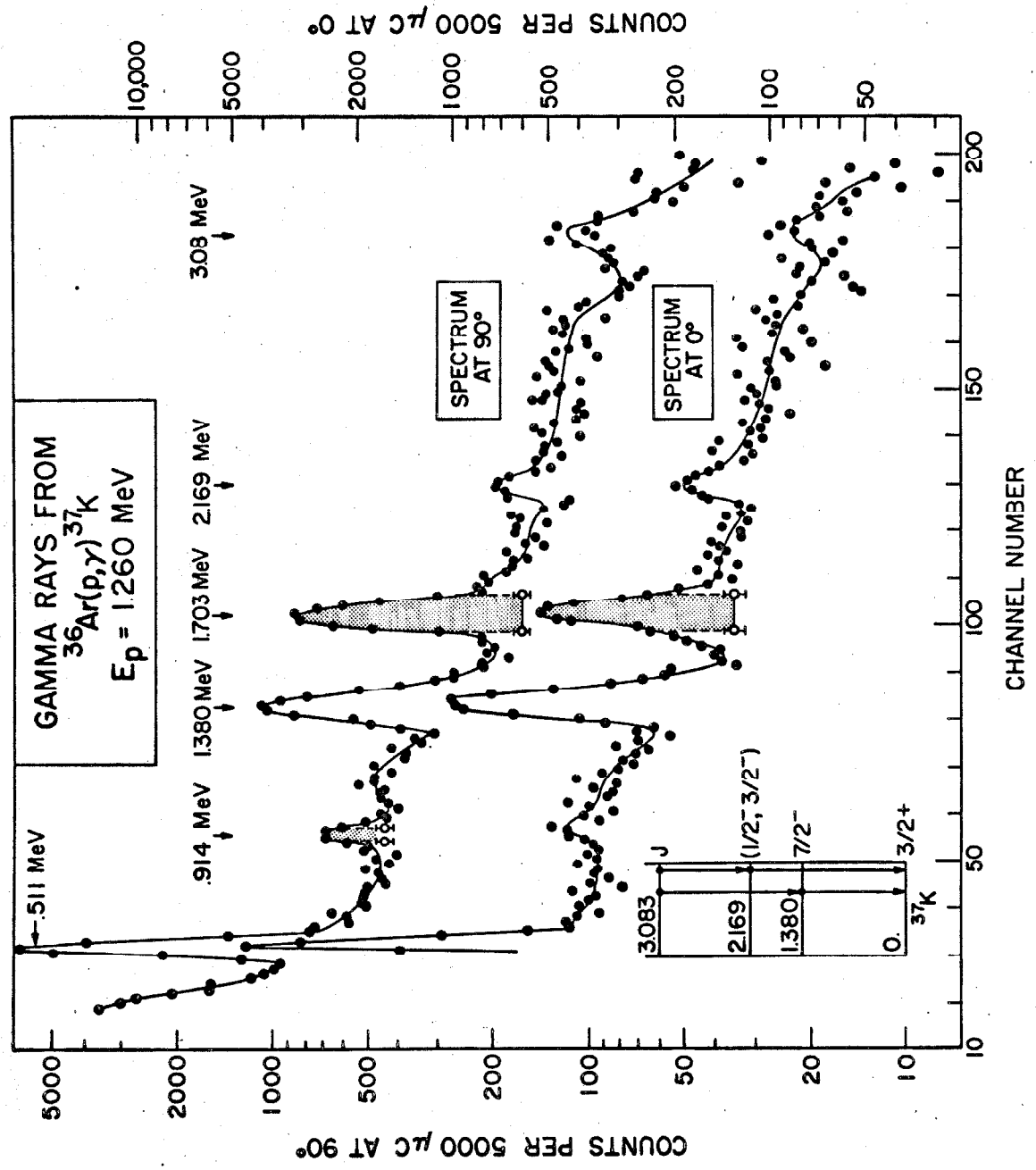
GAMMA RAYS FROM
$^{36}Ar(p,\gamma)^{37}K$
E_p = 1.260 MeV
.511 MeV
.914 MeV
1.380 MeV
1.703 MeV
2.169 MeV
3.08 MeV
SPECTRUM AT 90°
SPECTRUM AT 0°
COUNTS PER 5000 μC AT 90°
COUNTS PER 5000 μC AT 0°
CHANNEL NUMBER
J
(1/2⁻, 3/2⁻)
7/2⁻
3/2⁺
3.083
2.169
1.380
0.
^{37}K

Figure 53.

Isobar diagram for the mirror nuclei ^{37}K and ^{37}Ar. The excitation energies in ^{37}Ar are those reported by McNally (1966) with the exception of the 1.611 MeV level, which was calibrated by the $^{34}S(\alpha, n)^{37}Ar$ reaction. Gamma-ray transitions shown are the principal ones only and are initiated by a solid dot and terminated by an arrow.
(page 68)

Figure 53

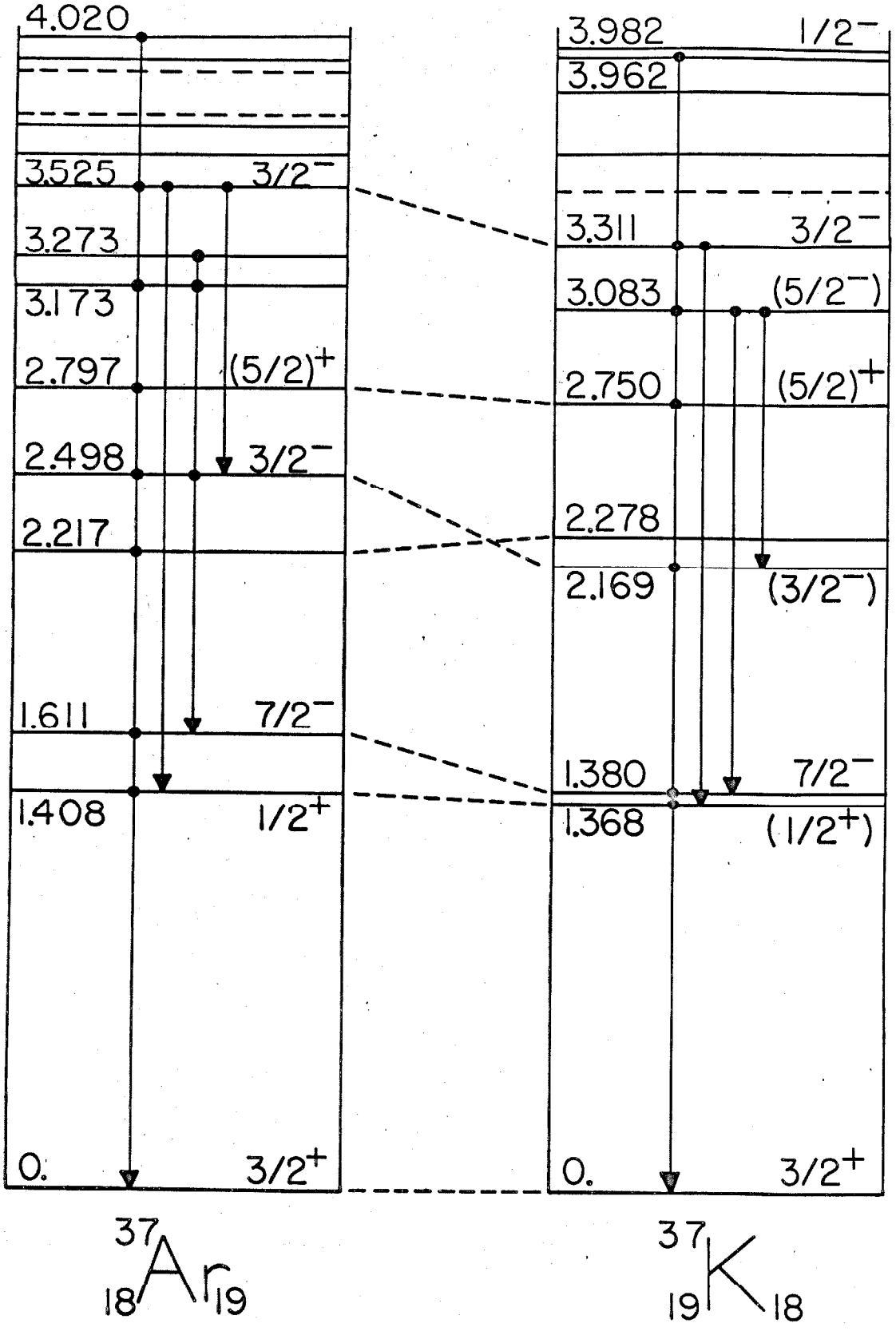
4.020
3.525
3/2⁻
3.273
3.173
2.797
(5/2)⁺
2.498
3/2⁻
2.217
1.611
7/2⁻
1.408
1/2⁺
0.
3/2⁺
3.982
1/2⁻
3.962
3.311
3/2⁻
3.083
(5/2⁻)
2.750
(5/2)⁺
2.278
2.169
(3/2⁻)
1.380
7/2⁻
1.368
(1/2⁺)
0.
3/2⁺
37 18 Ar 19
37 19 K 18

Figure 54.

The present energy-level diagram of ^{37}K. Gamma-ray transitions are initiated by a solid dot and are terminated by an arrow. A broad line represents the principal gamma-ray decay mode of a given level. Quantitative information on the gamma-ray widths is given in table 2 and figure 55. (page 69)

Figure 54

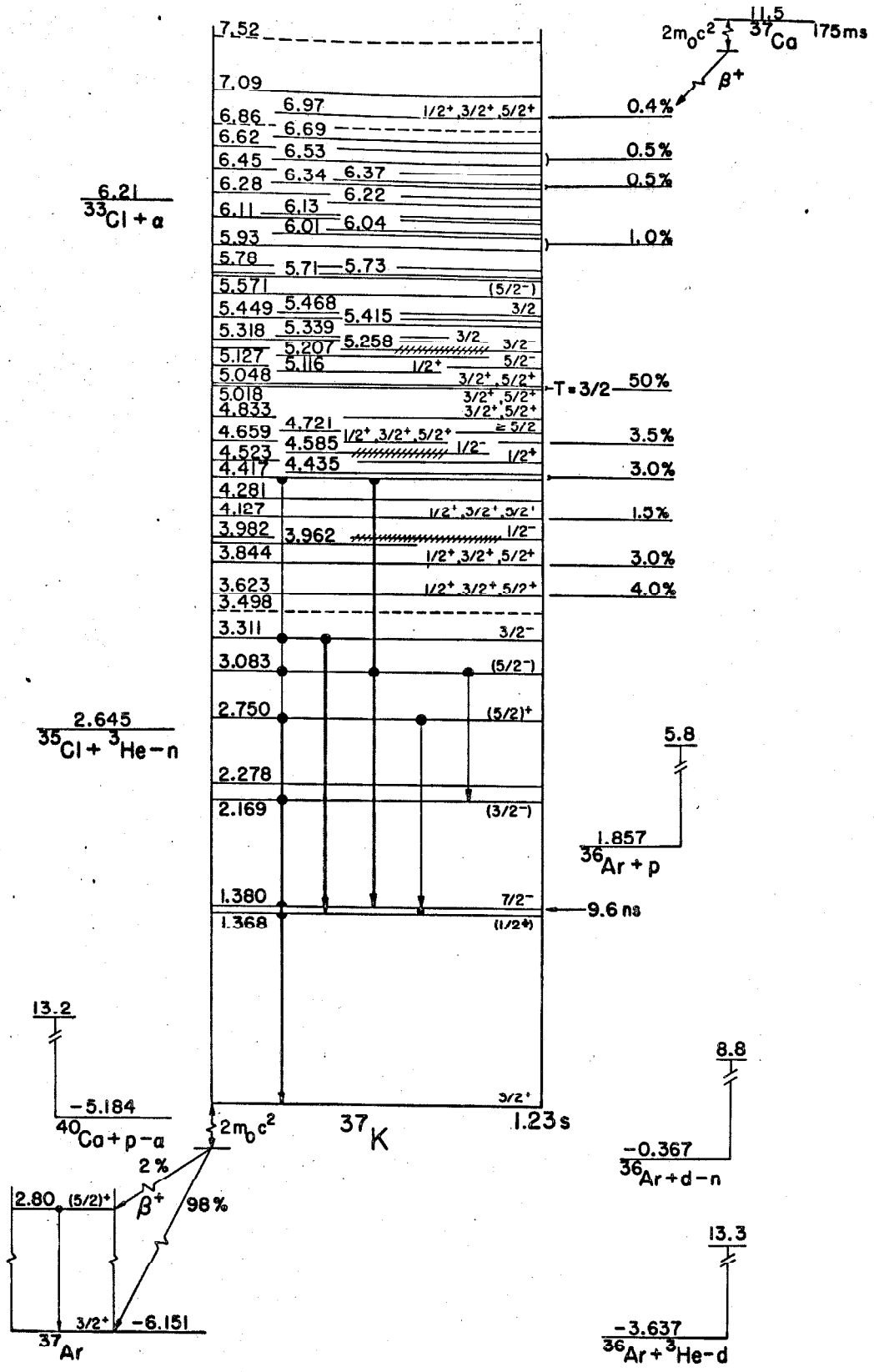
11.5
2m0c2
37Ca
175ms
β+
0.4%
0.5%
0.5%
1.0%
7.52
7.09
6.97
1/2+,3/2+,5/2+
6.86
6.69
6.62
6.53
6.45
6.34
6.37
6.28
6.22
6.11
6.13
6.01
6.04
5.93
5.78
5.71
5.73
5.571
(5/2−)
5.449
5.468
5.415
3/2
5.318
5.339
5.258
3/2
5.207
3/2
5.127
5.116
1/2+
5/2−
5.048
3/2+,5/2+
T=3/2
50%
5.018
3/2+,5/2+
4.833
3/2+,5/2+
4.659
4.721
1/2+,3/2+,5/2+
≥5/2
3.5%
4.523
4.585
1/2−
1/2+
4.417
4.435
3.0%
4.281
4.127
1/2+,3/2+,5/2+
1.5%
3.982
3.962
1/2−
3.844
1/2+,3/2+,5/2+
3.0%
3.623
1/2+,3/2+,5/2+
4.0%
3.498
3.311
3/2−
3.083
(5/2−)
2.750
(5/2)+
2.278
2.169
(3/2−)
1.380
7/2−
9.6 ns
1.368
(1/2+)
3/2+
6.21
33Cl + α
2.645
35Cl + 3He − n
5.8
1.857
36Ar + p
13.2
−5.184
40Ca + p − α
2m0c2
37K
1.23 s
2%
β+
98%
2.80
(5/2)+
3/2+
−6.151
37Ar
8.8
−0.367
36Ar + d − n
13.3
−3.637
36Ar + 3He − d

Figure 55.

The gamma-ray decay of levels in ^{37}K. The numbers are branching ratios expressed in percent. The value of X for the ground-state branch of the decay of the 2.750 MeV level is the ratio of reduced E2 to M1 matrix elements, and is written in the sign convention used by Poletti (1965). This value is correct only if the spin of the 2.750 MeV level is $5/2^+$. The transition from the 3.982 MeV level to the 2.169 MeV level may involve cascades, and all dashed transitions are tentative. (page 71)

Figure 55

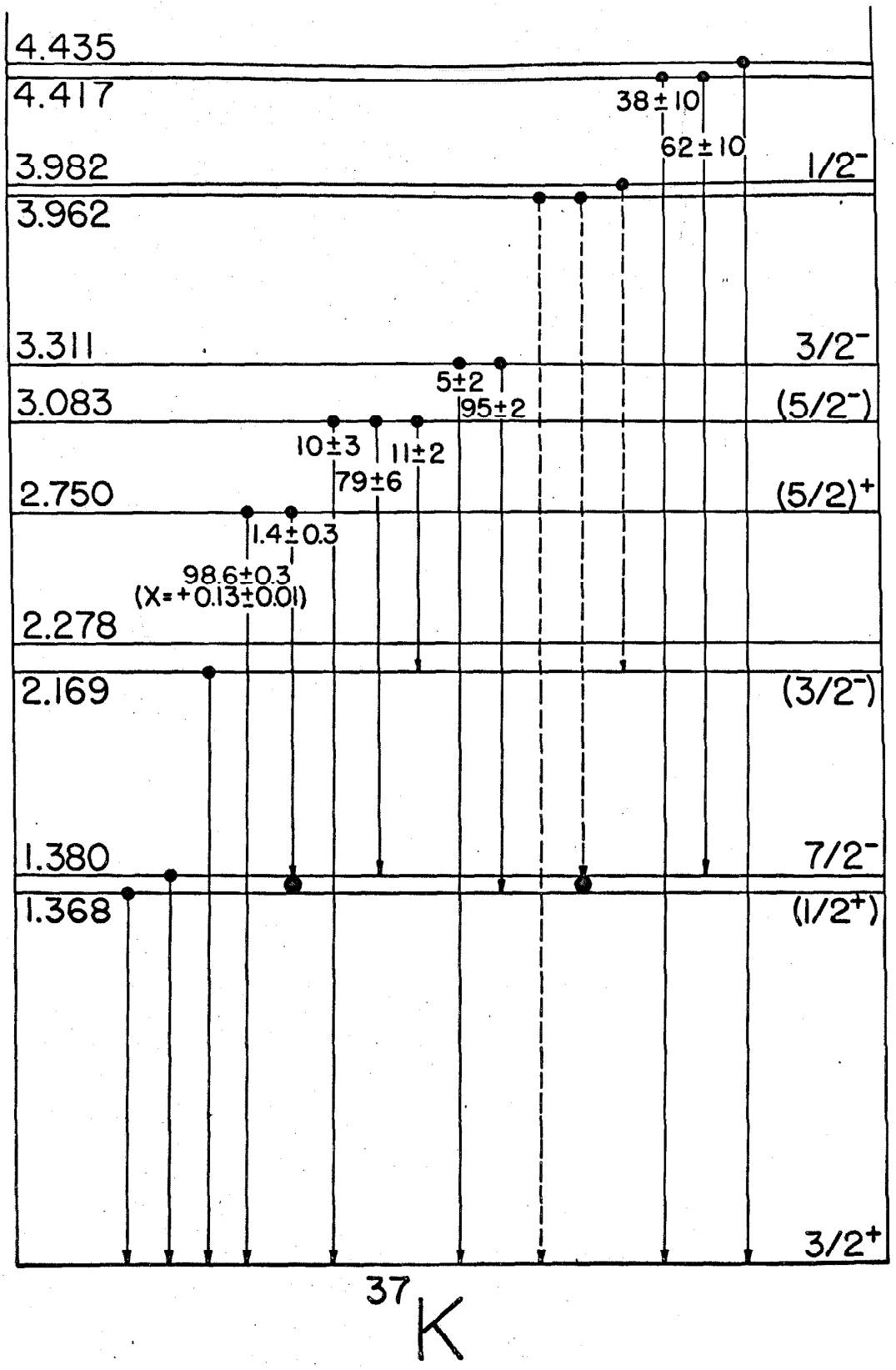
4.435
4.417
38±10
62±10
3.982
1/2⁻
3.962
3.311
3/2⁻
5±2
95±2
3.083
(5/2⁻)
10±3
11±2
79±6
2.750
(5/2)⁺
1.4±0.3
98.6±0.3
(X=+0.13±0.01)
2.278
2.169
(3/2⁻)
1.380
7/2⁻
1.368
(1/2⁺)
3/2⁺
37K